**First draft-unedited – 8.1.2017**

# Information Relativity: The Special and General Theory

**Ramzi Suleiman**[a]

"*Nature is pleased with simplicity. And Nature is no dummy*." - Isaac Newton.
*"Simplicity is the ultimate sophistication."* - Leonardo da Vinci.

**Abstract**

We propose a simple, axiom-free modification of Galileo-Newton's dynamics of moving bodies, termed Information Relativity theory. We claim that the theory is capable of unifying physics. The claimed unification is supported by the fact that the same derived set of simple and beautiful transformations, apply successfully to predicting and explaining many phenomena and findings in cosmology, quantum mechanics, and more. Our modification of classical physics is done simply by accounting for the time travel of information about a physical measurement, from the reference frame at which the measurement was taken, to an observer in another reference frame, which is in motion relative to the first frame. This minor modification of classical physics turns out to be sufficient for unifying all the dynamics of moving bodies, regardless of their size and mass. Since the theory's transformations and predictions are expressed only in terms of observable physical entities, its testing should be simple and straightforward.

For quantum mechanics the special version of the theory for translational inertial motion predicts and explains matter-wave duality, quantum phase transition, quantum criticality, entanglement, the diffraction of single particles in the double slit experiment, the quantum nature of the hydrogen atom. For cosmology, the theory constructs a relativistic quantum cosmology, which provides plausible and testable explanations of dark matter and dark energy, as well as predictions of the mass of the Higgs boson, the GZK cutoff phenomena, the Schwarzschild radius of black holes (without interior singularity), and the timeline of ionization of chemical elements along the history of the universe. The general version of the theory for gravitational and electrostatic fields, also detailed in the paper, is shown to be successful in predicting and explaining the strong force, quantum confinement, and asymptotic freedom.

**Keywords**: Information; Inertial systems; Relativity; Time dilation; Length contraction; Lorentz Invariance; Michelson-Morley experiment; Sagnac effect; Neutrino velocity experiments; OPERA; ICARUS; Higgs boson; ATLAS; CMS; quantum theory; Bell's inequality; EPR; Matter-wave duality; Quantum phase transition; Quantum criticality; Entanglement; Double slit experiment; Hydrogen atom problem; Dark matter; Dark energy; GZK cutoff; ΛCDM cosmologies; Black hole; Schwarzschild's radius; ionization; evolution of chemical elements; Gravitation, Electrostatic force; Strong force; Quantum confinement; Asymptotic freedom.

(a) Department of Psychology, University of Haifa, & Department of Philosophy, Al Quds University. Email: Suleiman@psy.haifa.ac.il

**Table of Contents**



## 1. Introduction

The Special Theory of relativity (SR) [1], and Lorentz's invariance principle (LI) have been with us for more than a century. Most physicist are confident that these two cornerstones of post-Newtonian physics will prevail forever. We do not wish to argue of whether these optimistic forecast are true or

false. However, we do argue, that a scientific discipline that is free from prejudice and dogmas, should allow a freedom of thought about other models of nature. In fact, without such freedom, many other theories, including quantum theories, some of which contradicts both SR and LI, would not have been developed, and our understanding of the microscopic world would have been impossible. Even for the macroscopic world, for which SR and GR are more applicable, some degree of freedom is witnessed in modifications of SR, include doubly special relativity (DSR) [2-4] and the "variable speed of light" (or VSL) theories [5-8]. In DSR not only the velocity of light, but also the maximum energy scale and minimum length scale (the Planck energy and Planck length) are observer-independent. In VSL theories the pillar of special relativity (constancy of the speed of light) is removed and in some versions a hard breaking of Lorentz symmetry is allowed.

In deriving his SR and GR [9], Albert Einstein adopted an ontological approach in his interpretation of the notion of relativity. For him, relativity is a real phenomenon. The famous time dilation effect is real. Stationary clocks with respect to an observer are predicted to run faster than moving clocks. The same ontological interpretation applies to the predicted distance (Lorentz) contraction, and mass increase, with increase in velocity. Modifications of the original theories, including DSR and VSL share the same ontological view of relativity. In the proposed theory, which we term *Information Relativity theory*, we take a completely different approach by proposing an epistemic interpretation of relativity. In our approach relativity is not an ontic, true state of nature, but an epistemic difference in the measurements taken by two or more observers, in relative motion with respect to each other, about some observable physical entity.

The basic idea behind the theory is extremely simple. Consider the case where information from a "moving" body of mass, is transmitted to a "stationary" observer by light signals. Assume that the start and end of an event on the body's reference frame, are indicated by two signals sent from the body's "moving" reference frame to the "stationary" observer. Since the light velocity is finite, the two signals will arrive to the observer's reference-frame in delays, which are determined by the distances between the body and the observer, at the time when each signal was transmitted. Suppose that the "moving" body is *distancing* from the observer. In this case the termination signal will travel a *longer* distance than the start signal. Thus the observer will measure a *longer* event duration than the event duration at the body's reference-frame (time dilation). For *approaching* bodies, the termination signal will travel a *shorter* distance than the start signal. Thus, the observer will measure a *shorter* event duration than the event duration at the body's reference-frame (time contraction). It is obvious from the above description that *no synchronization of the clocks at the two reference-frames is required*.

In fact, Information Relativity theory is nothing more than "relativizing" Newtonian physics, accomplished by taking into account the time travel of information from one reference frame to another. The theory has no constraints formulated as axioms (e.g., constancy of c), nor hypothetical constructs (e.g., spacetime). The theory is also local and realistic, and all its elements are observable physical entities. It departs from classical physics only in the minimal "adjustment" described above.

We shall demonstrate hereafter that despite its unprecedented simplicity, Information Relativity is successful in unifying quantum mechanics and cosmology. By treating the dynamics at cosmic scales, in the same manner we treat the dynamics of small particles, we shall throw a new light on the mysteries of dark matter and dark energy. In the following section we shall present the

formal derivation of the theory's transformations of time interval, length, mass, and energy, relating measurements transmitted by the information sender, to the corresponding information registered by the receiver. In section 3 we shall summarize the main features and predictions of the theory; in section 4 we use the theory to prediction the seminal Michelson-Morley's "null" result, and the time dilation of decaying muons; in section 5 we use the theory to derive a theoretical expression for the Sagnac effect; in section 6 we show that the theory predicts with precision the values of $\frac{v-c}{c}$ reported by OPERA and other collaborations; in section 7 we explain why the theory cannot be forbidden by Bell's theorem, and apply it to predict and explain several key quantum phenomena, including entanglement, particles' diffraction in the double-slit experiment, and the quantization of orbits of hydrogen atom problem; in section 8 we use the theory to construct a new quantum cosmology, and utilize it to several important predictions, and to infer about the nature of dark matter and dark energy, which the theory interprets as quantum matter and matter's dual-wave energy as cosmic scales. We also use the cosmological version of the theory to predict the mass of the Higgs boson and the time-line of evolution of chemical elements. In section 8 we summarize and make a few concluding remarks.

## 2. Derivation of Information Relativity transformations

In this article we limit ourselves to the case of two frames of reference in inertial motion with respect to each other. Thus for simplicity, but without losing generality, all the derivations hereafter are made for a one dimensional space. Generalization to the three dimensional configuration space is technically trivial. Generalization to accelerated systems due to a gravitational or electrostatic force is developed elsewhere [10].

### 2.1 Time duration transformation

We consider a system of two reference frames $F$ and $F'$ distancing from each other with constant velocity $v$. For the sake of simplicity, but without loss of generality, assume that the observers in $F$ and $F'$ synchronizes their clocks, just when they start distancing from each other, such that $t_1 = t_1' = 0$, and that at time zero the points of origin of $F$ and $F'$ were coincided (*i.e.*, $x_1 = x_1' = 0$). Suppose that at time zero in the two frames, an experiment started in $F'$at the point of origin, terminating exactly $\Delta t'$ seconds according to the clock stationed in $F'$, and that promptly with the termination of the experiment, a signal is sent by the observer in $F'$ to the observer in $F$. The "experiment" can be any event at the origin with duration of $\Delta t'$ (as measured in $F'$).

After $\Delta t'$ seconds, the point at which the event took place stays stationary with respect $F'$ (i.e., $x_2' = x_1' = 0$), while relative to frame $F$ this point would have departed by $x_2$ equaling:

$$x_2 = v\,\Delta t' \tag{1}$$

Notably, in eq. 1 the left side includes a measurement of distance taken in $F$, while the right side includes a measurement of time duration taken in $F'$. The validity of equation could be verified by an experimentally feasible method. As example, if the observer in $F$ conducts an identical experiment, to the experiment conducted in $F'$. Because the laws of physics are the same everywhere, he or she will conclude that when the event at $F'$ has terminated, $F'$ was at a distance of $x_2 = v\,\Delta t'$ away as measure in $F$.

If the information carrier sent from the observer in $F'$ to the observer in $F$ traveled with velocity $V_F$ relative to $F$, then it will be received by the observer in $F$ after a delay of:

$$t_d = \frac{x_2}{V_F} = \frac{v\,\Delta t'}{V_F} = \frac{v}{V_F}\,\Delta t' \tag{2}$$

Since $F'$ is distancing from $F$ with velocity $v$, we can write:

$$V_F = V_0 - v \tag{3}$$

Where $V_0$ denotes the information carrier's velocity in the light-source rest frame ($F'$). Substituting the value of $V_F$ from eq. 3 in eq. 2, we obtain:

$$t_d = \frac{v\,\Delta t'}{V_0 - v} = \frac{1}{\frac{V_0}{v} - 1}\,\Delta t' \tag{4}$$

Due to the information time-delay, the event's time duration $\Delta t$ that will be registered by the observer in $F$ will be:

$$\Delta t = \Delta t' + t_d = \Delta t' + \frac{1}{\frac{V_0}{v} - 1}\,\Delta t' = \left(1 + \frac{1}{\frac{V_0}{v} - 1}\right)\Delta t' = \left(\frac{\frac{V_0}{v}}{\frac{V_0}{v} - 1}\right) = \left(\frac{1}{1 - \frac{v}{V_0}}\right)\Delta t' \tag{5}$$

Denoting $\frac{v}{V_0}$ by $\beta$ eq. 5 becomes:

$$\frac{\Delta t}{\Delta t'} = \frac{1}{1 - \beta} \tag{6}$$

For $\beta << (v << V_0)$ eq. 6 reduces to the classical Newtonian equation $\Delta t = \Delta t'$, while for $\beta \to 1$ $(v \to V_0)$, $\Delta t \to \infty$ for all positive $\Delta t'$.

For a communication medium to be fit for transmitting information between frames in relative motion, a justifiable condition is to require that the velocity of the carrier is larger than the velocity of the relative motion, i. e. $|\beta| < 1$.

Before proceeding to the more technical part of this article, some remarks regarding eq. 1 are in order:

1. In the derivation of eq. 6 (to be detailed hereafter) synchronization between clocks is unnecessary. The time interval $\Delta t'$ is equal to $t'_2$ - $t'_1$, where $t'_1$ and $t'_2$ are respectively the start and end time of the event, as measured by a clock stationed on the event's rest-frame. On the other hand, the observer on the other frame will calculate the time interval $\Delta t$ as being equal to $t_2$ - $t_1$, where $t_1$ and $t_2$ are the readings of a clock stationed on the observer's frame of the arrivals of the signals indicating the start, and the end of the same event, respectively. There is no requirement for synchronization between the two clocks, as long as the two are identical clocks that tick at the same rate.

2. Evidently, eq. 6's prediction disobeys the Lorentz invariance principle. It is asymmetric with respect to the direction of the transverse velocity vector, predicting time dilation for distancing frames and time contraction for approaching frames. Most physicists view Lorentz's symmetry principle as the corner-stone of current physics. We argue that such view is unfounded. First and foremost, numerous experiments and astronomical observations attest to the possibility of Lorentz invariance breaking (cf. [11-17]), particularly in the high energy sector (cf. [18-19]). Second, despite the continued efforts for unification between Einstein's relativity and quantum theory, it is well-known that quantum mechanics contradicts with not only with Lorentz's invariance, and the subsequent Special Relativity's Lorentz factor and Lorentz contraction [20-21], but also with the fundamental assumption of local-realism [22-24]. The quantum phenomenon which presents the contradiction between Special Relativity and quantum theory and experimental results in a most profound way is the phenomenon of quantum entanglement [25-26]. Recent experimental tests of Bell's theorem provide convincing evidence that information between two entangled particles passed faster than light [27-30].

3. Note that eq. 6, derived for the time travel of moving bodies with constant velocity, is quite similar to the Doppler Effect formula [31-32], derived for the wave-length (frequency) of waves emitted from traveling bodies. In both cases *the direction of motion matters*. In the Doppler effect a wave emitted from a distancing body will be red-shifted (longer wavelength), whereas a wave emitted from an approaching body with be blues-shifted (shorter wavelength). In both cases the degree of red or blue shift will be positively correlated with the body's velocity. The same applies to the time duration of an event occurring at a stationary point of a moving frame. If the frame is distancing from the observer, time will be dilated, whereas if the frame is approaching the observer will contract. Interestingly, while eq. 6 predicts that the time dilation for distancing bodies approaches infinity when $\beta \rightarrow 1$, it puts a testable theoretical limit on the time contraction to for approaching bodies, since for $\beta \rightarrow -1$, it predicts a time contraction of exactly $\frac{1}{2}$.

4. It is especially important to note that the above derived transformation applies to *all* carriers of information, including *acoustic*, *optic*, etc. For the case in which information is carried by light or by electromagnetic waves with equal velocity, we have $\beta = \frac{v}{c}$, where *c* is the velocity of light in the light-source rest frame.

**2.2 Relativity of length**

To derive the distance transformation, consider the two reference-frames $F$ and $F'$ discussed above. Without loss of generality assume as before that when $F$ and $F'$ start distancing from each other $t_1 = t_1' = 0$, and $x_1 = x_1' = 0$. Assume further that $F'$ has onboard a rod placed along its $x'$ axis between the points $x' = 0$ and $x' = x_2'$ (see Figure 1) and that the observer in $F'$ uses his clock to measure the length of the rod (in its rest frame) and communicates his measurement to the observer in *F*. As before, assume that the information carrier from frame $F'$ to frame $F$ is light or another electromagnetic wave with velocity *c* (as measured in the light source rest frame). To perform the measurement of the rod's length, at $t_1' = t_1 = 0$ a light signal is sent from the rare end of the rod, i.e., from $x' = x_2'$ to the observer at the point of origin $x' = 0$.

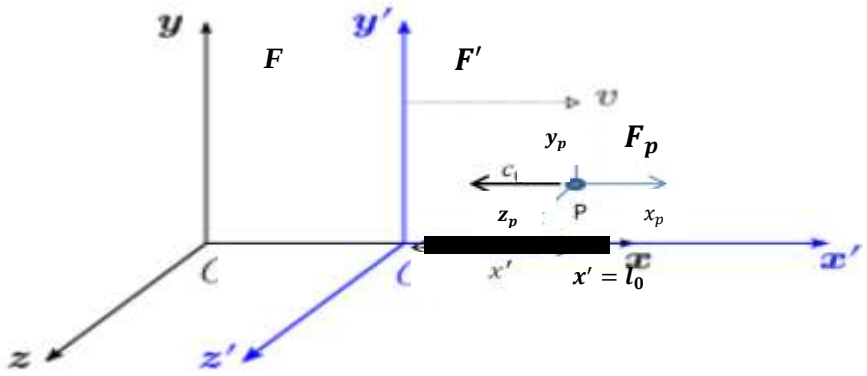


**Figure 1**: Two observers in two reference frames, moving with velocity *v* with respect to each other.

Denote the reference frame of the first light photon by $F_p$ (see Fig 1) and the time duration in $F_p$ for the light photon to arrive the observer in $F'$ by $\Delta t_p$. If the signal arrives to the observer in $F'$ at time $t' = t'_2$, then he or she can calculate the length of the rod as being:

$$l_0 = x'_2 = c\, t'_2 \tag{7}$$

Using eq. 6 $t'_2$ as a function of $\Delta t_p$ can be expressed as:

$$t'_2 = \frac{1}{1-\frac{-v}{c}}\,\Delta t_p = \frac{1}{1+\frac{v}{c}}\,\Delta t_p \tag{8}$$

Which could be rewritten as:

$$\Delta t_p = (1 + \frac{v}{c})\, t'_2 \tag{9}$$

Because $F'$ is departing $F$ with velocity *v*, the light signal reach and observer in $F$ at time $t_2$ equaling:

$$t_2 = \Delta t_p + \frac{v t_2}{c} = \Delta t_p + \frac{v}{c}\, t_2 \tag{10}$$

Substituting the value of $\Delta t_p$ from eq. 9 in eq. 10 yields:

$$t_2 = (1 + \frac{v}{c})\, t'_2 + \frac{v}{c}\, t_2, \tag{11}$$

Which could be rewritten as:

$$t_2 = \frac{(1+\frac{v}{c})}{(1-\frac{v}{c})}\, t'_2 \tag{12}$$

Substituting the value of $t'_2$ from eq. 7 we get:

$$t_2 = \frac{(1+\frac{v}{c})}{(1-\frac{v}{c})}\frac{l_0}{c} \quad (13)$$

Thus, the observer in *F* will conclude that the length of the rod is equal to:

$$l = \mathrm{c}\ t_2 = \frac{(1+\frac{v}{c})}{(1-\frac{v}{c})}\ l_0 \quad (14)$$

Or:

$$\frac{l}{l_0} = \frac{1+\beta}{1-\beta} \quad (15)$$

Where $\beta = \frac{v}{c}$.

The above derived relativistic distance equation predicts *distance contraction only when the two reference-frames approach each other*. On the other hand, in contradiction of the famous Lorentz contraction, for distancing frames eq. 15 predicts *length extension*.

The theoretical corollaries of the predicted length extension cannot be exaggerated. As it opens the door for a plausible unification between the physics of relativity and quantum mechanics.

will incur a relativistic "stretch". This means that at sufficiently high $\beta$, two particles, although distanced from each other, could remain spatially connected. We briefly note that the relationship between relativistic length and time could be easily derived from equation 6 and 15 yielding:

$$\frac{l}{l_0} = 2\frac{\Delta t}{\Delta t_0} - 1 \quad \ldots. (16)$$

Figure 2 depicts the relativistic time and distance as a function of $\beta$. As examples, for $\beta = \frac{1}{4}, \frac{1}{3}, \frac{1}{2}, \frac{2}{3}, \frac{3}{4}$, for $\frac{\Delta t}{\Delta t_0}$ and $\frac{l}{l_0}$ we get $\frac{4}{3}$ , $\frac{3}{2}$, 2, , 3, 4, and $\frac{5}{3}$, 2, 3, 5, 7, respectively.

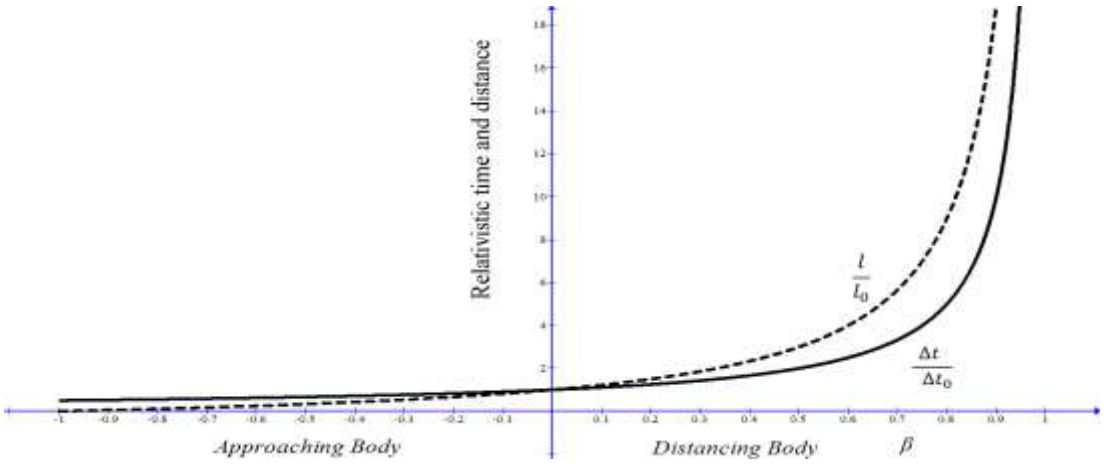


**Figure2**: Relativistic time and distance as a function of $\beta$

### 2.3 Mass and kinetic energy transformations

Let us assume that that the rod has a total rest-mass $m_0$ distributed uniformly along the *x* axis. According to eq. 15 an approaching rod will contract causing the mass density along the x axis to increase. On the other hand, a distancing rod will extend causing its mass density along the x axis to dilute. Denote the body's density in its rest-frame by $\rho'$, then its mass density distribution will be given by $\rho' = \frac{m_0}{A\, l_0}$, where *A* is the area of the body's cross section, perpendicular to the direction of movement. In *F* the density is given by: $\rho = \frac{m_0}{Al}$, where *l* is the object's length in *F*. Using the distance transformation (eq. 15) we can write:

$$\rho = \frac{m_0}{Al} = \frac{m_0}{A\ l_0\ (\frac{1+\beta}{1-\beta})} = \frac{1-\beta}{1+\beta}\,\rho_0 \tag{17}$$

Or,

$$\frac{\rho}{\rho_0} = \frac{1}{l/l_0} = \frac{1-\beta}{1+\beta} \tag{18}$$

As could be seen from eq. 18 the relativistic mass density is inversely proportional to the distance transformation. It is predicted to increase for approaching bodies and a decrease for distancing bodies. The relativistic kinetic energy density is given by:

$$e_k = \frac{1}{2}\rho\, v^2 = \frac{1}{2}\rho_0\, c^2\ \frac{(1-\beta)}{(1+\beta)}\,\beta^2 = e_0\,\frac{(1-\beta)}{(1+\beta)}\,\beta^2 \tag{19}$$

Where $e_0 = \frac{1}{2}\rho_0\, c^2$. For $\beta \to 0$ (or $v << c$) eq. 18 reduces to $\rho = \rho_0$ and eq. 19 reduces to $e_k = \frac{1}{2}\rho_0\, v^2$, which are the classical Newtonian expressions.

As shown by Figure 3 the relativistic kinetic energy density for *approaching* bodies is predicted to increase with *β,* up to infinitely high density values as $\beta \to -1$.

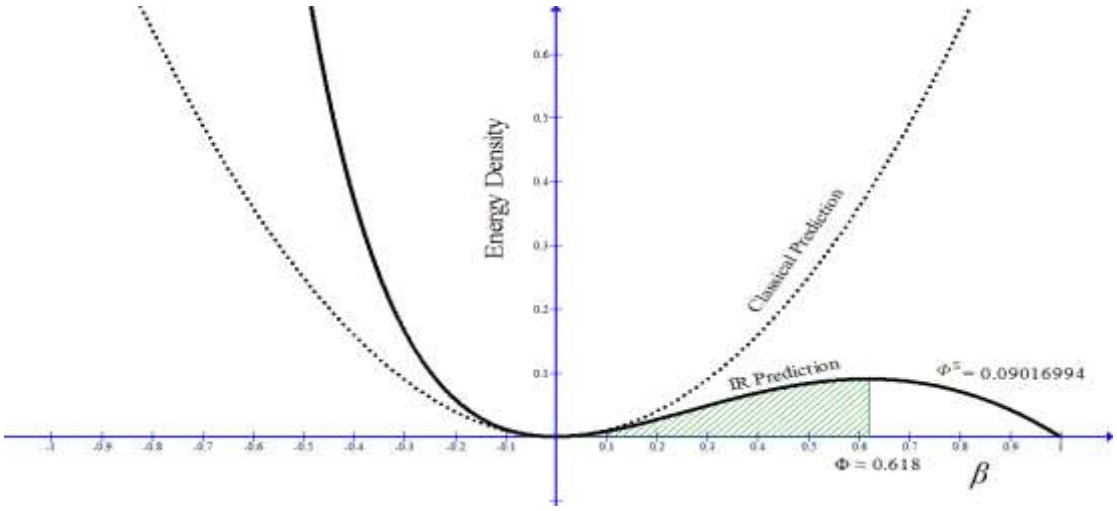


**Figure 3.** Kinetic energy density as a function of velocity

Strikingly, for distancing bodies the kinetic energy displays a non-monotonic behavior. It increases with β up to a maximum at velocity $\beta = \beta_{cr}$ , and then decreases to zero at β = 1. The obtained asymmetry in the kinetic energy density in its dependence on $\beta$ is a natural result of our axiom-free epistemic, in which no symmetry enforcing restrictions were introduced. Nevertheless, emerging type of non-monotonicity is quite astonishing and difficult to anticipate. Before we suggest what we strongly believe is what such behaviors tells, it is helpful to calculating the critical velocity $\beta_{cr}$ at which the kinetic energy density reaches its maximal value. Deriving eq. 19 with respect to $\beta$ and equating the result to zero yields:

$$\beta^2 + \beta - 1 = 0 \tag{20}$$

Which solves for:

$$\beta_{cr} = \frac{\sqrt{5}-1}{2} = \Phi \approx 0.618 \tag{21}$$

Where Φ is the famous Golden Ratio [33-34]. Substituting $\beta_{cr}$ in the energy expression (eq. 19) yields:

$$(e_k)_{max} = e_0 \ \ \Phi^2 \ \frac{1-\Phi}{1+\Phi} \tag{22}$$

From eq. 20 we can write: $\Phi^2 + \Phi - 1 = 0$, which implies $1 - \Phi = \Phi^2$ and $1+ \Phi = \frac{1}{\Phi}$. Substitution in eq. 22 gives:

$$(e_k)_{max} = \Phi^5 \, e_0 \approx 0.09016994 \ e_0 \tag{23}$$

The result above, depicted for the energy term in Fig. 3, are astonishing for more than one aspect. Mathematically, they are beautiful with fascinating Golden Ratio symmetries. Second, they suggest a relativistic interpretation of the phase transition of matter from a normal (baryonic) phase to a quantum phase. According to the suggested explanation, in transverse motion of the type analyzed above, the relativistic matter density of a distancing body is diluted as a function of its distancing velocity (see, eq. 18). For velocities below the Golden ratio ($\beta < \Phi$) the kinetic energy carried by the matter displays a semi-classical behavior, in the sense that an increase in the bodies velocity cause an increase in its kinetic energy, although considerably less than what would be predicted by Newton's quadratic relationship (see Fig. 3). However, a dramatic transition in the distancing matter dynamics is predicted for distancing velocities exceeding the Golden ratio. We propose that the point of transition discovered by our relativistic approach is the point of quantum transition. A strong support for our conjecture comes from a recent *Science* article [35] reporting that applying a magnetic field at right angles to an aligned chain of cobalt niobate atoms, makes the cobalt enter a quantum critical state, in which the ratio between the frequencies of the first two notes of the resonance equals the Golden Ratio. Another support for our conjecture is the fact the maximal kinetic energy at the point of phase transition is

proportional to $\Phi^5 \approx 0.09016994$, which equals to the eighth decimal digit to Hardy's maximum probability of obtaining an event which contradicts local realism [36].

**2.4 Matter-wave duality**

Another conjecture, inspired by de Broglie-Bohm model of matter-wave duality (e.g., [37-41]), is that the "relativistic loss" in kinetic energy is carried by the matter's dual-wave. To further investigate our conjecture, subtracting the relativistic term in eq. 19 from the nonrelativistic (Newtonian) term: $e_N = \frac{1}{2}\rho_0 v^2 = \frac{1}{2}\rho_0 v_c^2 \beta^2$, yielding:

$$e_w = e_N - e_k = \frac{1}{2}\rho_0 v_c^2 \beta^2 - \frac{1}{2}\rho_0 v_c^2 \frac{1-\beta}{1+\beta}\beta^2 = \left(\frac{1}{2}\rho_0 v_c^2\right)\frac{2\beta^3}{1+\beta} = \frac{2\beta^3}{1+\beta} e_0 \quad (24)$$

Where $e_0 = \frac{1}{2}\rho_0 v_c^2$.

In agreement with de Broglie's model, for bodies distancing with a fixed velocity β the matter and wave energies are predicted to be in a state of equilibrium. As shown in Figure 4, the predicted wave-energy density component increases rapidly with velocity. At relatively low velocities, the bulk of the particle's energy is carried by its matter. The energy carried by matter, and the energy carried by the wave, are predicted to be equal precisely at $\beta = \frac{1}{3}$, corresponding to a stretch equaling $\frac{l}{l_0} = \frac{1+\frac{1}{3}}{1-\frac{1}{3}} = 2$. For higher velocities, the matter density becomes very dilute and the accompanying wave becomes the primary carrier of the total energy. Surprisingly, at velocity $\beta_{cr} = \Phi \approx 0.618$ at which a distancing body undertakes a phase transition, seizing to behave classically, the value of the kinetic energy density reaches its maximum and this maximum is exactly equal to $\Phi^5 e_0$, which amounts to $\approx 0.09016994\ e_0$. The amount of the wave energy density at this critical point is equal to $\frac{2\Phi^3}{1+\Phi} = 2\Phi^4 \approx 0.29179607$. These results are striking given the role played by this type of symmetry, in nature, technology and the arts, including in the structure of plants [42-44], physics [35, 45-47], structure of the human brain [48], music [49-50], aesthetics [51], social sciences [52-53], and more.

**3. Information Relativity theory's main features**

The main transformations of the theory are depicted in Table 1. In the equations $\beta = \frac{v}{v_c}$, where $v$ is the relative velocity between the moving body and the observer, $v_c$ is the velocity of the information carrier, and $e_0 = \frac{1}{2} m_0 v_c^2$. As could be seen in Table 1 and Figure 1, the theory transformations are simple and beautiful, two qualities that are believed to be important features of good theories (cf. [54]).

Inspection of the table reveals that Information Relativity has four unique predictions, which distinguish it from all other relativity theories: 1. The time interval transformation is asymmetric in its dependence on the relative velocity (see eq.1), predicting time dilation for distancing bodies, and time contraction for approaching bodies. 2. The length and mass density transformations are also asymmetric with velocity, predicting length extension (and mass density dilution) for distancing bodies, and length contraction (mass density increase) for

approaching bodies. 3. The kinetic energy density for distancing bodies exhibits a non-monotonous dependence on velocity, with a unique maximum (see Fig. 4), and 4. A relativistic dual wave is predicted to emerge (see eq. 24 and Figures 4a & 4b). As shown in the figures, for any given velocity, the total energy of a distancing body is predicted to be carried jointly by the corpuscle, and its and pilot wave. At relatively low velocities, most of the body's energy is normal energy, carried by the corpuscle, while at very high velocities, most of the body's energy is carried by its pilot wave. Interestingly, at a recession velocity $\beta = \frac{1}{3}$ the energy densities of the corpuscle, and its pilot wave, are predicted to be equal.

**Table 1**
**Information relativity main transformations for inertial translational motion**

| **Variable** | **Mathematical expression** | **Main properties** |
|---|---|---|
| Time interval | $\frac{1}{1-\beta}$ (I) | Contraction for approaching bodies. Increase for distancing bodies; |
| Length $\frac{l}{l_0}$ | $\frac{1+\beta}{1-\beta}$ (II) | Contraction for approaching bodies; Extension for distancing bodies. |
| Mass density $\frac{\rho}{\rho_0}$ | $\frac{1-\beta}{1+\beta}$ (III) | Increases with $\beta$ for approaching bodies; Decreases for distancing bodies. |
| Kinetic energy density $\frac{e_k}{e_0}$ | $\frac{1-\beta}{1+\beta}\beta^2$ (IV) | Increases with $\beta$ for approaching bodies; non-monotonous for distancing bodies, with maximum equaling $\Phi^5$ at $\beta = \Phi \approx 0.618$ . |
| Wave energy density $\frac{e_w}{e_0}$ | $\frac{2\,\beta^3}{1+\beta}$ (V) | Increases with $\beta$ for distancing bodies. For $\beta < \frac{1}{3}$, $e_w < e_k$ ; For $\beta = \frac{1}{3}$, $e_w = e_k$, and for $\beta > \frac{1}{3}$ $e_w > e_k$. |

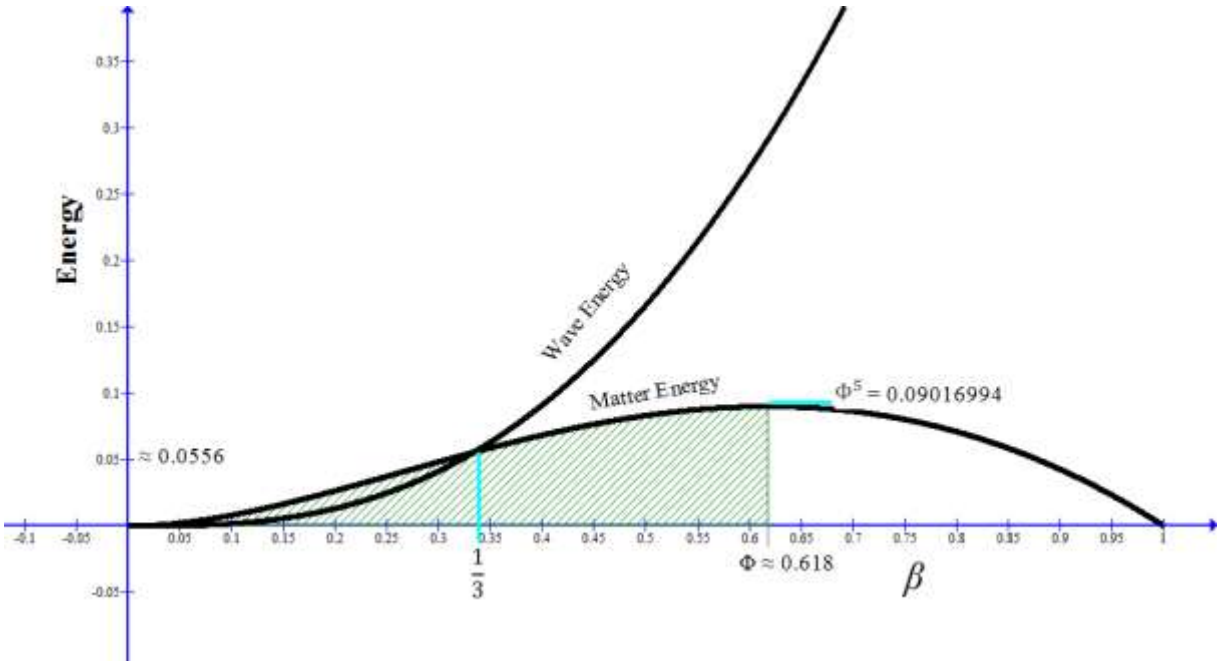


**Figure 4a.** Matter and dual wave energy densities for a distancing body as functions of velocity

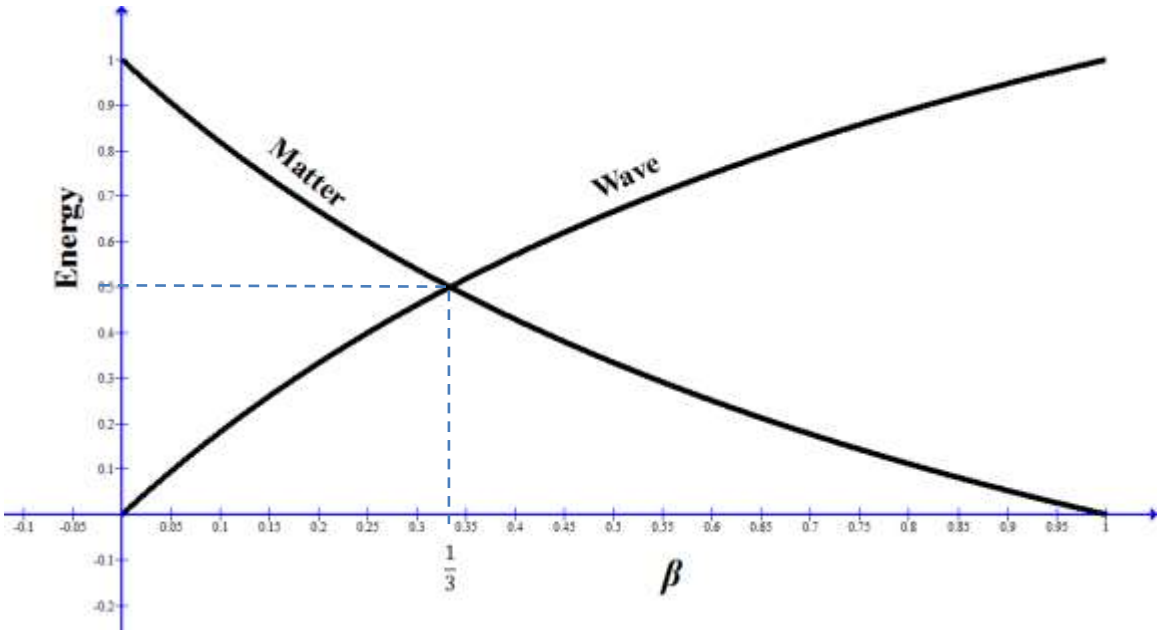


**Figure 4b.** The ratios of matter and wave energy densities out of the total energy, as functions of velocity

Two subtle, but extremely important features of the theory, enables its application to ALL physical systems:

First, since in the derivation of the theory transformation we did not restrict ourselves to light or another electromagnetic wave as the information carrier, all the transformations depicted in Table 1 should apply to classical systems, such as thermodynamic, acoustic, and seismic systems. The only requirement for applying the theory to a physical system that the velocity of the information carrier in the system must be higher than the relative velocity (i. e. , $v_c > v$).

Second, and no less important, Information Relativity theory applies to all moving bodies, regardless of their mass or spatial dimension. The logic behind this inference is straightforward: Since in the mathematical derivation of the equations we did not put any constraints on the body's rest mass density and length ($\rho_0$ and $l_0$), the derived equations should be applicable to all masses and all lengths. In fact, any other inference would contradict the basic principles of logic and mathematics. In section 8.1 we explain why Information Relativity is not forbidden by Bell's theorem [22-24] from predicting quantum phenomena, and in sections 8.2-8.5 we demonstrate it predictions and explanations of a sample of quantum phenomena, including quantum phase transition, entanglement, and the diffraction of particles in the double-slit experiment.

Since we claim that Information Relativity is universal, applying to all physical systems, the transformations depicted in Table 1, should to all physical systems, irrespective of mass and size. In what follows we demonstrate the universality of the theory by deriving predictions and proposing explanations to of microscopic and macroscopic phenomena.

## 4. Prediction of seminal relativistic results

### 4.1 Michelson-Morley's "null" result

Whether Einstein was motivated by the seminal Michelson -Morley's "null" experiment [55] or not, the success of special relativity theory in accounting for the experiments results is many times spoken of as a turning point in the history of physics, from Galileo-Newton's ether physics, in which time was considered absolute, to the non-classical, Einstein's relativistic physics. Another famous experiment, which was the first to confirm special relativity's prediction of time dilation is the Frisch and Smith experiment on decaying muons.

For a typical Michelson-Morley's type interferometer, the fringe shift calculated based on Information Relativity theory (for details see [56]) is given by:

$$\Delta x = D_0 \frac{1+\beta^2}{1-\beta^2}\beta^2 \tag{25}$$

Where $\Delta x$ is the fringe Shift, $D_0$ is the interferometer's arm length, $\beta = \frac{v}{c}$, c ≈ 299792.458 $km/_s$, and $v$ is the velocity of Earth around the sun ($v \approx 29.78\ km/_s$).

The comparable prediction provided by Special Relativity is given by $2\,D_0\left(\sqrt{1-\beta^2}\,\beta^2\right)$. Table 2 summarizes experimental results of several M&M type experiments, together with the corresponding predictions of Information Relativity and Special Relativity.

As could be clearly seen in the table, the "null" result is also accounted for by the proposed theory. In fact, the differences between the predictions of the two theories are either zero or in the order of magnitude of $10^{-10}$.

**Table 2**
**Predictions of findings reported by classical Michelson-Morley type experiments**

| Experiment | Arm length (meters) | Expected Fringe shift | Measured Fringe shift | Resolution | ER prediction | SR prediction |
|---|---|---|---|---|---|---|
| Michelson and Morley [55] | 11.0 | 0.4 | $< 0.02$ or $\leq 0.0$ | 0,01 | $\approx 4.34 \times 10^{-}$ | $\approx 4.34 \times 10^{-}$ |
| Miller [57] | 32.0 | 1.12 | $\leq 0.03$ | 0.03 | $\approx 1.27 \times 10^{-}$ | $\approx 1.26 \times 10^{-}$ |
| Tomaschek [58] | 8.6 | 0.3 | $\leq 0.02$ | 0.02 | $\approx 3.40 \times 10^{-}$ | $\approx 3.40 \times 10^{-}$ |
| Illingworth [59] | 2.0 | 0.07 | $\leq 0.0004$ | 0.0004 | $\approx 7.89 \times 10^{-}$ | $\approx 7.90 \times 10^{-}$ |
| Piccard & Stahel [60] | 2.8 | 0.13 | $\leq 0.0003$ | 0.0007 | $\approx 1.11 \times 10^{-7}$ | $\approx 1.11 \times 10^{-7}$ |
| Michelson et al. [61] | 25.9 | 0.9 | $\leq 0.01$ | 0.01 | $\approx 1.02 \times 10^{-}$ | $\approx 1.02 \times 10^{-}$ |
| Joos [62] | 21.0 | 0.75 | $\leq 0.002$ | 0.002 | $\approx 8.30 \times 10^{-}$ | $\approx 8.30 \times 10^{-}$ |

### 4.2 Time dilation of decaying muons

Muons generated when cosmic rays strike the upper levels of the Earth's atmosphere are unstable particles, with a lifetime of $\tau = 2.2\ \mu\ s$. Using counters of muons traveling within a velocity of 0.99450**c** to 0.9954**c**, and comparing their flux densities at different altitudes (e.g., top and bottom of a mountain), reveals that the rate of decay near earth level is much higher than the one resulting from classical calculations (cf., [63-65]). In the renowned muon decay experiment [63], assuming a velocity of 0.992c of muons in air, Frisch and Smith found that the percentage of the surviving muons descending from the top of Mt. Washington to the sea level ($d \approx 1907$ m.) was (72.2 ± 2.1) %, considerably higher than 36.79%, the expected percentage resulting from non-relativistic calculation.

Calculation based on Information Relativity (see details in [56]) shows that the flux density at time *t* on earth is given by:

$$N(t) = N(0)\, e^{-\frac{(1-\beta)t}{\tau}} \tag{26}$$

where $N(0)$ is the count at the mountain's level, $\tau$ is the muon lifetime at its rest-frame and $\beta = \frac{v}{c}$.

For $\beta$ =0.992, Figure 5 depicts the rates of decay predicted by Information Relativity, Special Relativity, and a nonrelativistic calculation. For an ascending time of $\delta t = \frac{d}{v} = \frac{1907\ m.}{2.998\text{x}\ 10^8} \approx 6.36$ μs., the predictions of Epistemic Relativity and Special Relativity are, respectively, $\frac{\mathrm{N}(t=6.36)_{CR}}{\mathrm{N}(0)}$ x 100= $e^{-\frac{(1-0.992)x\ 6.36}{2.2}}$ x 100 ≈ 97.7% and $\frac{\mathrm{N}(t=6.36)_{SR}}{\mathrm{N}(0)}$ x 100 = $e^{-\frac{\sqrt{1-\ 0.992^2}\ x\ 6.36}{2.2}}$ x 100 ≈ 69.42%. By contrast, according to nonrelativistic considerations, the expected percentage of surviving muons is only $\frac{\mathrm{N}(t=6.36)_{NR}}{\mathrm{N}(0)}$ x 100= $e^{-\frac{6.36}{2.2}}$ x 100 ≈ 5.55%.

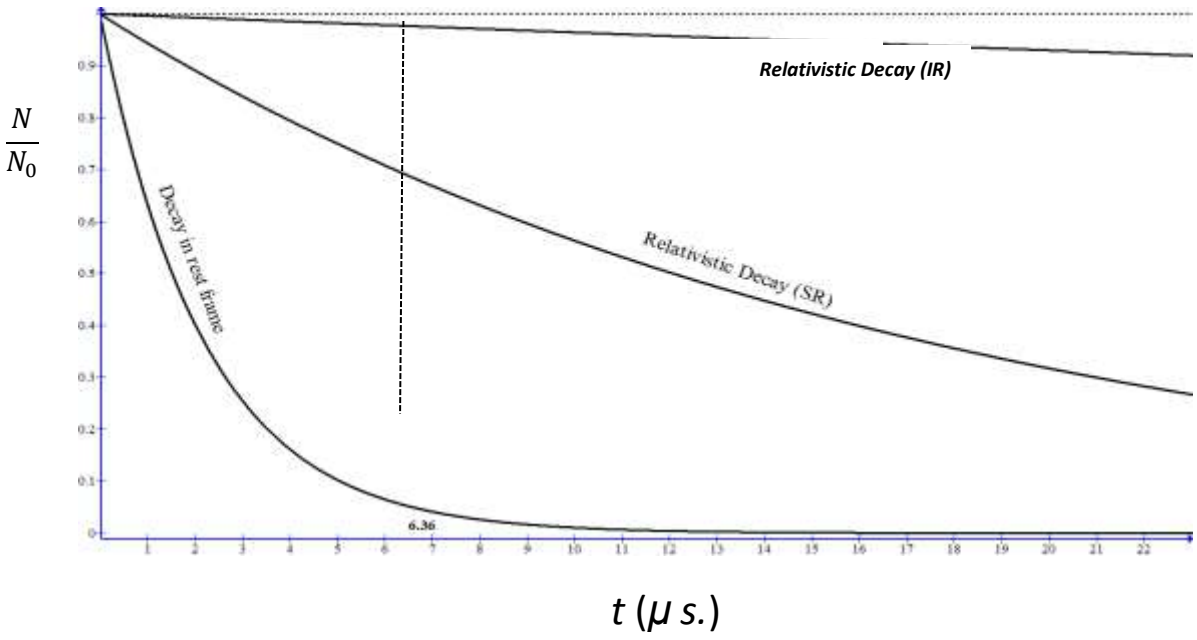


**Figure 2**: Predicted rates of muon decay

## 5. Predicting the Sagnac effect

The Sagnac effect, named after its discoverer in 1913 [66], has been replicated in many experiments (for reviews, see [67-71]). The Sagnac effect has well-known and crucial applications in navigation [67-68, 71] and in fiber-optic gyroscopes (FOGs) [72-76]. In the Sagnac effect, two light beams, sent clockwise and counterclockwise around a closed path on a

rotating disk, take different time intervals to travel the path. For a circular path of radius *R*, the time difference can be represented as $\Delta t = \frac{2\,v\,l}{c^2}$, where $v=\omega R$ and *l* is the circumference of the circle ($l=2\pi R$). Today, FOGs have become highly sensitive detectors measuring rotational motion in navigation. In the GPS system, the speed of light relative to a rotating frame is corrected by $\pm\,\omega\,R$, where $\omega$ is the radial velocity of the rotating frame and *R* is the rotation radius. A plus/minus signs is used depending on whether the rotating frame is approaching the light source or departing from it, respectively.

Many physicists claim that because the Sagnac effect involved a radial motion, it does not contradict SR and that it should be treated in the framework of general relativity [77-78]. However, Wang at al. [79-80] strongly refute this claim in two well-designed experiments that show unambiguously that an identical Sagnac effect appearing in uniform radial motion occurs in linear inertial motion. For example, Wang et al. [79] tested the travel-time difference between two counter-propagating light beams in uniformly moving fiber. Contrary to the LI principle and to the prediction of SR, their findings revealed a travel-time difference of $\frac{2v\,\Delta l}{c^2}$, where $\Delta l$ is the length of the fiber segment moving with the source and detector at a v, whether the segment was moving uniformly or circularly. This finding in itself should have raised serious questions about the validity of the LI principle and SR. If the Sagnac effect can be produced in linear uniform motion, then the claim that it is a characteristic of radial motion is simply incorrect. Because the rules SR apply to linear uniform motion, the only conclusion is that SR is incorrect. Strikingly, the unrefuted detection of a linear Sagnac effect and its diametrical contradiction with SR has hardly been debated.

For the linear Sagnac effect, using the time transformation depicted in eq. 6, the difference between the arrival times of the two light beams is given by:

$$\Delta t = \frac{\Delta l}{c-v} - \frac{\Delta l}{c+v} = \frac{2v\,\Delta l}{(c-v)(c+v)} = \frac{2v\,\Delta l}{c^2-v^2} \approx \frac{2v\,\Delta l}{c^2} \tag{27}$$

Which is in agreement with the analysis and results reported in [79].

## 6. Predicting the neutrino velocities reported by OPERA and other collaborations

Several collaborations, including OPERA have recently reported results indicating that neutrinos velocity is not significantly different from the velocity of light. For example, OPERA [81] reported an early neutrino arrival time of $\delta t = (6{:}5 \pm 7.4\,(\text{stat.})\,^{+8.3}_{-8.0}\,(\text{sys.}))$ ns. The corresponding relative difference of the muon neutrino velocity and the speed of light is:
$\frac{v-c}{c} = (2.7 \pm 3.1\,(\text{stat.}) + ^{+3.8}_{-2.8}\,(\text{sys.})) \times 10^{-6}$. A similar "null" result was also reported by other collaborations, including ICARUS, LVD, and Borexino [82-85].

In two recent papers [86-87] we demonstrated that Information Relativity yields precise point prediction of the $\frac{v-c}{c}$ values reported in all the aforementioned experiments. In the framework of Information Relativity, contrary to Special Relativity, the direction of motion matters (see eq. 6). Thus, the neutrino source and detector are treated in the theory as being stationed in two different

reference frames. For a typical neutrino-velocity experiment, our analysis (see [87]) yielded a value of $\frac{v-c}{c}$ equaling:

$$\frac{v-c}{c} = \sqrt[2]{\frac{2}{1-\frac{c\ \delta t}{d}} - 1} - 1 \tag{28}$$

Where $d$ is the travel distance. $\delta t$ is the early neutrino arrival time with respect to the velocity of light c. For the OPERA experiment [81], substituting $d$ = 730.085 km, and $\delta t$ = 6.5 n. s. yields:

$$\frac{v-c}{c} = \left(\frac{2}{1-\frac{299792.458\ x\ 6.5\ x\ 10^{-9}}{730.085}} - 1\right)^{\frac{1}{2}} - 1 \approx 2.67 \text{ x } 10^{-6} \tag{29}$$

Which is almost identical to the reported result of $\frac{v-c}{c}$ $(Exp.)$ = (2.7 ± 3.1 $(stat.)$ $\pm^{+3.8}_{-2.8}$ (sys.)) $\times 10^{-6}$. Applying eq. 28 to the experiments cited above by OPERA, ICARUS, LVD, and Borexino collaborations, yielded the results summarized in Table 3.

**Table 3**
**Predictions of ER for six neutrino-velocity experiments**

| **Experiment** | **Experimental** $\frac{v-c}{c}$ | **Predicted** $\frac{v-c}{c}$ |
|---|---|---|
| OPERA 2012 (corrected result) [81] | **(2.7 ± 3.1 (stat.) $+^{+3.8}_{-2.8}$ (sys.)) ×10$^{-6}$** | **2.67 x 10 $^{-6}$** |
| OPERA 2013 [82] | **(- 0.7 ± 0.5 (stat.) $+^{+2.5}_{-1.5}$ (sys.)) ×10$^{-6}$** | **- 0.66 x 10$^{-6}$** |
| ICARUS 2012 [83] | **(0.4 ± 2.8(stat.) ± 9.8 (sys.)) ×10$^{-7}$** | **0.41 x 10$^{-7}$** |
| LVD [84] | **(1.2 ± 2.5(stat.) ± 13.2 (sys.)) ×10$^{-7}$** | **1.23 x 10$^{-7}$** |
| Borexino [85] | **(3.3 ± 2.9(stat.) ± 11.9 (sys.)) ×10$^{-7}$** | **3.28 x 10$^{-7}$** |

As the table shows, the theory yields precise predictions for all the tested experiments. Since Information Relativity contradicts both Special Relativity and the Lorentz invariance principle, by asserting that the direction of relative motion matters, the success of Information Relativity in predicting all the above discussed results, is yet another indication of their inadequacy as physical laws.

## 7. Explaining quantum mechanics

For more important, since Information Relativity theory is scale independent, it hold the promise of a unified physics of everything. We shall demonstrate convincingly enough, not only that the proposed theory is successful in explaining and predicting various quantum phenomena, it also opens the door for a new quantum cosmology, according to which cosmological entities, such as dark matter, and cosmological phenomena, such as the well-known GZK cutoff redshift, are in fact quantum entities and phenomena at the cosmic scale.

Two main properties enable the application of Information Relativity to quantum phenomena: 1. The emergence of a matter dual-wave, discussed in section 2.4 (see figures 4a and 4b). 2. The predicted extension of distancing bodies. In the following section we explain why the second property enables Information Relativity to bypass Bell's theorem, and in the following sections we demonstrate the validity of our claim by reproducing some of the main predictions of quantum theory.

### 7.1 Bypassing Bell's inequality

Before proceeding to explain quantum mechanical phenomena, we must justify why our endeavor is not blocked by the impossibility asserted by Bell's inequality, by forbidding any local realistic theory from reproducing the predictions of quantum theory. In a recent paper [88], we showed that, despite being local-realistic Information Theory cannot be forbidden by Bell's theorem. The argument supporting our conclusion is simple: As evident from eq. 2 in Table 1, given a sufficiently high velocity $\beta$, a distancing particle from an observer's rest-frame, will extend enough to keep the particle at spatial proximity with the observer's rest frame. Thus, even when locality in time is eliminated, locality in configuration space could be maintained. This type of locality, which we term "spatial locality", was not considered previously, most probably due to the firm belief in the Lorentz contraction effect, a prediction of SR which in fact has never been established experimentally.

### 7.2 Quantum phase transition and quantum criticality

Quantum phase transition point [89-90] is explained by the theory as the point at which matter departs qualitatively in it dynamical behavior from a classical or quasi-classical behavior. For an inertial system, like the one discussed here, the point of quantum criticality is the aesthetically appealing Golden Ratio, $\varphi \approx 0.618$ (see Fig. 4a). The corresponding maximal matter energy density at $\beta = \varphi \approx 0.618$ is equal to $\varphi^5 \approx 0.09016994\ e_0$, where $e_0 = \frac{1}{2} m_0 c^2$.

### 7.3 Entanglement

For an EPR bipartite system comprised of two identical particles moving away from each other [91], the argument given in section 4.2.1 implies that given enough velocity, the two particles could maintain spatial locality, even when the particles have distanced enough to eliminate the possibility of temporal (not faster than light) locality. In [92] we found that the cross correlation between the energy densities of two particles A and B, distancing from each other with velocity $\beta$ is given by:

$$r(\hat{l}) = e_A * e_B = \int_{\hat{l}\geq 1} e_k(\xi)\, e_0(\xi + \hat{l})\, d\hat{l} = ln\left(\frac{\hat{l}+1}{\hat{l}}\right) - \frac{4}{(\hat{l}+1)(\hat{l}+2)} \qquad (30)$$

Where $\hat{l} = \frac{l}{l_0}$, is the relative "stretch" (given by eq. 15) of particle A in the rest-frame of particle B (see or vice versa). Figure y depicts $r(\hat{l})$ as a function of $\hat{l}$. The unique maximum appearing in the figure is found by derivation with respect to $\hat{l}$, to be the solution of the following polynomial:

$$\hat{l}^3 - 3\,\hat{l}^2 - 4\,\hat{l} + 4 = 0 \qquad (31)$$

Which for $\hat{l} \geq 1$ solves at $\hat{l} \approx 3.7785$, corresponding to a maximum cross correlation of $r_{max} \approx 0.08994$ (see Figure 5).

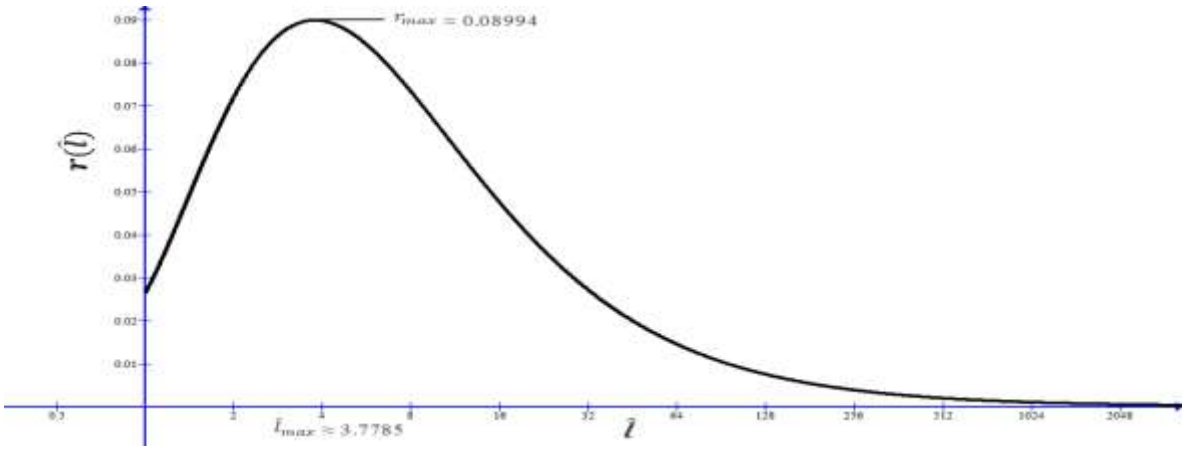


The energies' functions cross-correlation in terms of the distancing velocity β is depicted in Figure 6. As shown in the figure, maximum correlation is predicted to occur at a distancing velocity of $\beta \approx 0.58145$.

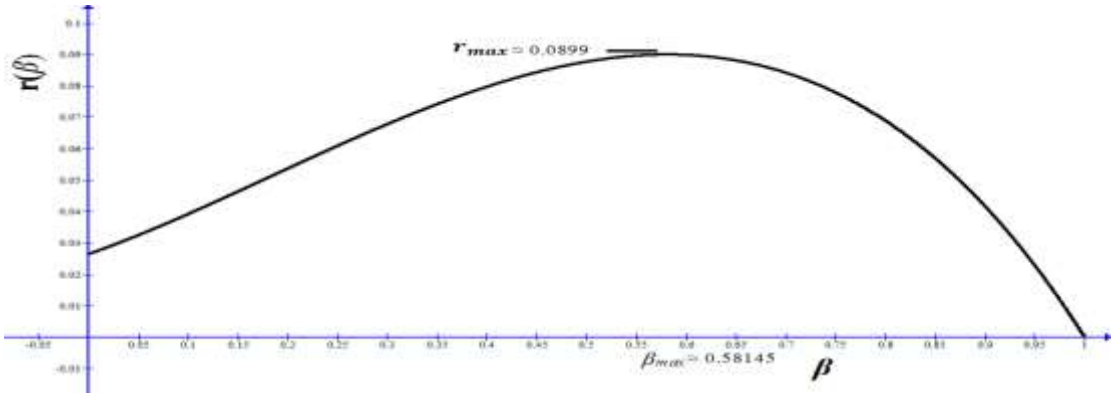


**Figure 6.** The cross-correlation between the energies of two distancing particles as a function of their distancing velocity $\beta$

### 7.4 Diffraction of particles in the double-slit experiment

The wave-like diffraction of corpuscles in Young's double-slit experiment has been demonstrated many times, using photons, electrons, neutrons, atoms, and molecules [93-100]. Nonetheless, it continues to be an unsolved mystery. Richard Feynman, who was very fond of the diffraction of particles in the double-slit experiment, called it: "a phenomenon which is impossible, absolutely impossible, to explain in any classical way, and which has in it the heart of quantum mechanics. In reality, it contains the only mystery. We cannot make the mystery go away by "explaining" how it works. In telling you how it works, we will have told you about the basic peculiarities of all quantum mechanics" [101]. In a recent article [102] we showed that Feynman's view is incorrect, and that the buildup of a particles' diffraction pattern in the double-slit experiment could be predicted and explained in the framework of Information Relativity theory.

To apply the proposed theory to the double-slit experiment, consider such an experiment in which electrons are fired, one at a time, from an electron gun, towards two open slits in a barrier separating the electron gun from an observation screen. According to Information Relativity, an electron traveling with sufficiently high velocity, will exhibit the particle-wave nature, from the first moment it is fired from the electron gun. In the experimenter's reference-frame, the corpuscular component will "stretch" along its travel path (see eq. 15,). Such predicted "stretch", resonates with Schrödinger's original thoughts, that particles in quantum states become physically "smeared out" over a region in configuration space. The energies carried by the corpuscular electron, and its pilot wave, as a function of the electron velocity, are given by equations 19 and 24, respectively (see also figures 4a & 4b). The corpuscular particle may either hit the barrier and bounce back, or pass through one of the two slits and hit the screen on its upper or lower part, depending on the slit from which it passed through. However, the pilot wave will pass through the *two* slits, generating two secondary waves, which will start propagating in phase from the two slits, while interfering with each other. If the particle passes through, it will be guided by the superposition of the two generated waves. When hitting the observation screen, the particle's velocity will decelerate very rapidly. As a result, the particle will shrink back to its rest-frame dimensions. The energy of the pilot wave will diminish dramatically and vanish (see Fig. 4a). Simultaneously, the corpuscular part will regain the energy lost to the wave, hitting the screen in one point with energy equaling the classical magnitude ($\frac{1}{2} m_0 v^2$). This prediction could be easily verified from equations 4 and 5 for the case $\beta << 1$.

As the reader might notice, the bulk of the above explanation resembles the explanation given by the de Broglie-Bohm theory. However, the proposed explanation does not suffer from the measurement problem. In our explanation, the "collapse" of the wave is a direct result of the corpuscle's collision with the screen, which causes its velocity to decrease sharply, resulting in the transfer of the wave energy to a classical kinetic energy of the corpuscle.

In [102] we derived quantitative predictions for particle's diffraction in the double-slit experiment. Using eq. 24 for the particle's dual wave energy, and the equation $E_w = h f$, where $E_w$ is the wave energy, $f$ is its frequency, and $h$ is the Planck constant ($h \approx 4.135667662\times10^{-15}$eV.s $\approx 6.62607004 \times 10^{-34} J.s$), we found that the wavelength of the particle's dual wave could be expressed in terms of the particle's velocity as:

$$\lambda = \frac{h}{m_0 c} \frac{1+\beta}{\beta^2} \tag{32}$$

Where $m_0$ is the electron rest mass, and $c$ is the velocity of light in the experiment's site with respect to its source. For a constructive interference to appear on the apparatus's observing screen, λ should satisfy the relationship:

$$d \sin\theta = n\lambda \qquad n = 1, 2, 3, \ldots \tag{33}$$

Where $d$ is the distance between the two slits, and $\theta$ is the angle between the orthogonal line connecting the center point between the two slits with the observing screen, and the line connecting the center point between the two slits, with a constructive interference point on the screen. For the far field, the distance between two constructive lines in the fringe pattern could be approximated as:

$$\Delta y \approx \frac{x}{d} \lambda \tag{34}$$

Where $x$ is the distance between the barrier and the observing screen (see Figure 7).

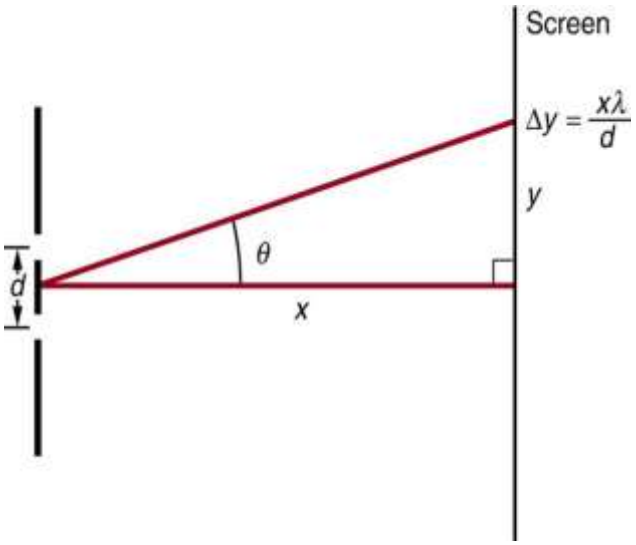


**Figure 7.** A schematic setup of a double-slit experiment.

Substituting the value of λ from eq. 32 in eq. 34 we get:

$$\Delta y \approx \frac{x}{d}\lambda \approx \frac{x}{d}\frac{h}{m_0 c}\frac{1+\beta}{\beta^2} \tag{35}$$

To demonstrate, for electrons, the rest mass is about $9.1 \times 10^{-31}$ *kg*. Thus:

$$\frac{h}{m_0 c} = \frac{6.62607004 \times 10^{-34}}{9.1 \times 10^{-31} \times 299\,792\,458} \approx 2.4293 \times 10^{-12}\ m = 0.024\ \text{Å}. \quad (36)$$

Substitution in eq. 32 gives:

$$\lambda = \frac{h}{m_0 c} \frac{1+\beta}{\beta^2} \approx 0.024 \frac{1+\beta}{\beta^2}\ \text{Å}. \quad (37)$$

Figure 8 depicts the length of the electron's pilot-wave ($\lambda$) a function of its velocity ($\beta$).

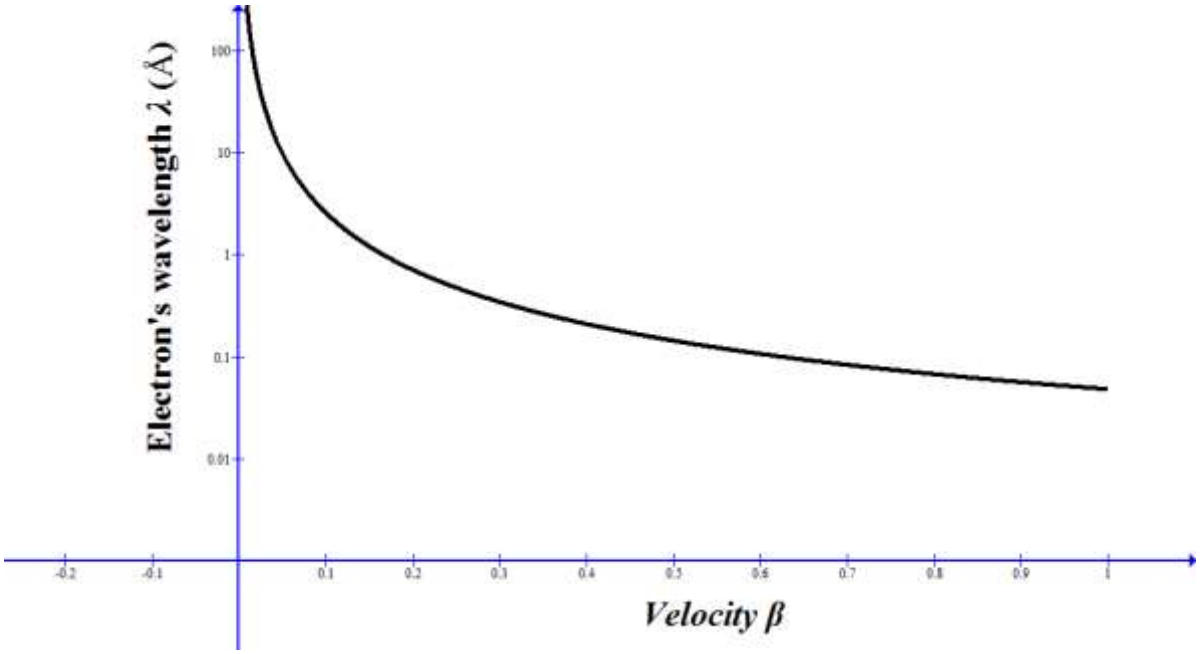


**Figure 8.** The length of the electron's pilot-wave, λ, as a function of the velocity $\beta$

Equation 35 yields two testable predictions: 1. That the fringe width should decrease hyperbolically with the increase in the corpuscle's rest-mass, and 2., that it should decrease even sharper with increase in the corpuscle's velocity.

Qualitative explanations of different variants of the double-slit experiments are also simple and plausible. For which-way experiments [103-105], installing detectors in front of the slits, causes the particle passing through one of the slits to slow down, due to its interaction with the detector. As a result, its velocity will decrease, causing the pilot wave to diminish and practically disappear. Thus, no interference will occur, which is exactly what happens in such experiments. This explanation conforms with the conclusion reached in [106], in which the disappearance of the diffraction pattern in the reported which-way experiment was attributed to correlations between the detector, and the atomic motion, rather than to the uncertainty principle.

In experiments in which the detectors are placed after the barrier, as in Wheeler's delayed choice experiments [107-108], a particle which has passed through one of the slits, will slow down upon

its interaction with the detector, causing its pilot wave to diminish and the interference to disappear.
To summarize, the proposed theories explanation is simple and sensible, with no "mysteries" involved. What goes on in the experimental apparatus of the double slit could be summarized as follows: 1. The corpuscular matter and its pilot wave exist *simultaneously* in the apparatus; 2. Their paths exist as real trajectories in the apparatus; 3. The "observer's effect" is caused by the mechanical interaction between the corpuscle and the measuring devices; 4. The collapse of the (real) wave occurs due to the particle's collision with the observation screen, causing its velocity to decrease rapidly to zero, and the wave to diminish, while giving away all its energy to the corpuscle, which by this restores its classical Newtonian energy.

**7.5 Solving the hydrogen atom problem**

It is well accepted that a satisfactory solution of the hydrogen atom problem, which is compatible with first principles and having first principles as the basis of quantization was never found [109] The classical model of the hydrogen atom proposed by Niels Bohr was in fact a straightforward application of Newton's laws of motion and Coulomb's law of electric force. However, the solution is with the electromagnetic theory, which predicts that the orbiting electron will radiate energy in the form of electromagnetic waves, and will eventually loose energy and fall spirally into the nucleus. To overcome this problem Bohr enforced a law of orbits quantization, according to which electron can orbit the nucleus only in specific orbits.

Quantum electrodynamics was proposed by Dirac in 1962 to provide a generalization of quantum mechanics for high energies in conformity with the theory of special relativity and to provide a consistent treatment of the interaction of matter with radiation. Dirac's quantum electrodynamics gave a more consistent derivation of the results of the correspondence principle, but it also brought about a number of new and serious difficulties. (1) It does not explain the non-radiation of bound electrons, (2) It admits solutions of negative rest mass and negative kinetic energy, (3) It leads to infinite kinetic energy and infinite electron mass for the interaction of the electron with the predicted zero-point field fluctuations, and (4) It still yielded infinities when Dirac used the unacceptable states of negative mass for the description of the vacuum [110, 111].

Information Relativity solves the hydrogen atom problem without enforcing quantization of the electron's orbits. For this purpose, we consider a simplified model of the hydrogen atom, in which the electron orbits the proton at the nucleus in a circular orbit (see Figure 9).
The centripetal force which binds the electron to the proton is equal to:

$$F = \frac{m_e v^2}{r} \tag{38}$$

Neglecting the gravitational force, we can write $F = F_e$, or:

$$\frac{m_e v^2}{r} = \frac{k_e e^2}{r^2} \tag{39}$$

Where $k_e$ is the electrostatic constant ($k_e$= 8.9875517873681764×$10^9$ N·$m^2$/$C^2$ ≈ 8.99×$10^9$ N·$m^2$/$C^2$**).** From eq. 39, the radius *r* could be written as:

$$r = \frac{k_e e^2}{m_e v^2} = \frac{k_e e^2}{m_e c^2 \beta^2} \tag{40}$$

Where $\beta = \frac{v}{c}$, and $c$ is the velocity of light (in the source rest frame).

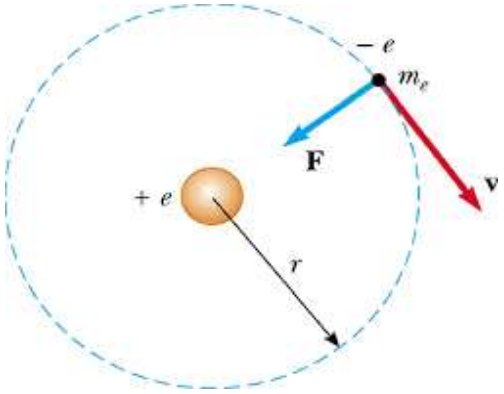


**Figure 9**. A simplified representation of the hydrogen atom

According to Information Relativity, the orbiting electron will stretch relative to the rest-frame of a fixed perimeter corresponding to a radius r is. Using eq. 15, the wavelength of the electron's dual-wave is given by:

$$\lambda = d = d_0 \frac{1+\beta}{1-\beta} = 2\, r_e \frac{1+\beta}{1-\beta} \tag{41}$$

Where $r_e$ is the radius of the electron at rest (i.e., the classical radius). The electron will stabilize in a given orbit with radius *r only* if the weave front of the electron's wave packet, arrives in complete phase synchronization with the wave's "tail", i.e., only if it constitutes a standing wave (see Fig. 10).

For this to occur, the wavelength $\lambda$ should satisfy:

$$n\,\lambda = 2\,\pi\, r\,, \quad n = 1,2,3,\ldots \tag{42}$$

Or:

$$\lambda = \frac{2\,\pi\, r}{n} \quad n = 1, 2, 3\ldots \tag{43}$$

Substituting the value of *r* from eq. 40 in eq. 43 we obtain:

$$\lambda = \frac{2\,\pi}{n} \frac{k_e e^2}{m_e c^2 \beta^2} \tag{44}$$

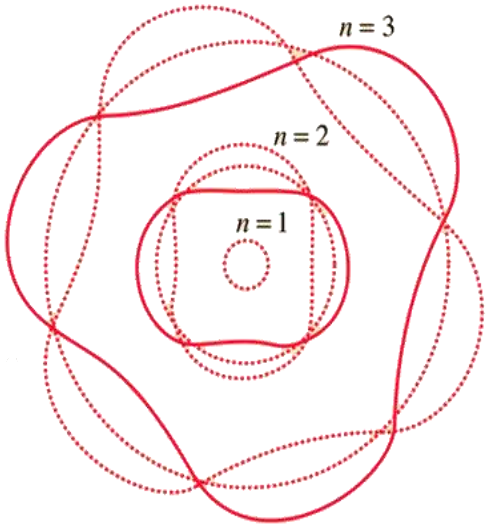


Figure 10: First three harmonics of a "standing wave"

Equating the expressions for λ in equation 41 and 44 we obtain:

$$\frac{2\,\pi}{n}\,\frac{k_e e^2}{m_e c^2 \beta^2} = 2r_e\,\frac{1+\beta}{1-\beta}, \qquad \text{n = 1, 2, 3…} \tag{45}$$

Which could be written as:

$$\frac{A_1}{n\,\beta^2} = \frac{1+\beta}{1-\beta} \tag{46}$$

Where $A_1 = \frac{\pi\, k_e e^2}{r_e\, m_e c^2}$. Defining $A_n = \frac{A}{n}$ eq. 46 could be written as:

$$\frac{A_n}{\beta^2} = \frac{1+\beta}{1-\beta} \tag{47}$$

Which could be simplified to yield:

$$\beta^3 + \beta^2 + A_n\,\beta - A_n = 0, \ \text{n = 1, 2, 3, …} \tag{48}$$

For n=1 we have:

$$A_1 = \frac{\pi\, k_e e^2}{r_e\, m_e c^2} = \frac{\pi\, x\, 8.99{\times}10^9 x\, (1.6021766208{\times}10{-}19)^2}{(9.10938356{*}10^{-31}{*}\,299792458^2)}\,\frac{1}{r_e} = 8.85523x10^{-15}\ \frac{1}{r_e} \tag{49}$$

There is no agreed upon length of the electron radius. For a midrange radius of 5.5x $10^{-13}$ m., reported in [114] we obtain:

$$A_1 = 8.85523x10^{-15}\ \frac{1}{r_e} = \frac{8.85523x10^{-15}}{5.5\text{x } 10\ -13} \approx 0.016 \qquad (50)$$

Substitution in eq.48 gives:

$$\beta^3 + \beta^2 + \frac{0.016}{n}\ \beta - \frac{0.016}{n} = 0, \qquad \text{n = , 2, 3, …} \qquad (51)$$

Table 4 depicts the radii of the electron's orbit for n=1, 2, … 6, together with the corresponding electron's velocity $\beta$. These relationships are also shown in Figures 11 and 12.

**Table 4**

**radii and corresponding electron velocity in the hydrogen atom**

| ***n*** | ***β*** | ***R (in m.)*** |
|---|---|---|
| 1 | 0.112929 | 2.212 x $10^{-13}$ |
| 2 | 0.0823563 | 4.156 x $10^{-13}$ |
| 3 | 0.0682074 | 6.059 x $10^{-13}$ |
| 4 | 0.059583 | 7.940 x $10^{-13}$ |
| 5 | 0.0536128 | 9.807 x $10^{-13}$ |
| 6 | 0.0491606 | 1.16610$^{-12}$ |

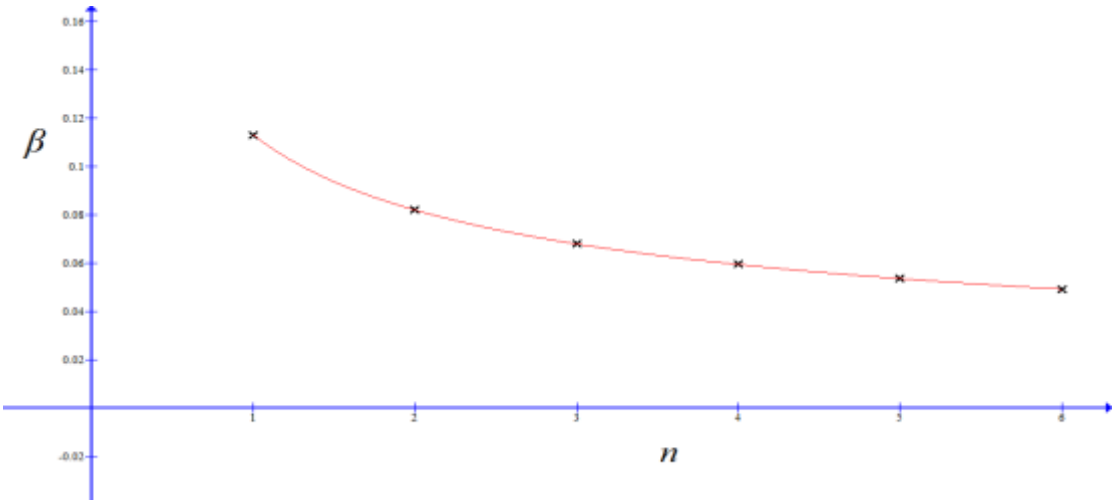


**Figure 11**. Velocity of the electron at various orbits (Trend line: β(n)=0.1132 $n^{-0.4642}$, $R^2$= 0.9999)

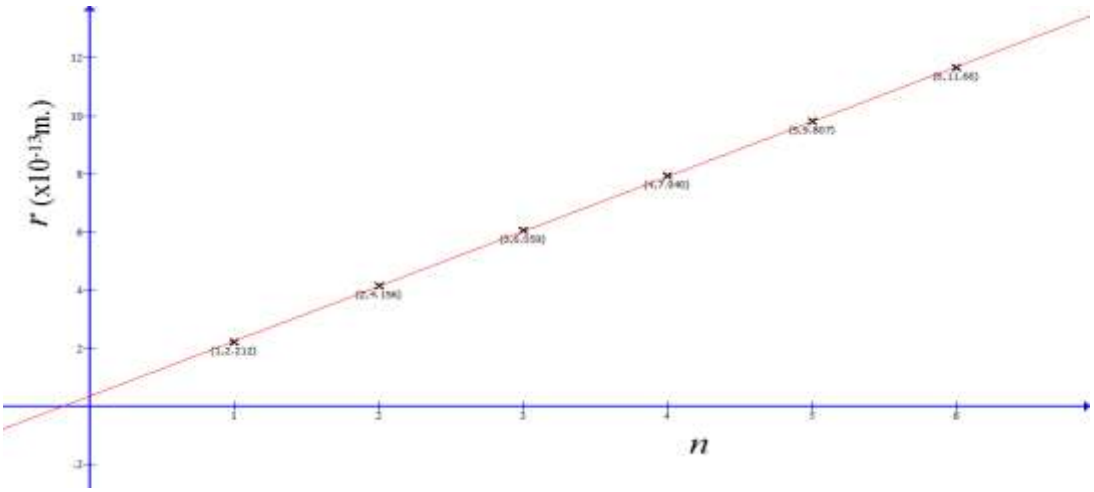


**Figure 12.** Radii of various electron orbits (Trend line: r(n)=1.8878*n+0.3649; $R^2$=0.9999)

It is important to stress that the above derivation of the hydrogen atom's permitted radii was accomplished without any assumptions about quantization as done by Bohr, and without any considerations of uncertainty, neither directly, nor through utilization of Planck's constant.

**8. A new relativistic quantum cosmology and astrophysics**

The proposed theory, without alteration or additional assumptions, provides a simple, yet adequate model of the cosmology of the universe, based only on the classical Doppler redshift (a z-cosmology). We term this model "quantum" because it treats the dynamics of receding galaxies using the same model of matter-wave duality utilized for explaining quantum mechanics. In the framework of Information Relativity, the scale of the system is of no importance. We shall show in the proceedings that dark matter is quantum matter at cosmic scale, and the amounts of "dark energy" reported in large scale ΛCDM observational studies.

**8.1 Information Relativity's cosmological transformations**

To apply the theory to cosmology, we rewrite the transformations in Table 1 in terms of the redshift z, instead of the velocity $\beta$. For deriving the relationship between redshift and velocity, consider an observer on earth who receives redshifted waves emitted from a receding galaxy. Assume that the recession velocity at the time the waves were emitted was equal to $v$. Using Doppler's formula, we can write:

$$z = \frac{\lambda_{ob} - \lambda_{em}}{\lambda_{em}} = \frac{f_{em} - f_{ob}}{f_{ob}} \tag{52}$$

Where $\lambda_{em}$ ($f_{em}$) is the wavelength (frequency) of the wave emitted by the galaxy and $\lambda_{ob}$ ($f_{ob}$) is the wavelength (frequency) measured by the observer. We also have $f_{em} = \frac{1}{\Delta t_{em}}$ and $f_{ob} = \frac{1}{\Delta t_{ob}}$,

Where $\Delta t_{em}\ and\ \Delta t_{ob}$ are the time intervals corresponding to $f_{em}$ and $f_{ob}$, respectively. Substitution in eq. 52 gives:

$$z = \frac{\frac{1}{t_{em}} - \frac{1}{t_{ob}}}{\frac{1}{t_{ob}}} = \frac{\Delta t_{ob}}{\Delta t_{em}} - 1 \tag{53}$$

From eq. 6 we have: $\frac{\Delta t_{ob}}{\Delta t_{em}} = \frac{1}{1-\beta}$ , where $\beta = \frac{v}{c}$. Substitution in eq. 53 yields:

$$z = \frac{1}{1-\beta} - 1 = \frac{\beta}{1-\beta} \tag{54}$$

And the recession velocity in terms of redshift is:

$$\beta = \frac{z}{z+1} \tag{55}$$

For blue-shift the same equation holds except that we must replace $\beta$ by - β. Substituting eq. 55 in the transformations depicted in Table 1 yields the transformation as functions of the redshift z depicted in Table 5.

**Table 5**
**Information relativity transformations in terms of redshift z**

| Physical Term | Relativistic Expression |
|---|---|
| Time interval | $\frac{\Delta t}{\Delta t_0} = z + 1$ (56) |
| Distance | $\frac{l}{l_0} = 2z + 1$ (57) |
| Mass density | $\frac{\rho}{\rho_0} = \frac{1}{2z+1}$ (58) |
| Kinetic energy density | $\frac{e_k}{e_0} = \frac{z^2}{(z+1)^2(2z+1)}$ (59) |
| Wave energy density | $\frac{e_w}{e_0} = \frac{2z^3}{(z+1)^2(2z+1)}$ (60) |

In previous articles [115-116] we applied equations 56-60 to construct a simple and plausible cosmology. Here we summarize the more important results:

### 8.2 The pattern of recession velocity

The recession velocity in eq. 55 fits well with current inflammation cosmological models. As could be seen in Figure 13, for very high redshifts (from z~8 to z~1089), the predicted recession velocity is close to the velocity of light, and its deceleration rate is low and relatively steady. This prediction confirms with accepted inflation theory [117-118] predicting an early period of accelerated expansion of the universe. For very low redshifts ($z \leq 0.1$), the recession velocity is predicted to be low and relatively steady. In the midrange of redshifts, between z~8 and z~0.1, the model predicts that the universe underwent a period of rapid deceleration.

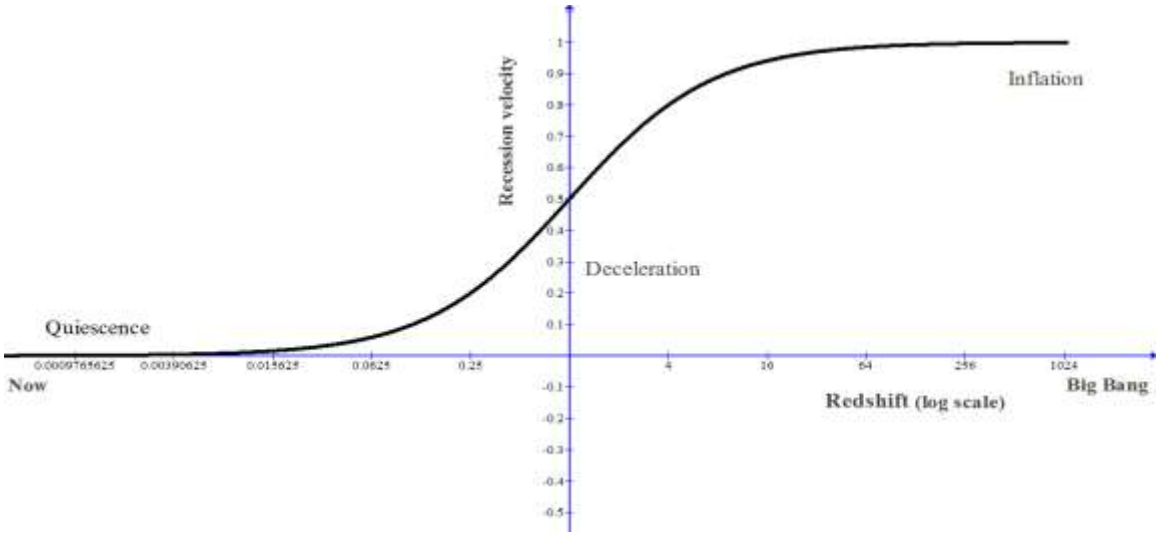


**Figure 13.** Recession velocity as a function of redshift z

### 8.3 Predicting the expanding universe

The constructed model predicts an expanding universe. From equations 56 and 57 it could be easily seen that:

$$\frac{l}{l_0} = 2\,\frac{\Delta t}{\Delta t_0} - 1 \tag{61}$$

Which predicts a unidimensional expanding universe, in which the relativistic spatial dimension increases linearly with the relativistic time interval.

### 8.4 Explaining dark matter and dark energy

Perhaps the most important result of applying Information Relativity to cosmology is the interpretation it provides for dark matter and dark energy. According to the theory dark matter is quantum matter at cosmic scales, whereas the measured amounts of what is believed to be negative dark energy is the energy of associated with the receding cosmological structures (e.g., galaxies) pilot waves. This explanation abolishes the mystery of the source and nature of dark energy.

The kinetic energy density, and the accompanying wave energy density as functions of redshift (in logarithmic scale), are depicted in Figure 14.

The predicted decline in kinetic energy density at $z \approx 1.618$ is in agreement with the well-known

GZK cutoff limit to the cosmic-ray energy spectrum [119-120]. In the proposed theory the GZK cutoff point is the point of cosmic quantum criticality. As shown in Fig 14, the maximal kinetic energy density is predicted to be at redshift $z = 1+\varphi \approx 1.618$. These predictions are in good agreement with the HiRes experiment show a break in the luminosity densities QSO's and AGN's at about z=1.6, as well as with numerous discoveries of quasars, galaxies, and AGNs, indicating a break in luminosity densities at about z=1.6 (e.g., [121-122]), including a recent discovery of galaxies at redshift equaling exactly 1.618 [123].

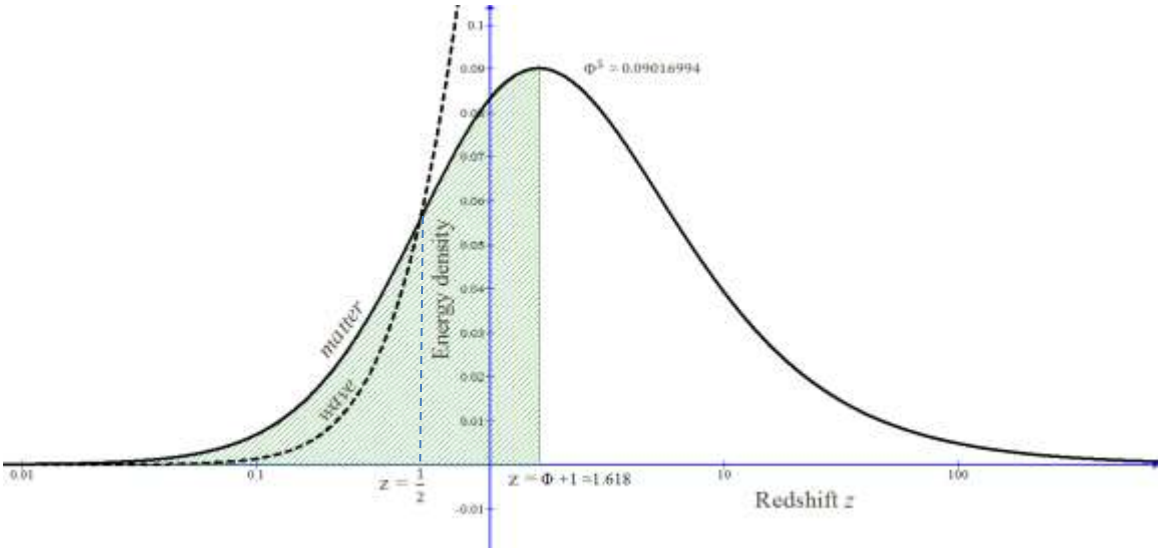


**Figure 14.** Matter and accompanying wave energy densities as functions of redshift

A testable prediction of the model is the prediction that at redshifts below $z = \frac{1}{2}$, (corresponding to recession velocity $\beta = \frac{1}{3}$) the universe is dominated by normal matter such that it's the kinetic energy density is larger than the energy density of the accompanying wave, while at redshifts higher than $z = \frac{1}{2}$ the universe is dominated by the accompanying wave (dark energy).

For a given redshift range $(z_1, z_2)$, $z_2 > z_1$, the amounts of matter and wave energies could be calculated by integrating over the functions in equations 59 and 60, yielding (see [116]):

$$\frac{e_k(z_1 - z_2)}{e_0} = = \frac{1}{2} ln\left(\frac{2z_2+1}{2z_1+1}\right) - \frac{z_2 - z_1}{(z_2+1)(z_1+1)} \quad (62)$$

And,

$$\frac{e_d(z_1 - z_2)}{e_0} = (z_2 - z_1) + 2\frac{(z_2 - z_1)}{(z_2+1)(z_1+1)} - 2\, ln\left(\frac{(z_2+1)}{(z_1+1)}\right) - \frac{1}{2}\ln\left(\frac{(2z_2+1)}{(2z_1+1)}\right) \quad (63)$$

### 8.5 Predicting the results of ΛCDM cosmologies

Calculations based on the above expressions are in good agreement with observationally based ΛCDM cosmologies. As example, for the redshift ranging 0.6-1, tested by Wittman et al. (2000) [124] , it was concluded that dark matter is distributed in a manner consistent with either an open universe, with $\Omega_b = 0.045$, $\Omega_{matter} - \Omega_b = 0.405$, $\Omega_\Lambda = 0$, or with a ΛCDM with $\Omega_b = 0.039$,

$\Omega_{matter}$ - $\Omega_b = 0.291$, $\Omega_\Lambda = 0.67$, where $\Omega_b$ is the fraction of critical density in ordinary (baryonic) matter, $\Omega_{matter}$ is the fraction of all matter, and $\Omega_\Lambda$ is the fraction of dark energy. In the open universe model, we have $\Omega_{matter}$ = 0.045 + 0.405 = 0.45, and $\Omega_\Lambda = 0$, whereas in the ΛCDM, we have $\Omega_{matter}$ = 0.039 + 0.291 = 0.33, and $\Omega_\Lambda = 0.67$. Calculating the ratios of kinetic and wave energies from equations 62 and 63 for the same redshift range gives:

$$\frac{e_k}{e_{tot}} = \frac{e_k}{e_k+e_w} = \frac{0.0300775}{0.0300775 + 0.0486354} \approx 0.382\ (\approx 38.2\%) \tag{64}$$

And,

$$\frac{e_w}{e_{tot}} = \frac{e_w}{e_k+e_w} = \frac{0.0486354}{0.0300775+0.0486354} \approx 0.618\ (\approx 61.8\%) \tag{65}$$

Which is in agreement with the observations based ΛCDM model with ($\Omega_m = \frac{1}{3}$, $\Omega_\Lambda = \frac{2}{3}$). For the entire range of semi-classical matter ($0 \leq z < 1.618$) we get: $\frac{e_k(0\ -1.618)}{e_0} \approx 0.1038$, and $\frac{e_w(0\ -\varphi)}{e_0} \approx 0.3420$, yielding:

$$\frac{e_k}{e_k + e_w} = \frac{0.138}{0.138+0.3420} \approx 0.233\ (\text{or } 23\%) \tag{66}$$

And,

$$\frac{e_w}{e_k + e_w} = \frac{0.3420}{0.138+0.3420} \approx 0.767\ (\text{or } 76.7\%) \tag{67}$$

Which is in excellent agreement with the ΛCDM cosmology with $\Omega_{matter}$ = 0.23, $\Omega_\Lambda$ = 0.77 (see, e.g., [125-127]), and quite close to the $\Omega_{matter}$ = 0.26, $\Omega_\Lambda$ = 0.74 cosmology (see, e.g., [128 -130 ]).

**8.6 Predicting the Schwarzschild radius of black holes.**

Karl Schwarzschild, while serving in the German Army on the Russian front, solved Einstein's field equations for a non-rotating, uncharged, spherical black hole [131-132]. For a star of a given mass, M, Schwarzschild found the critical radius $R = \frac{2\ G\ M}{c^2}$, where G is the gravitational constant and *c* is the velocity of light, at which light emitted from the surface would have an infinite gravitational redshift, and thereby infinite time dilation. Such a star, Schwarzschild concluded, would be undetectable by an external observer at *any* distance from the star.

Our understanding of the processes involved in the evolution and decay of black holes is largely due to quantum mechanical and thermodynamic theories. Early in 1974, Stephen Hawking predicted that a black hole should radiate like a hot, non-black ("gray") body [133]. Hawking's theory of black holes, is consistent with Bekenstein's generalized second law of thermodynamics [134], stating that the sum of the black-hole entropy and the ordinary thermal entropy outside the black hole cannot decrease. According to this prediction, black holes should have a finite, non-zero, and non-decreasing temperature and entropy.

The first X-ray source, widely accepted to be a black hole, was Cygnus X-1 [135]. Since 1994, The Hubble Space Telescope, and other space-crafts and extremely large ground telescopes [see, e.g., 136-139], have detected numerous black holes of different sizes and redshifts. We now know that black holes exist in two mass ranges: small ones of ($M \lesssim 10\ M_{\odot}$) ($M_{\odot}$, solar mass), believed to be the evolutionary end points of the gravitational collapse of massive stars, and supermassive black holes of $M \gtrsim 10^6\ M_{\odot}$, responsible for the powering of quasars and active galactic nuclei (AGN) [140-142]. Supermassive black holes, residing at the centers of most galaxies, are believed to be intimately related to the formation and evolution of their galaxies [140- 142].

The Schwarzschild solution to Einstein's field equations yielded a critical hole radius of $R = \frac{2\,GM}{c^2}$. However, Schwarzschild's solution suffers from a serious pathology, because it predicts a singularity whereby the fabric of spacetime is torn, causing all matter and radiation passing the event horizon to be ejected out to an undefined spacetime, leaving the black hole empty, thus, in violation of the laws of thermodynamics and contradiction with quantum mechanics [e.g., 143-144]. Many believe that the black holes (and the Big Bang) singularities mark a breakdown in GR.

Attempts to solve the singularity problem are aplenty. Bardeen was the first to propose a regular black hole model [145]. In 1968, he produced a famous model, conventionally interpreted as a counterexample to the possibility that the existence of singularities may be proved in black hole spacetimes without assuming either a global Cauchy hyper-surface or the strong energy condition. Other regular "Bardeen black holes" models have been also proposed [e.g., 146-151], but none of these models is an exact solution to Einstein equations [152]. Other solutions to produce singularity-free black hole come from quantum mechanics [e.g., 153-157], and string theory [e.g., 158-159], and. As examples, Ashtekar and others proposed a loop quantum gravity model that avoids the singularities of black holes and the Big Bang. Their strategy was to utilize a regime that keeps GR intact, except at the singularity point, at which the classical spacetime is bridged by a discrete quantum one. Although the solution is mathematically difficult, its strategy is simple. It begins with semi-classical state at large late times ("now"), and evolves it back in time, while keeping it semi-classical until one encounters the deep Planck regime near the classical singularity. In this regime, it allows the quantum geometry effects to dominate. As the state becomes semi-classical again on the other side, the deep Planck region serves as a quantum bridge between two large, classical spacetimes [153].

To derive Information Relativity solution for an uncharged, non-rotational black hole, consider Figure 15 which depicts a schematic representation of a supermassive black hole with mass M and radius *R* residing at the center of its host galaxy. The figure shows three particles, with equal masses and velocities, at different distances from the center of the black hole. As depicted in the figure, the more distant particle will be deflected toward the black hole, but will escape it due to its large distance, and continue its travel in space. By contrast, the closest particle to the black hole will experience a strong enough gravitational force to cause its absorption into the black hole. Now consider the third particle, which rotates around the black hole at radius *r*. Such particle could be a baryon or wave quanta entrapped at a critical distance, ensuring that it rotates around the black hole. For such particle, the acceleration $|\vec{a}|$ supporting a uniform radial motion with radius *r* should satisfy:

$$a = |\vec{a}| = \frac{v^2}{r} = \frac{c^2}{r}\,\beta^2 \tag{68}$$

The force supporting such motion, according to Newton's second law, could be expressed as:

$$F = \frac{\partial P}{\partial t} = \frac{\partial (mv)}{\partial t} = m\,\frac{\partial (v)}{\partial t} + v\,\frac{\partial (m)}{\partial t} =$$

$$m\,a + v\,\frac{\partial (m)}{\partial v}\,\frac{\partial (v)}{\partial t} = m\,a + v\,a\,\frac{\partial (m)}{\partial v} \;=\; (m + v\,\frac{\partial (m)}{\partial v})\,a \tag{69}$$

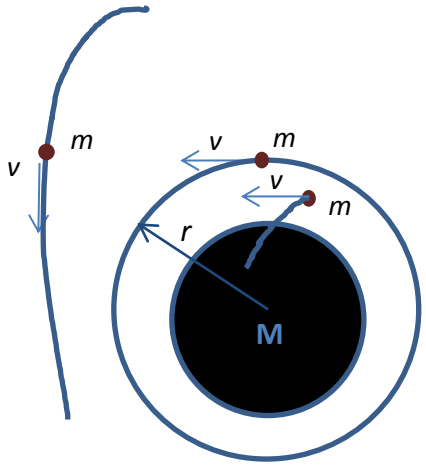


**Figure 15.** Three particles near a black hole

Substitution the term for *m* from eq. 18 in eq. 69, and deriving m with respect to *v* yields:

$$F = \frac{1-2\beta-\beta^2}{(1+\beta)^2}\;\; m_0\;\; a \tag{70}$$

Substitution the value of *a*, from Eq. 68 in Eq. 70 yields:

$$F = \frac{1-2\beta-\beta^2}{(1+\beta)^2}\;\; m_0\;\; a = \frac{1-2\,\beta-\beta^2}{(1+\,\beta)^2}\,m_0\;\;\frac{v^2}{r} = \;m_0\,c^2\,\frac{1-2\,\beta-\beta^2}{(1+\,\beta)^2}\,\beta^2\,\frac{1}{r} \tag{71}$$

Using Newton's general law of gravitation, we get:

$$\mathrm{G}\,\frac{m_0\,M}{r^2} = m_0\,c^2\,\frac{1-2\,\beta-\beta^2}{(1+\,\beta)^2}\,\beta^2\,\frac{1}{r} \tag{72}$$

Solving for $r$ yields:

$$r = \frac{G\,M}{c^2}\ \frac{(1+\beta)^2}{1-2\,\beta-\beta^2}\ \beta^2 \tag{73}$$

Assuming spherical symmetry, eq. 73 describes the dynamics of the host galaxy as a function of velocity. For a light photon ($\beta = 1$), we have:

$$r\,(\beta = 1) = R = \frac{2\,G\,M}{c^2} \tag{74}$$

Which exactly equals the Schwarzschild radius, ***but with no singularity in the hole's interior***. Interestingly, the solution (eq. 73) has a naked *spatial* singularity at $\beta$ satisfying:

$$1 - 2\,\beta - \beta^2 = 0 \tag{75}$$

Solving for $\beta$, we have:

$$\beta = \sqrt[2]{2}\ \text{-}1 \approx 0.4142 \tag{76}$$

With corresponding redshift of:

$$z = \frac{\beta}{1-\beta} = \frac{1}{\sqrt[2]{2}} \approx 0.707 \tag{77}$$

It is important to stress that the predicted singularity is in space and not in spacetime, as prescribed by General Relativity's field equations. In fact, Information Relativity in general, including in its present application to the black hole problem, does not require reference to the notion of spacetime. Rather, it is a straightforward relativistic extension of Galileo-Newton's physics, and as such, it treats space and time independently of each other.

To express the derived radius in terms of redshift, we substitute the value of $\beta$ from eq. 55 in Eq. 73 and solve for $r$, yielding:

$$r = \left(\frac{G\,M}{c^2}\right) \frac{z^2(1+2z)^2}{(1+z)^2\,(1-2z^2)} \tag{78}$$

Figure 16 depicts the ratio $r$, normalized by $\frac{GM}{c^2}$, as a function of z.

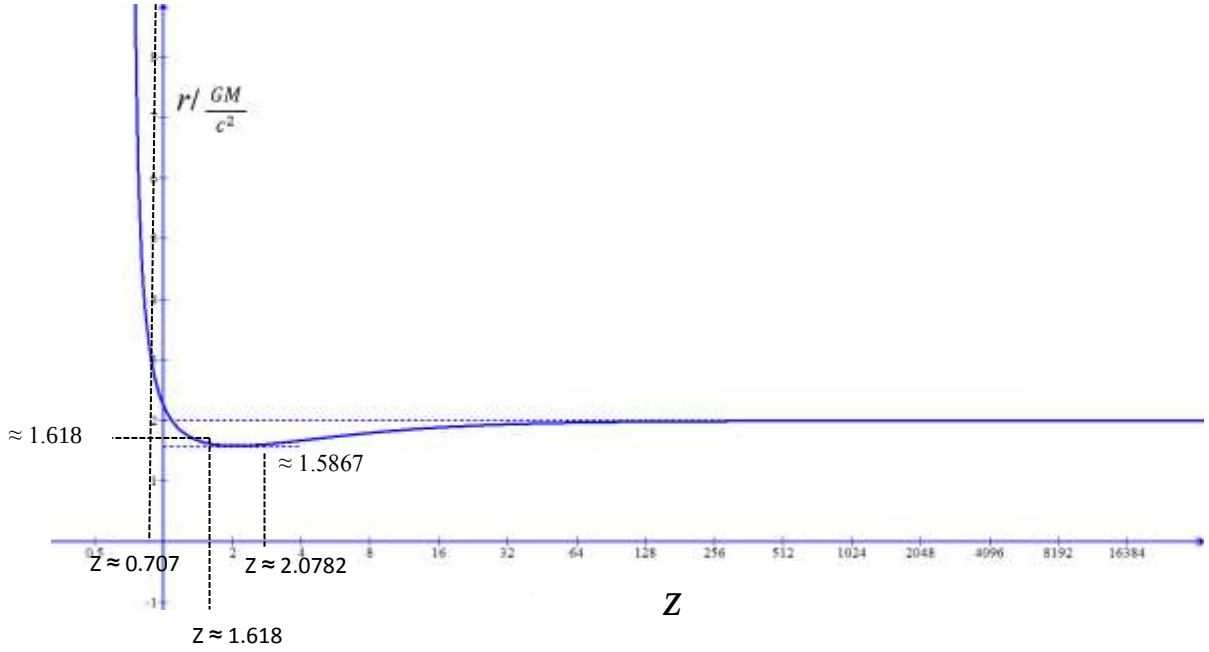


**Figure 16**. $r\ /\ (\frac{GM}{c^2})$ as a function of redshift

As shown by the figure, for very high redshifts $r$ converges to $2\,\frac{G\,M}{c^2}$ (the Schwarzschild radius). Moreover, the result in eq. 78 has some interesting properties: (1) $r$ has a naked *spatial singularity*, at $z = \frac{1}{\sqrt[2]{2}} \approx 0.707$, (2) It displays a striking Golden Ration symmetry, such that for z = φ ≈ 1.618, $r\ /\ (\frac{G\,M}{c^2}) \approx 1.618$, (3) It has a point of minimum in the range between the above mentions redshifts. To find the point of minimum we derive $r\ /\ (\frac{G\,M}{c^2})$ with respect to z and equate the result to zero, yielding:

$$4\,z^4 - 2\,z^3 - 10\,z^2 - 6\,z - 1 = 0 \tag{79}$$

Which solves at $z_m \approx 2.078$, yielding:

$$r_m \approx 1.5867\ (\frac{G\,M}{c^2}) \tag{80}$$

The prediction of an extreme galactic activity at $z \approx 0.707$ is supported by many observational studies, which reported the detection of quasars, blazars and other AGNs at $z \approx 0.707$ [e.g., 160 -163]. For example, a recent study by Steinhardt et al. [160] reported the discovery of a Type 1 quasar, SDSS 0956+5128, with extreme velocity offsets at redshifts z = 0.690, 0.714, and 0.707. The prediction of AGNs at z ≈ 2.078 is also confirmed by observations [e.g. 164-165].
I also compared the dynamical dependence of *r* on redshift (eq. 19) with the dynamics reported in [166] for a cosmology of $\Omega_M = 0.3$ and $\Omega_\Lambda = 0.7$, $H_0 = 70$ km $s^{-1}$ $Mpc^{-1}$. Figure 17a depicts the predicted radius *r* (in Km) as a function of redshift for intermediate and massive black holes

and Figure 17b depicts comparable results reported in [166]. Comparison of the two figures, despite differences in scaling, reveals a remarkable similarity between the results of the two models.

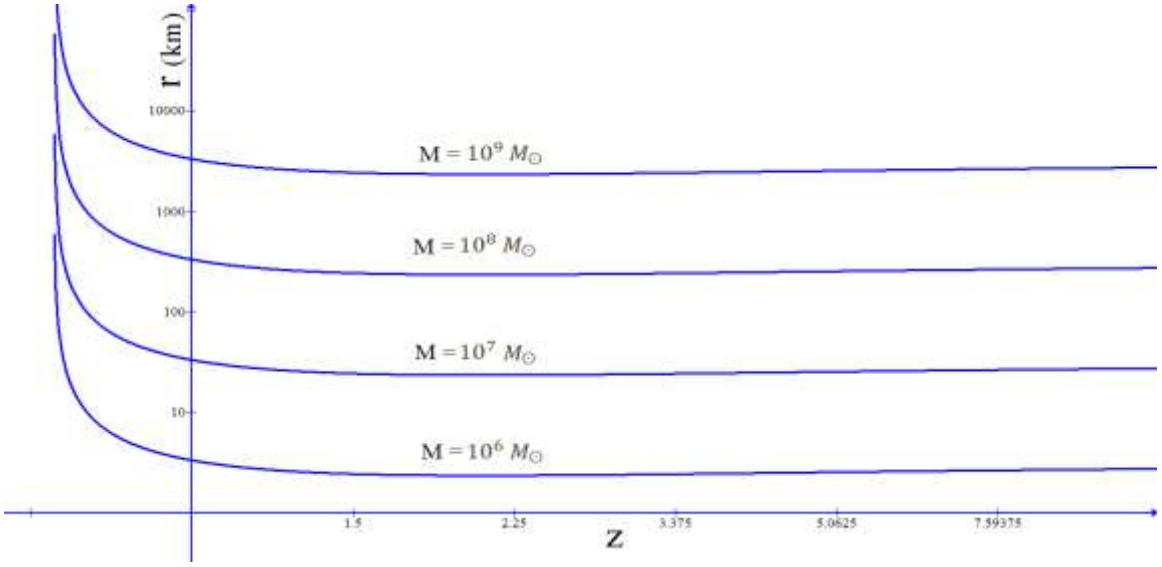


**Figure 17a**

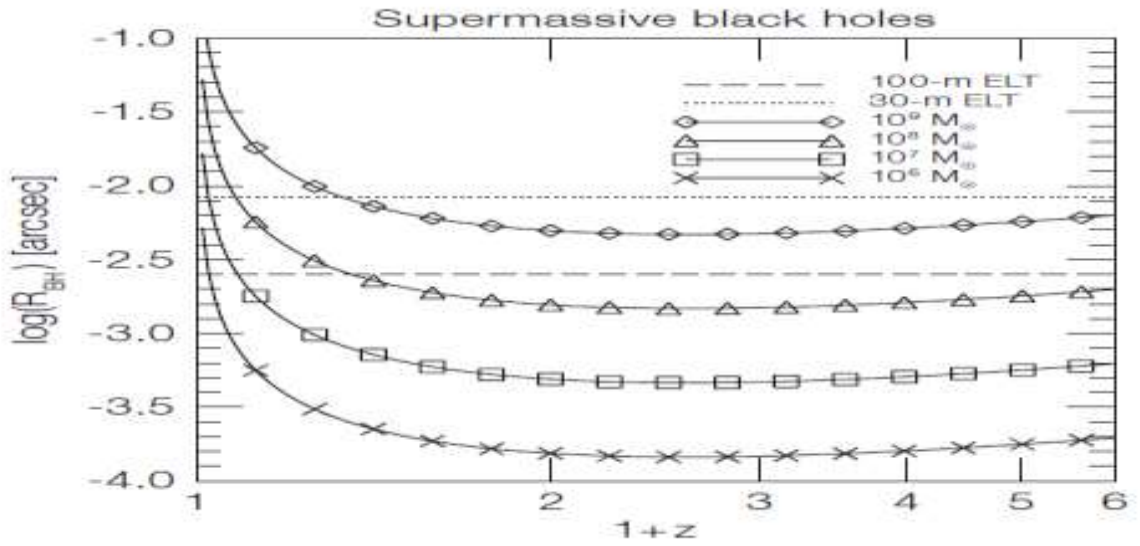


**Figure 17b**

**Figure 17**. Predicted *r* as a function of z (Fig. 17a) and comparable results based on ΛCDM model ($\Omega_M = 0.3,\ \Omega_\Lambda = 0.7$, $H_0 = 70$ km $s^{-1}$ $Mpc^{-1}$) reported by Hook (2005) [166] (Fig 17b).

### 8.7 Predicting the mass of the Higgs boson

The possibility of existence of the recently discovered Higgs boson [167-168] was proposed more than forty years ago. In the Standard Model (SM), electroweak symmetry breaking (EWSB) is

achieved by invoking the Higgs mechanism, which requires the existence of the Higgs boson [169-172]. In the SM, the Higgs boson mass, $m_H$, is a priori unknown. However, for a given $m_H$ hypothesis, the production cross sections and branching fractions of each decay mode are predicted, which enables a combined search with data from several decay channels [167]. In July 2012, the ATLAS [167] and CMS [168] collaborations announced that they had discovered a new particle with a mass ~125 GeV, which qualifies as a candidate for the theorized Higgs boson. ATLAS reported a particle mass $m_H \sim 126$ GeV with a local significance of 3.5 σ, and CMS reported a mass $m_H = 125.3 \pm 0.4(\text{stat.}) \pm 0.5(\text{syst.})$ GeV, with a local significance of 5 σ. In the signal region of (5.56 – 5.68) GeV, the reconstructed mass of $\Lambda_b^0$ and $\overline{\Lambda}_b^0$ using up to 4.6 $fb^{-1}$ at 7 TeV of pp collision data is shown in Figure 18 (see [173-174]).

To predict the mass of the Higgs boson we took a cosmological view of the creation of the unstable Higgs boson (e.g., [175-178]). Like the W and Z bosons, the Higgs boson gets its mass from the Higgs mechanism. It is assumed that this process has occurred at an epoch in the early universe, characterized by an unstable phase transitions [[178]. This assumption fits well with the prediction of Information Relativity theory, which predicts that quantum phase transition is predicted to have happened at a redshift equaling $z = 1+ \varphi \approx 1.618$ (see Fig 14).

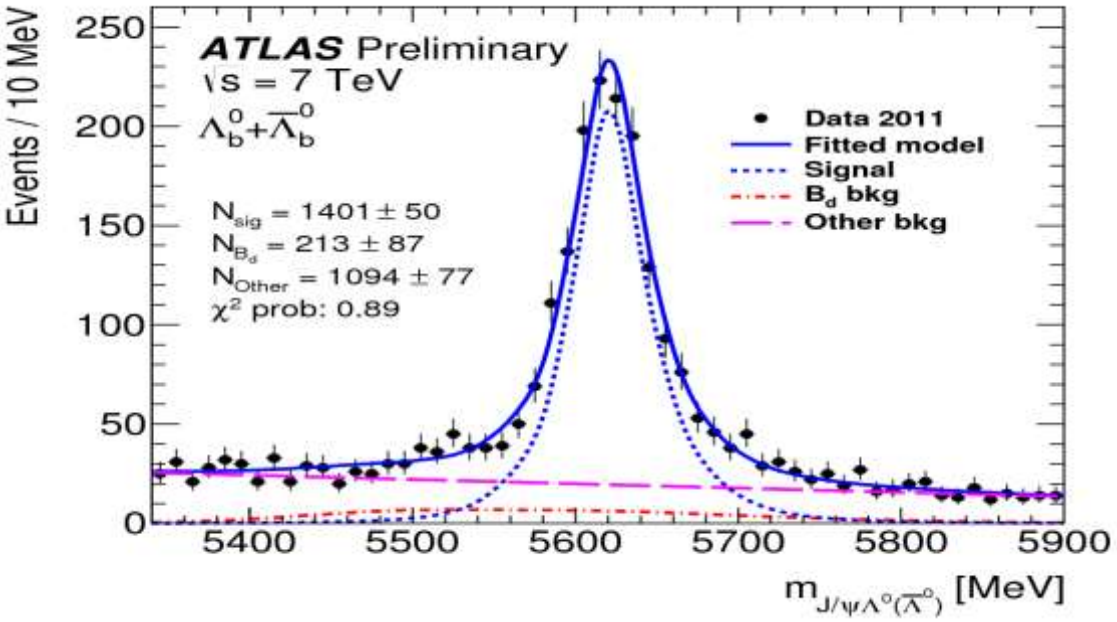


**Figure 18.** The reconstructed mass of $\Lambda_b^0$ and $\overline{\Lambda}_b^0$ candidates, fitted with a three-component PDF (blue solid curve) consisting of signal (blue dashed curve), combinatorial (magenta long-dashed straight line) and $B_d^0$ background (red dot-dashed curve, bottom). (Source: [173])

To calculate the Higgs mass, from eq. 23, which gives the kinetic energy at redshift $z \approx 1.618$, we can write:

$$(e_k)_{max} = \Phi^5 e_0 = \Phi^5 \times \frac{1}{2} m_0 c^2, \quad (81)$$

Or:

$$m_0\, c^2 \;= 2\, \Phi^{-5}\;\; (e_k)_{max} \tag{82}$$

For the lower bound of the signal region of (5.56 – 5.68) GeV, reported by ATLAS, we have:

$$m_0\, c^2 = 2 \text{ x } (\tfrac{\sqrt{5}-1}{2})^{-5} \text{ x } 5.56 \text{ (GeV)} \approx 22.180 \text{ x } 5.56 \text{ (GeV)} \approx 123.321 \text{ GeV}. \tag{83}$$

And for the upper bound we have:

$$m_0\, c^2 = 2 \text{ x } (\tfrac{\sqrt{5}-1}{2})^{-5} \text{ x } 5.68 \text{ (GeV)} \approx 22.180 \text{ x } 5.68 \text{ (GeV)} \approx 125.983 \text{ GeV}. \tag{84}$$

And the average mass is equal to:

$$m_0\, c^2 \approx \tfrac{123.321+125.982}{2} \approx 124.652 \text{ GeV}. \tag{85}$$

Which highly agrees with the reported results of the mass of the Higgs boson.

**8.8 Predicting the evolutionary timeline of chemical elements**

Currently, the details of the ionization history are not well understood [179], but it is believed to exist at as early as $z \sim 20$ [180]. It is well accepted that fusion reactions (starting with hydrogen into helium) inside stars synthesize the elements up to iron, and that elements heavier than iron cannot be formed by fusion, and that they are synthesized as a result of slow and fast neutron-capture reactions, known as n-capture [180].

The proposed theory can be used to make predictions about the cosmic ionization of light and of heavy elements. This highly important issue goes far beyond the scope of the present paper, and will hopefully be addressed in a subsequent paper. Here, I only give a glimpse of the topic by applying the theory for predicting the times of formation, after the Big Bang, of two light elements, Carbon ${}^{6}_{12}\mathrm{C}$ and Oxygen ${}^{6}_{12}\mathrm{C}$.

For this purpose, consider the generic nuclear fusion of the type

$$_k\mathrm{X} + \;_l\mathrm{Y} = \;_m\mathrm{Z} + \;\omega + E_k \tag{86}$$

Where *k, l,* and *m* are the atomic weights of the elements X, Y, and Z, respectively, ω is some elementary particle, and $E_k$ is the emitted kinetic energy. Denote the difference in atomic mass between the interacting and the produced elements by Δm. Assuming that all the emitted kinetic energy is carried by the newly formed particle Z, from eq. 59, we have the following:

$$E_k = (\frac{1}{2} m\, c^2)\, \frac{z^2}{(z+1)^2(2z+1)} = \frac{1}{2} \Delta m\, c^2 \quad (87)$$

Solving for $\frac{\Delta m}{m}$, we get:

$$\frac{\Delta m}{m} = \frac{z^2}{(z+1)^2(2z+1)} \quad (88)$$

The right-side term in eq. 88 is identical to the kinetic energy term (see eq. 59), implying that the dependence of $\frac{\Delta m}{m}$ on z mimics the dependence on z of the kinetic energy density depicted in Figure 4, with maximum obtained at z ≈ 1.618. Inspection of eq. 88 (see also Figure 14) reveals that for very high redshifts, the rate of increase in atomic mass, $\frac{\Delta m}{m}$, is very low, suggesting the differences between the atomic masses of very heavy elements are predicted to be small. A similar prediction applies to the differences between the atomic masses of very light elements. As we move from epochs of very low redshifts to epochs of larger redshifts (or from epochs of very high redshifts to earlier epochs), $\frac{\Delta m}{m}$ is predicted to increase, reaching a crest at z = φ ≈ 1.618.

To derive the term for the dynamical dependence of $\frac{\Delta m}{m}$ on time, denote the redshift corresponding to the Big Bang moment by $z_T$ (≈ 1089), with corresponding time of T (≈ 13.789 BY). From eq. 56, we can write the following:

$$\frac{T}{t'} = z_T + 1 \quad (89)$$

For any time, *t*, and redshift *z*, using equation 66 and 89 we can write:

$$\frac{t}{T} = \frac{z+1}{z_T+1} \quad (90)$$

Which yields:

$$z = (z_T + 1)\frac{t}{T} - 1 \quad (91)$$

Substituting *z* from eq. 91 in eq. 88, we get:

$$\frac{\Delta m}{m} = \frac{((z_T+1)\frac{t}{T} - 1)^2}{\left((z_T+1)\frac{t}{T}\right)^2 (2(z_T+1)\frac{t}{T} - 2 + 1)} \quad (92)$$

For $z_T \approx 1089 >> 1$, solving eq. 92 for $\frac{t}{T}$ gives:

$$\frac{t}{T} \approx \frac{1}{2z_T \frac{\Delta m}{m}} \approx \frac{1}{2178 \frac{\Delta m}{m}} \tag{93}$$

For T ≈ 13.789 BY, we get:

$$t \approx \frac{1}{2178 \frac{\Delta m}{m}} \text{ . } 13.789 \text{ BY} \tag{94}$$

In principle, given any nucleuses reaction, eq. 92 could be used to explore the timeline for the formation of the various chemical elements. Solving eq. 92 for *z* gives:

$$2\, z^3 + (5 - \frac{1}{(\frac{\Delta m_i}{m_i})})\, z^2 + 4\, z + 1 = 0 \tag{95}$$

To demonstrate, we apply the model for estimating the redshifts and times for the cosmic formation of two important elements: Carbon ${}^{6}_{12}\mathrm{C}$ and Oxygen ${}^{8}_{16}\mathrm{O}$. Carbon ${}^{6}_{12}\mathrm{C}$ is produced by the nuclear fusion:

$${}^{4}_{8}\mathrm{Be} + {}^{2}_{4}\mathrm{He} \rightarrow {}^{6}_{12}\mathrm{C} + E_k \tag{96}$$

Thus,

$$\frac{\Delta m}{m} = \frac{(m_{b-8} + m_{He-4}) - m_{C-12}}{m_{C-12}} = \frac{(8.00530510 + 4.0026020) - 12}{12} \approx 0.000658925 \tag{97}$$

Substituting $\frac{\Delta m}{m}$ = 0.000658925 in eq. 95 and solving for *z* yields:

$z_h \approx 756$, and $z_l \approx 0.027$ .

Using eq. 90, we have:

$$t_h = \frac{z_h+1}{z_T+1} \text{T} = \frac{756+1}{1089+1} \text{ x } 13.789 \approx 9.6 \text{ BY.} \quad (98)$$

And:

$$t_l = \frac{z_l+1}{z_T+1} \text{T} = \frac{0.027+1}{1089+1} \text{ x } 13.789 \approx 0.013 \text{ BY} = 13 \text{ MY.} \quad (99)$$

For Oxygen ${}^{8}_{16}\text{O}$ , the nuclear fusion reaction is:

$${}^{6}_{12}\text{C} + {}^{2}_{4}\text{He} \rightarrow {}^{8}_{16}\text{O} + E_k \quad (100)$$

Thus,

$$\frac{\Delta m}{m} = \frac{(m_{C-12} + m_{He-4}) - m_{O-16}}{m_{C-12}} = \frac{(12.0107 + 4.002602)\text{u} - 15.9994\text{u}}{15.9994\text{u}} \approx 0.00086891 \quad (101)$$

Substituting $\frac{\Delta m}{m}$ = 0.00086891 in eq. 95 yields:

$z_h \approx 573$, and $z_l \approx 0.031$

Which correspond to:

$$t_h = \frac{573+1}{1089+1} \text{ x } 13.789 \approx 7.26 \text{ BY.} \quad (102)$$

And,

$$t_l = \frac{z_l+1}{z_T+1} \text{T} = \frac{0.031+1}{1089+1} \text{ x } 13.789 \approx 0.013 \text{ BY} = 13 \text{ MY.} \quad (103)$$

The above results are consistent with observations. The low redshift predictions are in agreement with the findings of several survey studies using highly ionized metal absorption lines in ultraviolet, and X-ray spectra. These findings revealed an abundance of Carbon and Oxygen in the Milky Way, at redshift z = 0.027 [50], and of Oxygen at z = 0.031 [179]. Precision tests for the predicted high redshifts are (still) unfeasible, but several survey findings were successful in tracing the formation of Carbon and Oxygen to early epochs, of $z \geq 5$ [180].

The above mentioned predictions are quite interesting, because they imply that Carbon ${}^{6}_{12}\text{C}$ and Oxygen ${}^{8}_{16}\text{O}$, and most probably all chemical elements, were created twice: once in massive galaxy structures in the early universe epochs, at redshifts z > 1.618 (golden ratio), and a second time in the more recent history of the universe, at redshifts $z \leq 1.618$. It is not unrealistic to conjecture

that the ionization of elements at low redshifts is indeed a second-round, or "re-ionization," probably in the internal galaxy of the observer (the Milky Way). Because the analysis applies to an observer in any galaxy, the theory predicts that the process of ionization that took place closer to the Big Bang repeats itself in all galaxies, with their massive black holes playing the role of the Big bang, mother of all black holes.

**9. Relativizing Newton's universal law of gravitation**

For the simple two-body gravitational system, the calculus involved in relativizing Newton's gravitation law is as simple as the one used in the inertial system case. To accomplish consider the two uncharged bodies in Fig. 19. To avoid unnecessary calculations, assume that the mass $m_0$ of the body on the left is distributed uniformly along its length $l_0$ and that there are no other masses to gravitate with any of the two bodies. For an observer in reference frame *F*, at a given time *t* along its movement due to the attraction by mass $M_0$, the "moving" body shown in figure 19 is predicted to stretch along its travel path, and its matter density is predicted to decrease (see equations II and III in Table 1). The mass of a segment *dx* is given by:

$$dm = \rho\, dx = \rho_0 \frac{1+\beta}{1-\beta}\, dx \tag{104}$$

And its attraction force with $M_0$ is given by:

$$dF_{RG} = \mathrm{G}\frac{dm\, M_0}{(r+x)^2} = \mathrm{G}\, M_0\ \rho_0 \frac{1+\beta}{1-\beta}\frac{dx}{(r+x)^2} \tag{105}$$

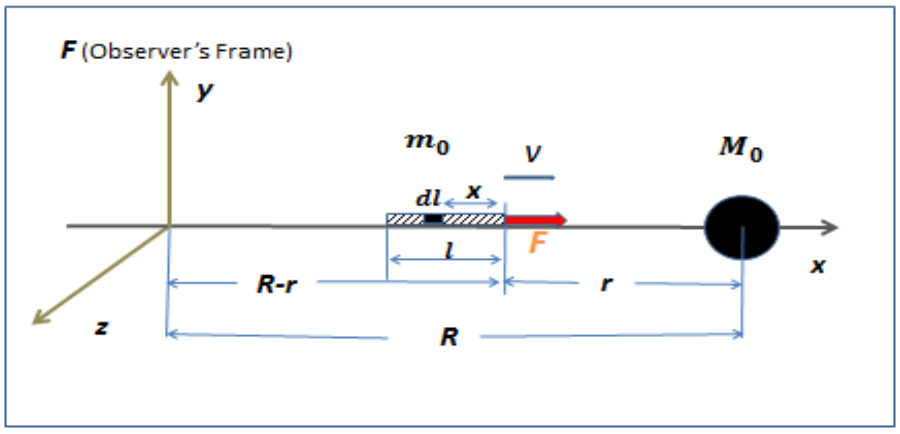


**Figure 19.** Two gravitational bodies in relative motion with respect to each other

The total relativistic gravitational force can be calculated by integrating $dF_R$ over $l$, yielding:

$$F_{RG} = \int_l \quad G\ M_0\ \rho_0\ \frac{1+\beta}{1-\beta}\ \frac{dx}{(r+x)^2} = G\ M_0\ \rho_0\ \frac{1+\beta}{1-\beta} \int_{x=r}^{x=r+l} \quad \frac{dx}{(r+x)^2}$$

$$= \ G\ M_0\ \rho_0\ \frac{1+\beta}{1-\beta}\left(\frac{1}{r} - \frac{1}{r+l}\right) = G\ M_0\ \rho_0\ \left(\frac{1+\beta}{1-\beta}\right)\frac{r+l-r}{r\ (r+l)}$$

$$= \ G\ M_0\ \rho_0\left(\frac{1+\beta}{1-\beta}\right)\frac{l}{r\ (r+l)} = G\ M_0\ \rho_0\left(\frac{1+\beta}{1-\beta}\right)\frac{l}{r^2\ (1+\frac{l}{r})}$$

$$= \text{G}\ \frac{M_0\ \rho_0}{r^2}\left(\frac{1-\beta}{1+\beta}\right)\frac{l_0\frac{1+\beta}{1-\beta}}{r^2\left(1+\frac{l}{r}\right)} = \text{G}\ \frac{M_0\ \rho_0 l_0}{r^2}\ \frac{1}{r^2\ (1+\frac{l}{r})} = \text{G}\ \frac{M_0\ m_0}{r^2}\ \ \frac{1}{1+\frac{l}{r}}$$

$$= \text{G}\ \frac{M_0\ m_0}{r^2}\ \ \frac{1}{1+\frac{l_0}{r}\left(\frac{1+\beta}{1-\beta}\right)} \tag{106}$$

Or:

$$F_{RG} = \frac{1}{1+\frac{l_0}{r}\left(\frac{1+\beta}{1-\beta}\right)}\ F_N \tag{107}$$

Fig. 20 depicts a three-dimensional graph of the ratio $\frac{F_{RG}}{F_N}$ as a function of the velocity β and the ratio $\frac{l_0}{r}$. A cross-section for selected $\frac{l_0}{r}$ values appears in Fig. 21. For stationary bodies (β =0), the classic law is recovered as long as the $l_0$/r is sufficiently small. For approaching bodies, the relativistic gravitational force is weaker than the classic force. It decreases with an increase of the ratio $\frac{l_0}{r}$. As shown in the figures, for very small $\frac{l_0}{r}$ ratios (small body dimensions relative to the distance *r* from the attracting mass), at all velocities, the relativistic force is very close to the classic Newtonian force. For large body dimensions relative to the distance *r* the relativistic force is predicted to reduce significantly, particularly at high approach velocities.

For velocities close to the velocity of light, the obtained result predicts a complete breakdown of gravitation. As $\beta$ approaches 1, the relativistic gravitational force goes down to zero. This theoretical result, derived solely from simple relativistic consideration, is in complete agreement with the important phenomenon occurring at strong interactions known as *asymptotic freedom* [181-182].

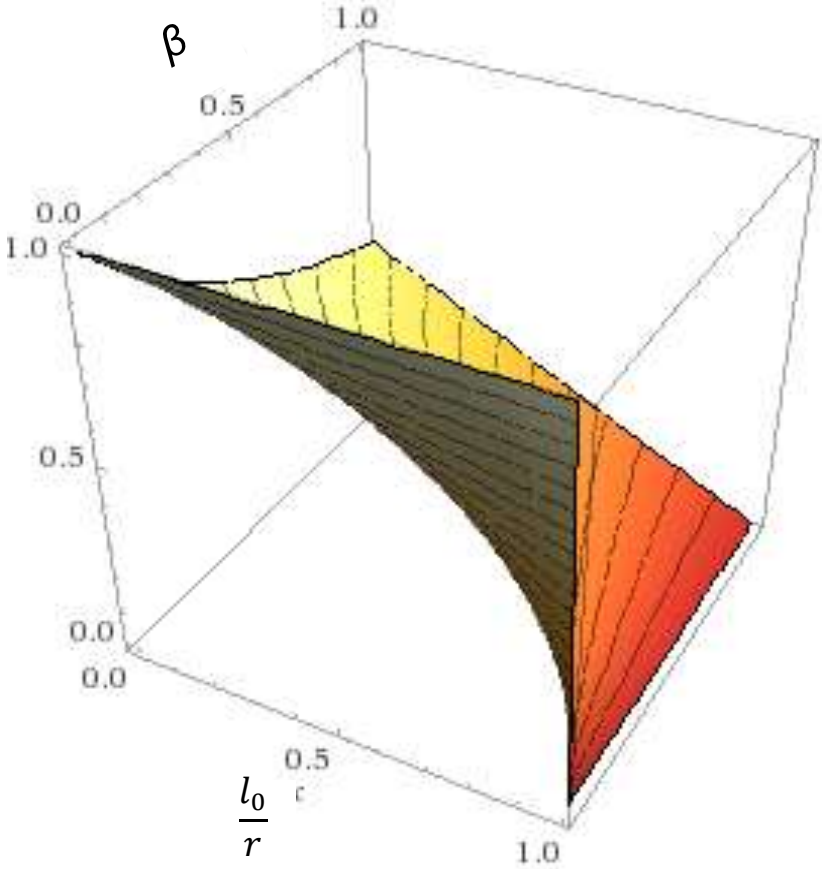


**Figure 20.** $\frac{F_{RG}}{F_N}$ as a function of the velocity β and the ratio $\frac{l_0}{r}$

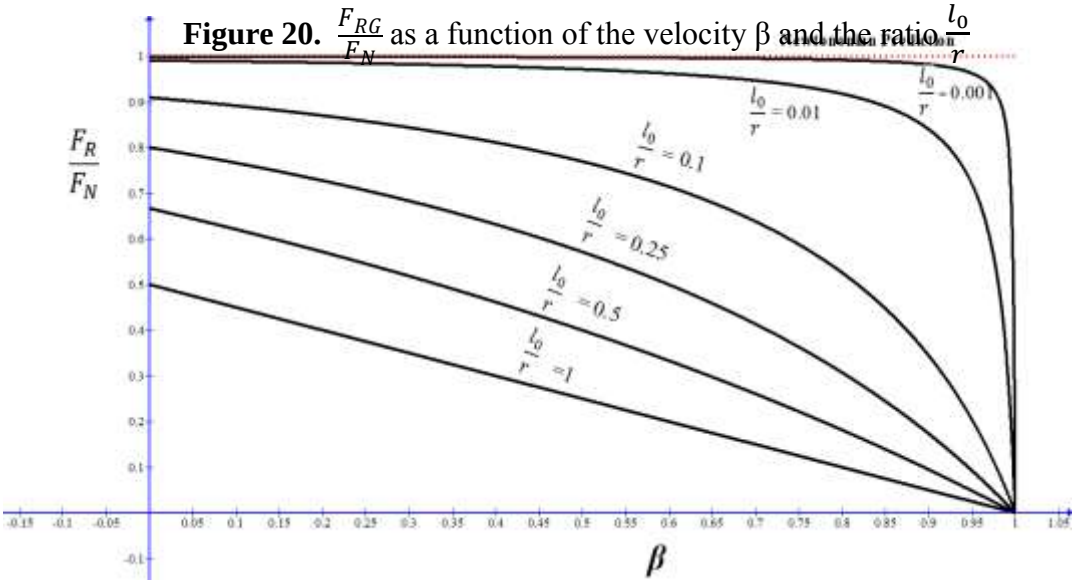


**Figure 21.** $\frac{F_{RN}}{F_N}$ as a function of the velocity for selected $\frac{l_0}{r}$ values

**9.1 Velocity as a function of distance from a gravitating body**

Without loss of generality, assume that at $t = 0$ the mass $m$ was at rest ($\beta_0 = 0$) at $r = R$ before it started moving due to its attraction by mass $M_0$. As $m$ moves along the horizontal axis, it will accelerate. At distance r from $M_0$, the incremental increase in its kinetic energy is given by:

$$de_k = dW = \boldsymbol{F}.\,\boldsymbol{d}r \tag{108}$$

Where $dW$ is the work done by the gravitational force $\boldsymbol{F}$ along the segment $\boldsymbol{dr}$. Using the kinetic energy transformation (see Table 1), we can write:

$$F = \frac{de_k}{dr} = \frac{de_k}{d\beta}\frac{d\beta}{dr} = \frac{1}{2} m_0 c^2 \frac{d\left(\frac{1-\beta}{1+\beta}\beta^2\right)}{d\beta}\frac{d\beta}{dr}$$

$$= m_0 c^2 \frac{(1-\beta-\beta^2)\beta}{(1+\beta)^2}\frac{d\beta}{dr} \tag{109}$$

Equating the expressions in equations 107 and 109, we get:

$$m_0 c^2 \frac{(1-\beta-\beta^2)\beta}{(1+\beta)^2}\frac{d\beta}{dr} = \mathrm{G}\frac{M_0 m_0}{r^2}\frac{1}{1+\frac{l_0}{r}\left(\frac{1+\beta}{1-\beta}\right)} \tag{110}$$

Which can be re-written as:

$$\frac{(1-\beta-\beta^2)\beta}{(1+\beta)^2}d\beta = \frac{G M_0}{c^2}\frac{\frac{dr}{r^2}}{1+\frac{l_0}{r}\left(\frac{1+\beta}{1-\beta}\right)} \tag{111}$$

For the case $\frac{l_0}{r} << 1$ the general term above reduces to:

$$\frac{(1-\beta-\beta^2)\beta}{(1+\beta)}d\beta = \frac{G M_0}{c^2}\frac{dr}{r^2} \tag{112}$$

Integrating on the path from $x=R$ (starting point) to x= $R$-$r$ (boundaries of $M_0$), we get:

$$\int_0^{\beta}\frac{(1-\beta-\beta^2)\beta}{(1+\beta)}d\beta = \frac{G M_0}{c^2}\int_R^{R-r}\frac{dr}{r^2} \tag{113}$$

Performing the integration gives:

$$(\beta(\beta+2)+ln(\frac{1-\beta}{1+\beta}))^2 = \frac{G M_0}{c^2}\left(\frac{1}{r}-\frac{1}{R}\right) \tag{114}$$

Solving for $\beta$ (after some calculations) gives:

$$\beta = -\frac{1-e^{\frac{G M_0}{c^2}\left(\frac{1}{r}-\frac{1}{R}\right)}}{1+e^{\frac{G M_0}{c^2}\left(\frac{1}{r}-\frac{1}{R}\right)}} = \tanh\left(\frac{1}{2}\frac{G M_0}{c^2}\left(\frac{1}{r}-\frac{1}{R}\right)\right) \tag{115}$$

Substituting $\frac{G M_0}{c^2} = \frac{R_{Sch}}{2}$, where $R_{Sch}$ is defined as the Schwarzschild radius of the attracting mass $M_0$, we can write:

$$\beta = \tanh\left(\frac{1}{4}\frac{R_{Sch}}{R}\left(\frac{R}{r} - 1\right)\right) \tag{116}$$

Fig. 22 depicts the velocity $\beta$ as a function of $\frac{r}{R}$ for selected $\frac{R_{Sch}}{R}$ values.

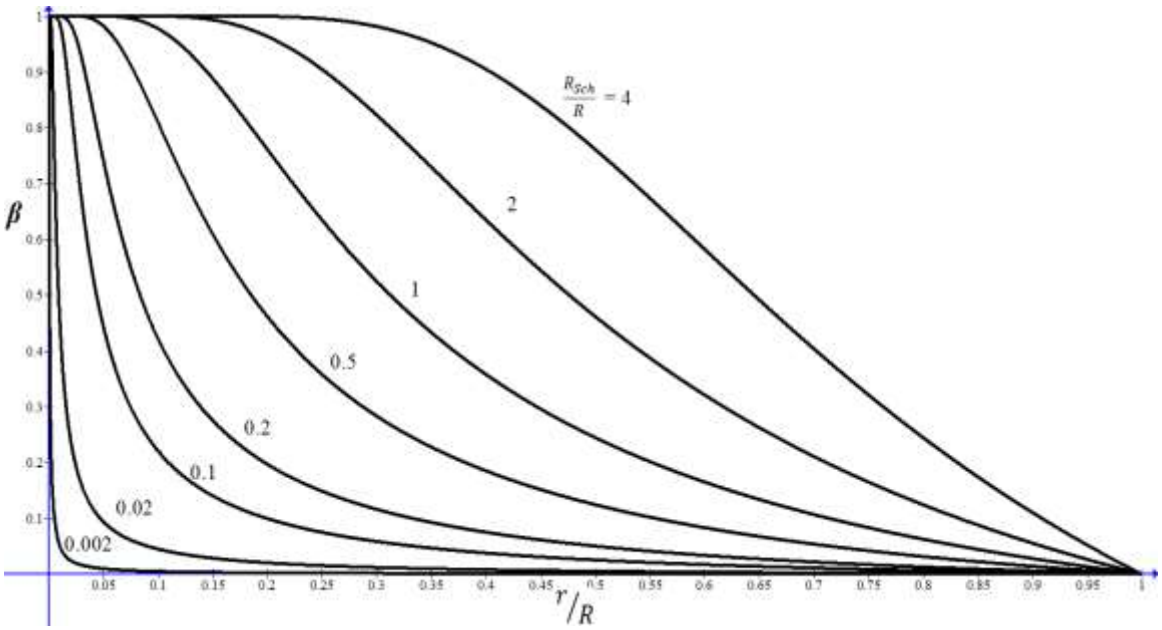


**Figure 22.** Velocity $\beta$ as a function of $\frac{r}{R}$ for selected $\frac{R_{Sch}}{R}$ values.

As shown in the figure, for a given dimension $R$ of the system, as the distance from the attracting mass $M_0$ becomes smaller, the velocity increases quite sharply when approaching $\beta$ =1 as r→0, and the predicted increase in velocity is steeper for larger attracting masses (larger $R_{Sch}$).

**9.2 Time duration and length transformations in a body's gravitational field**

Using the transformations in Table 1, we can write the gravitational transformations for time duration and length as:

$$\left(\frac{\Delta t}{\Delta t_0}\right)_G = \frac{1}{1-\beta} = \frac{1}{1-\beta_0-\tanh\left(\frac{1}{4}\frac{R_{Sch}}{R}\left(\frac{R}{r}-1\right)\right)} \tag{117}$$

And

$$\left(\frac{l}{l_0}\right)_G = \frac{1+\beta}{1-\beta} = \frac{1+\beta_0+\tanh\left(\frac{1}{4}\frac{R_{Sch}}{R}\left(\frac{R}{r}-1\right)\right)}{1-\beta_0-\tanh\left(\frac{1}{4}\frac{R_{Sch}}{R}\left(\frac{R}{r}-1\right)\right)} \tag{118}$$

For $\beta_0$ = 0, we get:

$$\left(\frac{\Delta t}{\Delta t_0}\right)_G = \frac{1}{1-tanh\left(\frac{1}{4}\frac{R_{Sch}}{R}\left(\frac{R}{r}-1\right)\right)} = \frac{1}{2}\left(e^{\left(\frac{1}{2}\frac{R_{Sch}}{R}\left(\frac{R}{r}-1\right)\right)}+1\right) \quad (119)$$

And:

$$\left(\frac{l}{l_0}\right)_G = \frac{1+\beta}{1-\beta} = \frac{1+tanh\left(\frac{1}{4}\frac{R_{Sch}}{R}\left(\frac{R}{r}-1\right)\right)}{1-tanh\left(\frac{1}{4}\frac{R_{Sch}}{R}\left(\frac{R}{r}-1\right)\right)} = e^{\left(\frac{R_{Sch}}{R}\left(\frac{R}{r}-1\right)\right)} \quad (120)$$

The relationships in equations 119 and 120 are depicted in figures 23 and 24, respectively.

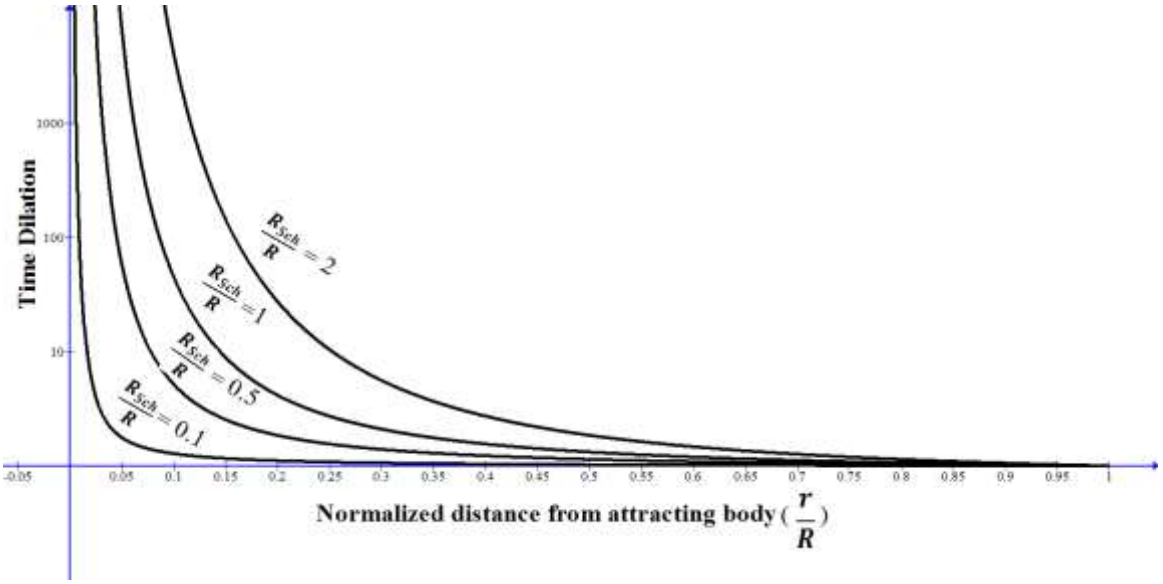


**Figure 23**. Time dilation as function of distance from attracting body

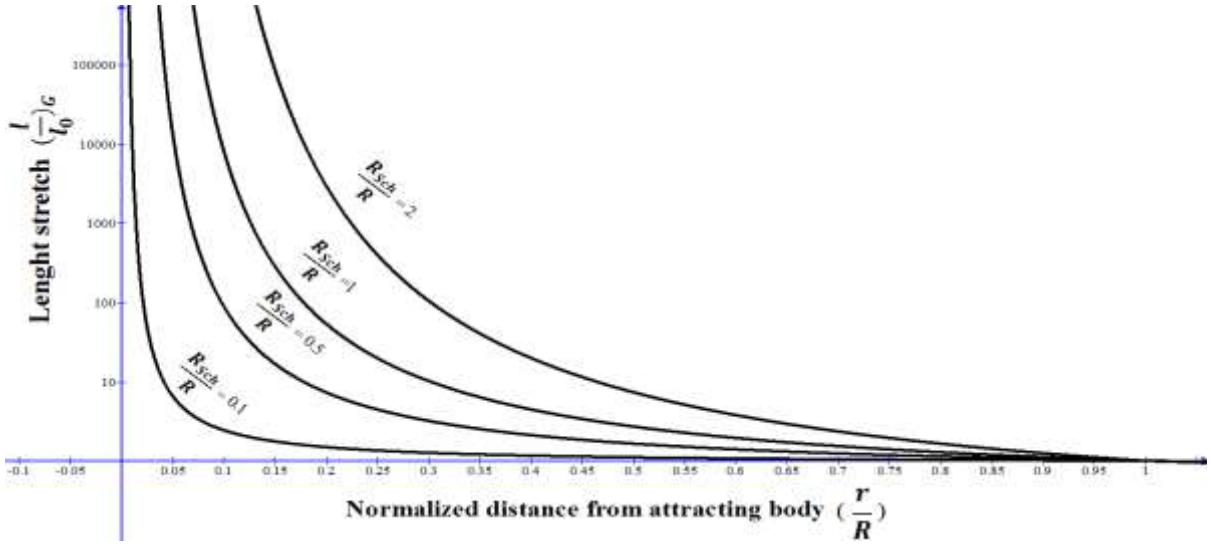


**Figure 24**. Length stretch as function of distance from attracting body

### 9.3 Relativistic force as a function of distance from a gravitating body

Substituting the expression for $\beta$ from eq. 116 in the relativistic gravitation force expression in eq. 107 and simplifying gives:

$$F_{RG} = \mathrm{G}\ \frac{M_0\ m_0}{r^2}\ \frac{1}{1+\frac{l_0}{r}e^{\frac{G\,M_0}{c^2}(\frac{1}{r}-\frac{1}{R})}} = \mathrm{G}\ \frac{M_0\ m_0}{r^2}\ \frac{1}{1+\frac{l_0}{r}e^{\frac{R_{Sch}}{2}(\frac{1}{r}-\frac{1}{R})}}$$

$$= \frac{1}{1+\frac{l_0}{r}e^{\frac{R_{Sch}}{2}(\frac{1}{r}-\frac{1}{R})}}\ F_N \qquad (121)$$

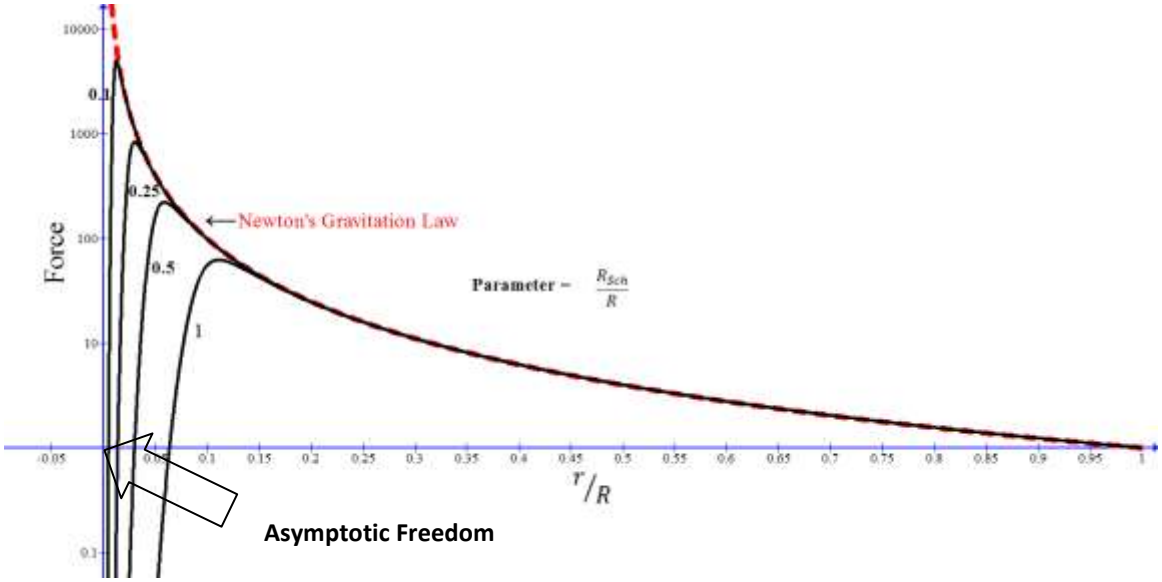


**Figure 25**. Gravitational force as function of the distance from attracting body

Figure 25 depicts the classic gravitational force as a function of the distance between two gravitating bodies alongside of its relativistic extension plotted for selected $\frac{l_0}{r}$ values. As could be seen from q. 121 and Fig. 25, at long distances from the gravitating body the relativistic force is almost equal to the Newtonian term. Strikingly, as the moving body gains more velocity while it approaches the attracting mass, the gravitational force drops sharply below the value predicted by Newton's law, reaching zero as the distance approaches zero. As noted above, this counterintuitive prediction is in complete agreement with quantum-theoretic explanation of *asymptotic freedom* [181-182], a demonstrated phenomenon [e.g., 183-184], which according to gauge theories results from an asymptotic decrease in the bonds between particles as energy increases and distance decreases. The region of asymptotic freedom emerges also in the following analysis of the moving body's kinetic energy during its travel towards the attractor $M_0$.

### 9.4 Matter-wave duality in a gravitational field

To calculate the expression for the matter kinetic energy, we substituted the value of β from eq. 116 in the energy equation in Table 1. After simplification we get:

$$\frac{e_K}{e_0} = e^{\frac{R_{Sch}}{R}} \frac{(e^{\frac{R_{Sch}}{r}} - e^{\frac{R_{Sch}}{R}})^2}{(e^{\frac{R_{Sch}}{r}} - e^{\frac{R_{Sch}}{R}})^3} \tag{122}$$

And the dual (pilot) wave energy as a function of the distance $r$ is given by:

$$\frac{e_W}{e_0} = \beta^2 - \frac{e_k}{e_0} = \beta^2 - e^{\frac{R_{Sch}}{R}} \frac{(e^{\frac{R_{Sch}}{r}} - e^{\frac{R_{Sch}}{R}})^2}{(e^{\frac{R_{Sch}}{r}} + e^{\frac{R_{Sch}}{R}})^3} \tag{123}$$

Substituting the value of β from Eq. 116 we get:

$$\frac{e_W}{e_0} = \beta^2 - \frac{e_k}{e_0} = tanh(\frac{1}{4} R_{Sch}(\frac{1}{r} - \frac{1}{R}))^2 - e^{\frac{R_{Sch}}{R}} \frac{(e^{\frac{R_{Sch}}{r}} - e^{\frac{R_{Sch}}{R}})^2}{(e^{\frac{R_{Sch}}{r}} + e^{\frac{R_{Sch}}{R}})^3} \tag{124}$$

Fig. 26 depicts the kinetic energy and dual wave energy of mass "$m_0$" for a "large" and a "small" gravitating mass (with $\frac{R_{Sch}}{R} = 1$ and 0.1, respectively).

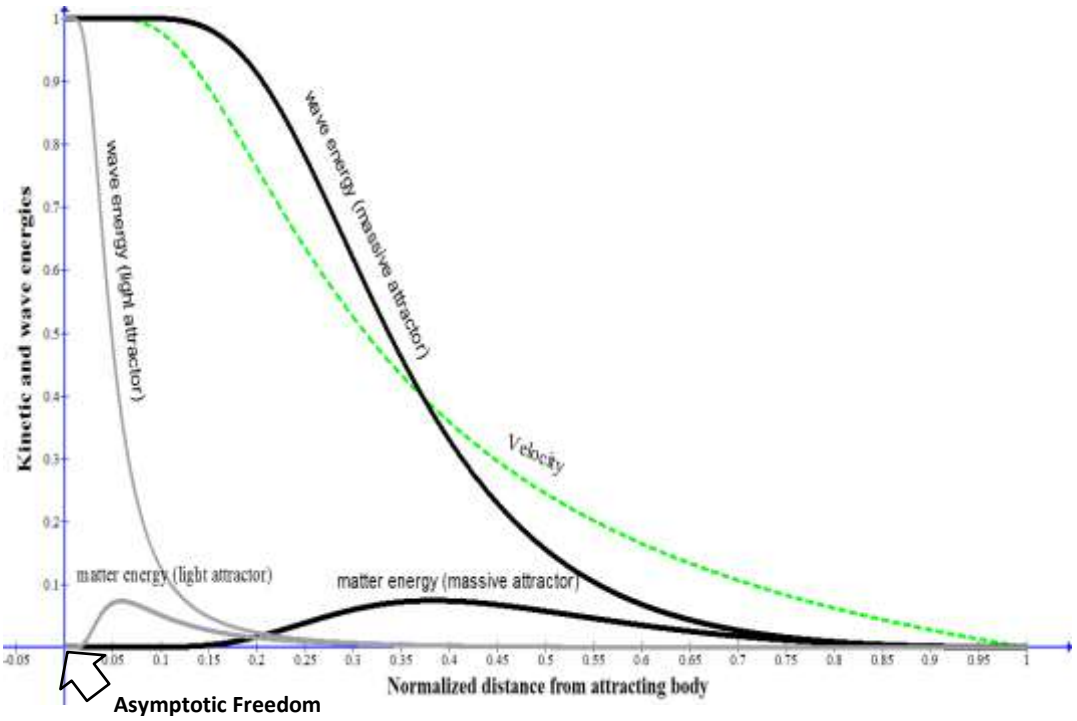


**Figure 26.** Matter and wave energies as functions of the distance from the attracting mass

The figure reveals some interesting features of the predicted matter-wave dynamics. As $m_0$ approaches $M_0$, the wave energy increases with acceleration, reaching the maximal value of $e_W = e_0$ at $r$ = 0, with the increase in wave energy being larger the larger the mass of the

attractor (the larger $\frac{R_{Sch}}{R}$) is. The kinetic energy of $m_0$ displays a non-monotonic pattern in its dependence on the proximity to the attractor. It increases at large normalized distances $\frac{r}{R}$, behaving somewhat classically, reaching a maximum after which classic physics breaks down, such that a further decrease in the distance from the attractor results in a decrease in kinetic energy, reaching zero as r → 0. Maximum kinetic energy is attained at a critical distance $r_{cr,}$ satisfying $\frac{\partial e_K}{\partial r}$ (r = $r_{cr}$)= 0. Performing the differentiation yields the following simple equation:

$$\frac{r_{cr}}{R_{Sch}} = \frac{1}{\frac{R_{Sch}}{R} + ln(5)} \tag{125}$$

For very large $\frac{R_{Sch}}{R}$ values we have $\frac{r_{cr}}{R} \approx 1$, while for $\frac{R_{Sch}}{R} \ll ln(5)$, $\frac{r_{cr}}{R} \approx \frac{\frac{R_{Sch}}{R}}{ln(5)} \approx 0.62133494$. Substituting $\frac{r_{cr}}{R_{Sch}}$ in Eq. 122, we get:

$$(\frac{e_K}{e_0})_{max} = e^{\frac{R_{Sch}}{R}} \frac{(e^{\ln(5)+\frac{R_{Sch}}{R}} - e^{\frac{R_{Sch}}{R}})^2}{(e^{ln\,(5)} + \frac{R_{Sch}}{R} + e^{\frac{R_{Sch}}{R}})^3} = \frac{e^{\frac{R_{Sch}}{R}} e^{2\frac{R_{Sch}}{R}} (e^{ln\,(5)} - 1)^2}{e^{3\frac{R_{Sch}}{R}} (e^{ln\,(5)} + 1)^3}$$

$$= \frac{(e^{ln\,(5)} - 1)^2}{(e^{ln\,(5)} + 1)^3} = \frac{2}{27}! \; (\approx 0.074074074074074\ldots) \tag{126}$$

Or:

$$(e_K)_{max} = \frac{2}{27} e_0 = \frac{2}{27} \frac{1}{2} \rho_0 \; c^2 = \frac{1}{27} \rho_0 \; c^2 \tag{127}$$

Strikingly, the maximal kinetic energy attained by $m_0$ is the same for all values $\frac{R_{Sch}}{R}$ (see figure). Moreover, the wave energy at the points of maximal kinetic energy is 5 times higher than the maximal kinetic energy (≈ 0.3704).

Fig. 27 depicts the proportions of matter and wave energies as functions of the normalized distance from the attracting mass $\frac{r}{R}$ for masses with normalized Schwarzschild radii $\frac{R_{Sch}}{R}$ of 1 (large) and 0.1 (small), respectively. As the figure shows, for any $\frac{R_{Sch}}{R} \neq 0$ there exists a critical distance at which the ratios of matter and wave energies are equal. That is a distance at which $\frac{e_K}{e_K + e_w} = \frac{e_w}{e_K + e_w} = \frac{1}{2}$. Substitution of the values of $e_k$ and $e_w$ from equations 122 and 124, and simplifying yields:

$$\frac{e^y (e^y - 1)^2}{(e^y + 1)^3} = \frac{1}{2} \tag{128}$$

Where y = $\frac{R_{Sch}}{R}\left(\frac{1}{\frac{r}{R}} - 1\right)$. Solving Eq. 128 for y yields y ≈ 1.9684, which corresponds to:

$$\frac{r}{R} = \frac{\frac{R_{Sch}}{R}}{\frac{R_{Sch}}{R} + y} \approx \frac{\frac{R_{Sch}}{R}}{\frac{R_{Sch}}{R} + 1.9684} \tag{129}$$

For $\frac{R_{Sch}}{R}$ = 1, substitution in the equation above gives: $\frac{r}{R} = \frac{\frac{R_{Sch}}{R}}{\frac{R_{Sch}}{R} + y} \approx \frac{1}{1 + 1.9684} \approx 0.336882$, and for $\frac{R_{Sch}}{R}$ = 0.1 we get: $\frac{r}{R} \approx \frac{0.1}{0.1 + 1.9684} \approx 0.048347$.

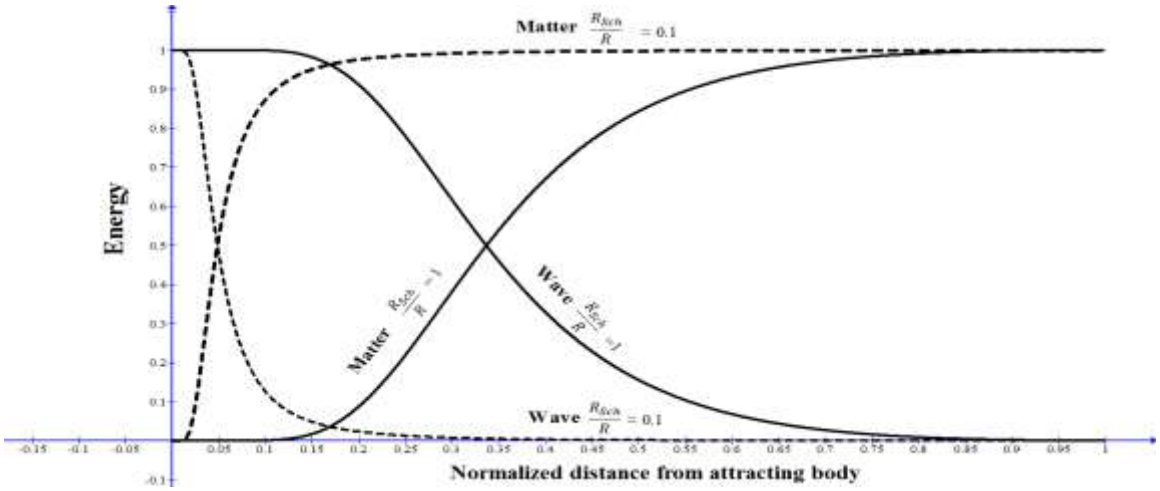


**Figure 27.** Ratios of matter and wave energies as functions of distance from a gravitating mass

### 9.5 Summary of main results

Table 6 summarizes the main predictions for the discussed two-body gravitational system. The picture emerging from the predicted matter-wave dynamics is the following: Assuming a closed gravitational two-body system with rest-masses $M_0$ and $m_0$, distanced by $R$, which start moving towards each other (from rest) due to gravitation. For an observer in F (the rest frame of $M_0$), Information Relativity theory predicts that as $m_0$ $approaches$ $M_0$, the wave energy of "$m_0$ will first increase with acceleration and then with deceleration leveling to $e_W = e_0 = \frac{1}{2}\rho_0 c^2$ at very short distances from $M_0's$ boundary. The matter (kinetic) energy is predicted to first increase with a decrease in distance up to a maximum reached at a critical distance determined by the spatial dimension of the system $R$ and the Schwarzschild radius of the gravitating mass (see eq. 122 and fig. 26). For shorter distances the kinetic energy decreases continually until it reaches zero at $r$ =0, where the two masses are predicted to move freely without any gravitational pull between them. Surprisingly, while the point of maximum kinetic energy density "shifts" closer to the gravitating body as its mass becomes smaller, the maximum kinetic energy remains constant at $(e_K)_{max} = \frac{2}{27} e_0$ (= $\frac{1}{27}\rho_0 c^2$).

**Table 6**

**Summary of main results**

| Physical Term | Relativistic expression as function of the distance *r* from the gravitating mass |
|---|---|
| Velocity (from rest) | $\beta = -\frac{1-e^{\frac{G M_0}{c^2}(\frac{1}{r}-\frac{1}{R})}}{1+e^{\frac{G M_0}{c^2}(\frac{1}{r}-\frac{1}{R})}} = \tanh(\frac{1}{4}\frac{R_{Sch}}{R}(\frac{R}{r} - 1))$ |
| Time dilation | $(\frac{\Delta t}{\Delta t_0})_G = \frac{1}{2}\ (e^{(\frac{1}{2}\frac{R_{Sch}}{R}(\frac{R}{r}-1))} + 1) = \frac{1}{1-tanh(\frac{1}{4}\frac{R_{Sch}}{R}(\frac{R}{r}-1))}$ |
| Length extension | $(\frac{l}{l_0})_G = e^{(\frac{R_{Sch}}{R}(\frac{R}{r}-1))} = \frac{1+tanh(\frac{1}{4}\frac{R_{Sch}}{R}(\frac{R}{r}-1))}{1-tanh(\frac{1}{4}\frac{R_{Sch}}{R}(\frac{R}{r}-1))}$ |
| Mass density | $(\frac{\rho}{\rho_0})_G = \frac{1}{e^{(\frac{R_{Sch}}{R}(\frac{R}{r}-1))}} = \frac{1-tanh(\frac{1}{4}\frac{R_{Sch}}{R}(\frac{R}{r}-1))}{1+tanh(\frac{1}{4}\frac{R_{Sch}}{R}(\frac{R}{r}-1))}$ |
| Force | $F_{RN} = \mathrm{G}\ \frac{M_0\ m_0}{r^2}\ \frac{1}{1+\frac{l_0}{r}e^{\frac{R_{Sch}}{2}(\frac{1}{r}-\frac{1}{R})}}$ |
| Kinetic energy density | $\frac{e_K}{e_0} = e^{\frac{R_{Sch}}{R}}\frac{(e^{\frac{R_{Sch}}{r}}-e^{\frac{R_{Sch}}{R}})^2}{(e^{\frac{R_{Sch}}{r}}+e^{\frac{R_{Sch}}{R}})^3}$ |
| Accompanying wave energy density | $\frac{e_W}{e_0} = tanh(\frac{1}{4}R_{Sch}(\frac{1}{r} - \frac{1}{R}))^2 - e^{\frac{R_{Sch}}{R}}\frac{(e^{\frac{R_{Sch}}{r}}-e^{\frac{R_{Sch}}{R}})^2}{(e^{\frac{R_{Sch}}{r}}+e^{\frac{R_{Sch}}{R}})^3}$ |
| Critical distance at which the proportion of matter and wave energies are equal | $\frac{r}{R} \approx \frac{\frac{R_{Sch}}{R}}{\frac{R_{Sch}}{R}+1.9684}$ |
| Critical distance at which matter KE is maximal | $\frac{r_{cr}}{R_{Sch}} = \frac{1}{\frac{R_{Sch}}{R}+ln(5)} \approx \frac{1}{\frac{R_{Sch}}{R}+1.6094}$ |
| Maximal kinetic energy | $(e_K)_{max} = \frac{2}{27}\ e_0 = \frac{1}{27}\ \rho_0\ c^2$ |

Inspection of the ratios of matter and wave energies out of the total energy (see fig. 27), provides insight into the dynamics between the two energy carrier components. At normalized distances exceeding a critical $\frac{r}{R}$ ratio, which is determined completely by the ratio $\frac{R_{Sch}}{R}$ (see eq. 129), the matter kinetic energy dominates its dual wave energy, while at normalized distances $\frac{r}{R}$ below the critical distance, the dual-wave's energy dominates the matter energy. In de Broglie's terminology, we may say that at distances above the critical distance the matter might guide the wave, whereas at distances below the critical value, the dual wave takes the lead and pilots its dual matter.

It is worth noting that by setting $M_0$= 0 ($R_{sch}$ = 0), all the transformations of in the table reduce to the transformations derived for inertial systems, which in turn reduce to the classical Newtonian terms for β = $\frac{v}{c}$ << 1. For example, setting $R_{sch}$ = 0 in Eq. 117 gives: $\frac{\Delta t}{\Delta t_0} = \frac{1}{1-\beta_0-tanh(0)} = \frac{1}{1-\beta_0}$, which for $\beta_0$ << 1 gives $\frac{\Delta t}{\Delta t_0}$ = 1. Similarly, the velocity term after the elimination of gravity gives $\beta = \beta_0 + tanh(0) = \beta_0$, and the kinetic energy becomes $e_k = e_0 \frac{1-\beta_0}{1+\beta_0} {\beta_0}^2$, which for $\beta_0$ << 1 gives $e_k = e_0 {\beta_0}^2 = \frac{1}{2} \rho_0 c^2 (\frac{v}{c})^2 = \frac{1}{2} \rho_0 v^2$.

**10. Relativizing Coulomb's law**

The classical Coulomb's law of the electrostatic force between two charged bodies is given by:

$$F_E = k_e \frac{q_1 q_2}{r^2} \tag{130}$$

Where $F_e$ is the electrostatic force, $k_e$ is Coulomb's electrostatic constant ($k_e$= 8.99 x $10^9$ $N m^2/C^2$), $q_1$ and $q_2$ are the charges of respective charged bodies, *r* is the distance between the two particles. For a two-body system like the one described in fig. 19, assume that the body with rest mass $m_0$ has a negative rest charge of - $q_0$, and the body with rest mass $M_0$ has a positive rest charge of $Q_0$. Also, assume that in the rest-frame of an observer, the electric charge of a "moving" body will distribute uniformly along its "stretched" physical dimension. The complete equivalence between Coulomb's law of electrostatic force and Newton's law of gravitation, implies that the derivation of the laws of motion of a negatively charged body in the rest-frame of a positively charged, in the rest-frame of the latter could be easily written by mimicking the derivation described in the previous section for the gravitational field. Thus, what seems very hard to achieve in quantum gravity or even in QCD theories, is floating on the surface of our theory.

Similarly, to eq. 106, the relativistic electrostatic force could be written as:

$$F_{RE} = k_e \frac{Q_0 \, q_0}{r^2} \quad \frac{1}{1+\frac{l_0}{r}(\frac{1+\beta}{1-\beta})} \tag{131}$$

Also, similarly to eq. 110, we can write:

$$m_0\, c^2\, \frac{(1-\beta-\beta^2)\,\beta}{(1+\beta)^2}\ \frac{d\beta}{dr}\ =\ k_e\, \frac{Q_0\ q_0}{r^2}\ \ \frac{1}{1+\frac{l_0}{r}(\frac{1+\beta}{1-\beta})} \tag{132}$$

Which can be re-written as:

$$\frac{(1-\beta-\beta^2)\,\beta}{(1+\beta)^2}\ d\beta\ =\ \frac{k_e\, Q_0\ q_0}{m_0\, c^2}\ \frac{\frac{dr}{r^2}}{1+\frac{l_0}{r}(\frac{1+\beta}{1-\beta})} \tag{133}$$

For the case $\frac{l_0}{r}$ << 1 the general term above reduces to:

$$\frac{(1-\beta-\beta^2)\,\beta}{(1+\beta)}\ d\beta\ =\frac{k_e\, Q_0\ q_0}{m_0\, c^2}\ \frac{dr}{r^2} \tag{134}$$

Integrating on the path from *x*=*R* (starting point) to x= *R*-*r* (boundaries of $M_0$), we get:

$$\int_0^{\beta} \frac{(1-\beta-\beta^2)\,\beta}{(1+\beta)}\ d\beta\ \ =\frac{k_e\, Q_0\ q_0}{m_0\, c^2}\ \int_R^{R-r}\ \frac{dr}{r^2} \tag{135}$$

Performing the integration gives:

$$(\beta\ (\beta+2)+ln(\tfrac{1-\beta}{1+\beta}))^2 = \frac{k_e\, Q_0\ q_0}{m_0\, c^2}\ (\frac{1}{r}\ -\ \frac{1}{R}) \tag{136}$$

Solving for $\beta$ (after some calculations) gives:

$$\beta = -\frac{1-e^{\frac{k_e\, Q_0\ q_0}{m_0\, c^2}(\frac{1}{r}-\frac{1}{R})}}{1+e^{\frac{k_e\, Q_0\ q_0}{m_0\, c^2}(\frac{1}{r}-\frac{1}{R})}} = \tanh(\frac{1}{2}\frac{k_e\, Q_0\ q_0}{m_0\, c^2}\ (\frac{1}{r}\ -\ \frac{1}{R})) \tag{137}$$

**10.1 Time duration and length transformations in a charged particle's electrostatic field**

Using the transformations in Table 1, we can write the relativistic time and d transformations for time duration and length in an electrostatic field as:

$$(\frac{\Delta t}{\Delta t_0})_{RE}\ =\ \frac{1}{1-\beta}\ =\ \ \frac{1}{1-\beta_0-\tanh(\frac{1}{2}\frac{k_e\, Q_0\ q_0}{m_0\, c^2}(\frac{1}{r}-\frac{1}{R}))} \tag{138}$$

And

$$(\frac{l}{l_0})_{RE}\ =\frac{1+\beta}{1-\beta}=\frac{1+\beta_0+\tanh(\frac{1}{2}\frac{k_e\, Q_0\ q_0}{m_0\, c^2}(\frac{1}{r}-\frac{1}{R}))}{1-\beta_0+\tanh(\frac{1}{2}\frac{k_e\, Q_0\ q_0}{m_0\, c^2}(\frac{1}{r}-\frac{1}{R}))} \tag{139}$$

For $\beta_0$ = 0, we get:

$$\left(\frac{\Delta t}{\Delta t_0}\right)_{RE} = \frac{1}{1-\tanh\left(\frac{1}{2}\frac{k_e Q_0 q_0}{m_0 c^2}\left(\frac{1}{r}-\frac{1}{R}\right)\right)} = \frac{1}{2}\left(e^{\frac{k_e Q_0 q_0}{m_0 c^2}\left(\frac{1}{r}-\frac{1}{R}\right)} + 1\right) \quad (140)$$

And:

$$\left(\frac{l}{l_0}\right)_{RE} = \frac{1+\beta}{1-\beta} = \frac{1+\tanh\left(\frac{1}{2}\frac{k_e Q_0 q_0}{m_0 c^2}\left(\frac{1}{r}-\frac{1}{R}\right)\right)}{1-\tanh\left(\frac{1}{2}\frac{k_e Q_0 q_0}{m_0 c^2}\left(\frac{1}{r}-\frac{1}{R}\right)\right)} = e^{\frac{k_e Q_0 q_0}{m_0 c^2}\left(\frac{1}{r}-\frac{1}{R}\right)} \quad (141)$$

**10.2 Matter-wave duality of a body moving in an electrostatic field**

To calculate the expression for the matter kinetic energy, we substituted the value of β from eq. 137 in the energy equation in Table 1, yielding:

$$\frac{e_K}{e_0} = \frac{1-\beta}{1+\beta} \quad \beta^2 = \frac{1-\tanh\left(\frac{1}{2}\frac{k_e Q_0 q_0}{m_0 c^2}\left(\frac{1}{r}-\frac{1}{R}\right)\right)}{1+\tanh\left(\frac{1}{2}\frac{k_e Q_0 q_0}{m_0 c^2}\left(\frac{1}{r}-\frac{1}{R}\right)\right)} \quad \left(\tanh\left(\frac{1}{2}\frac{k_e Q_0 q_0}{m_0 c^2}\left(\frac{1}{r}-\frac{1}{R}\right)\right)\right)^2$$

$$= \frac{\left(e^{\frac{k_e Q_0 q_0}{m_0 c^2}\left(\frac{1}{r}-\frac{1}{R}\right)}-1\right)^2}{\left(e^{\frac{k_e Q_0 q_0}{m_0 c^2}\left(\frac{1}{r}-\frac{1}{R}\right)}+1\right)^2} \; e^{-\frac{k_e Q_0 q_0}{m_0 c^2}\left(\frac{1}{r}-\frac{1}{R}\right)} \quad (142)$$

And the dual (pilot) wave energy as a function of the distance *r* is given by:

$$\frac{e_W}{e_0} = \beta^2 - \frac{e_k}{e_0} = \beta^2 - \frac{\left(e^{\frac{k_e Q_0 q_0}{m_0 c^2}\left(\frac{1}{r}-\frac{1}{R}\right)}-1\right)^2}{\left(e^{\frac{k_e Q_0 q_0}{m_0 c^2}\left(\frac{1}{r}-\frac{1}{R}\right)}+1\right)^2} \; e^{-\frac{k_e Q_0 q_0}{m_0 c^2}\left(\frac{1}{r}-\frac{1}{R}\right)} \quad (143)$$

Substituting the value of β from Eq. 116 we get:

$$\frac{e_W}{e_0} = \left(-\frac{1-e^{\frac{k_e Q_0 q_0}{m_0 c^2}\left(\frac{1}{r}-\frac{1}{R}\right)}}{1+e^{\frac{k_e Q_0 q_0}{m_0 c^2}\left(\frac{1}{r}-\frac{1}{R}\right)}}\right)^2 - \frac{\left(e^{\frac{k_e Q_0 q_0}{m_0 c^2}\left(\frac{1}{r}-\frac{1}{R}\right)}-1\right)^2}{\left(e^{\frac{k_e Q_0 q_0}{m_0 c^2}\left(\frac{1}{r}-\frac{1}{R}\right)}+1\right)^2} \; e^{-\frac{k_e Q_0 q_0}{m_0 c^2}\left(\frac{1}{r}-\frac{1}{R}\right)}$$

$$= \frac{\left(e^{\frac{k_e Q_0 q_0}{m_0 c^2}\left(\frac{1}{r}-\frac{1}{R}\right)}-1\right)^2}{\left(e^{\frac{k_e Q_0 q_0}{m_0 c^2}\left(\frac{1}{r}-\frac{1}{R}\right)}+1\right)^2}\left(1- e^{-\frac{k_e Q_0 q_0}{m_0 c^2}\left(\frac{1}{r}-\frac{1}{R}\right)}\right) \quad (144)$$

Figure 28 depicts the kinetic energy and dual wave energies as a function of the normalized distance $\frac{r}{\left(\frac{k_e Q_0 q_0}{m_0 c^2}\right)}$ from the attracting charge. The ratio of each energy from the body's total energy is depicted in Figure 29.

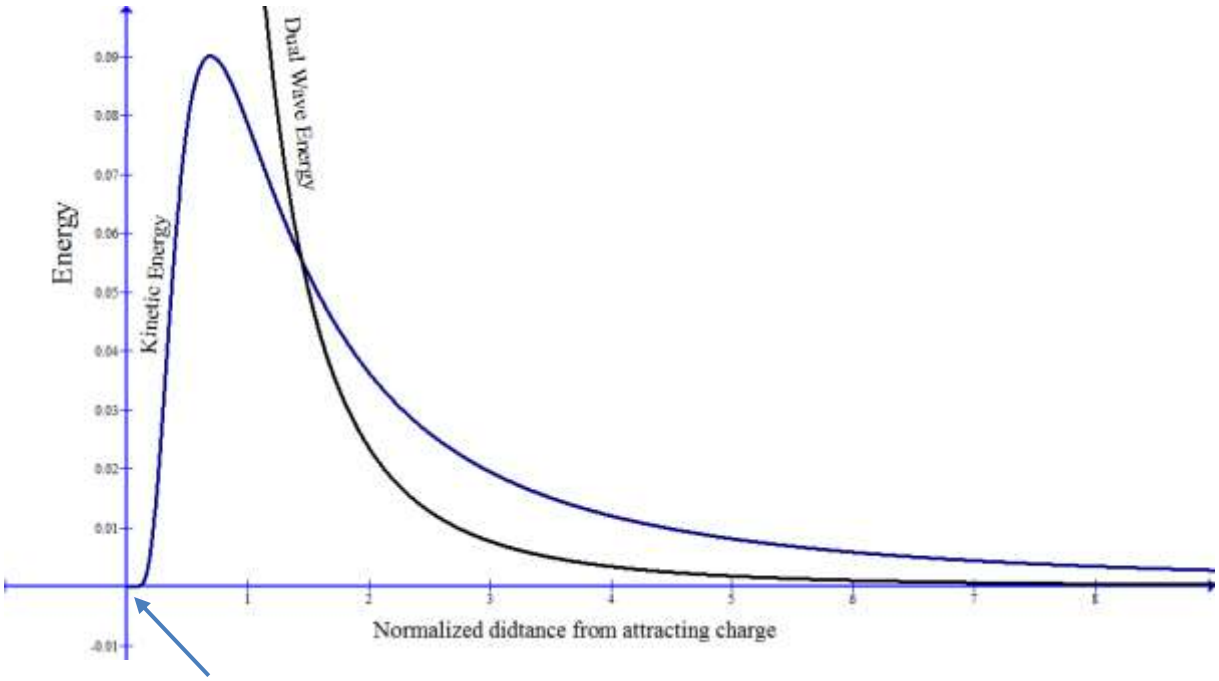


**Figure 28**. Matter and dual-wave energies as functions of the distance from an attracting charge

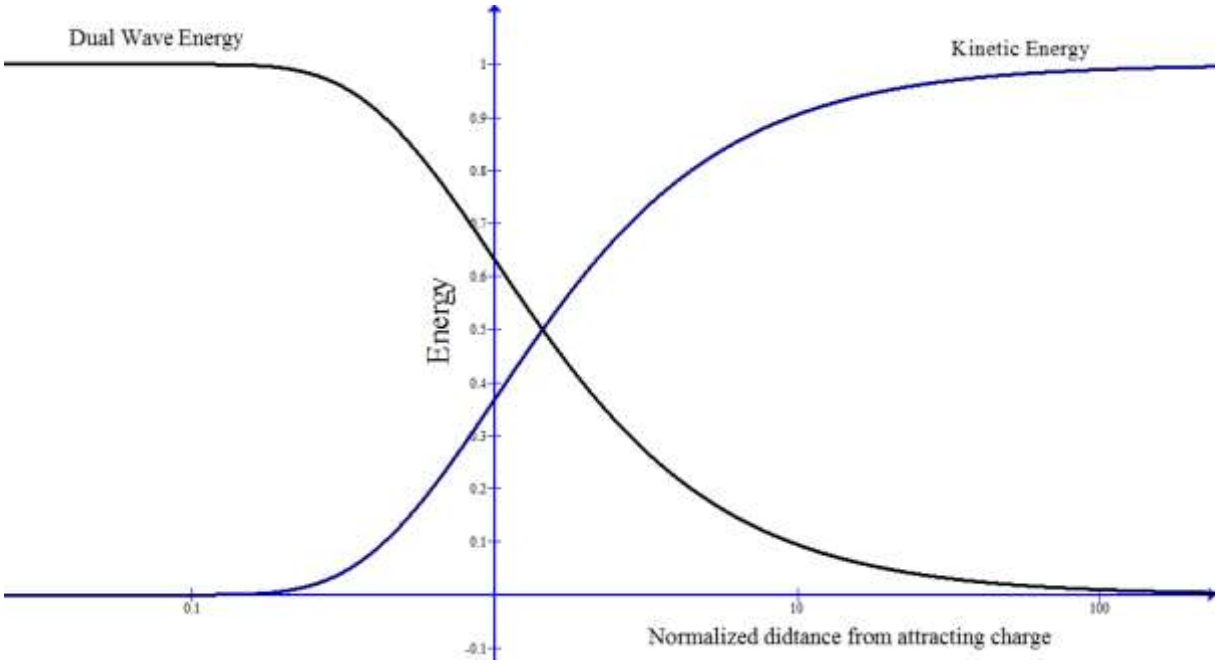


**Figure 29**. Ratios of matter and wave energies as functions of the distance from an attracting charge

The distance at which the matter energy reaches is maximum is calculated by deriving the kinetic energy term in eq. 142 with respect to r and equating the derivative to zero, which after simplification yields:

$$r^* = \frac{1}{\frac{ln(2+\sqrt{5})}{(\frac{k_e\, Q_0\ q_0}{m_0\, c^2})} + \frac{1}{R}} \tag{145}$$

For R>>1 the above expression becomes:

$$r^* = \frac{(\frac{k_e\, Q_0\ q_0}{m_0\, c^2})}{ln(2+\sqrt{5})} \approx 0.3413884\, \frac{k_e\, Q_0\ q_0}{m_0\, c^2} \tag{146}$$

The distance from the attracting body at which the matter and dual wave energies are predicted to be equal could be found by equating the expressions in equations 142 and 144, which after simplification yields:

$$r^{**} = \frac{1}{\frac{ln(2)}{(\frac{k_e\, Q_0\ q_0}{m_0\, c^2})} + \frac{1}{R}} \tag{147}$$

Which for R>>1 reduces to:

$$r^{**} = \frac{(\frac{k_e\, Q_0\ q_0}{m_0\, c^2})}{ln(2)} \approx 1.4426950\ \frac{k_e\, Q_0\ q_0}{m_0\, c^2} \tag{148}$$

In order to account for both electrodynamics and gravitation, we simply relativize both forces or fields, and then sum up the forces vectors.

**11. A brief note on the theory's application to radial motion**

In the previous section we investigated the relativistic dynamics of bodies in translational motion. However, most physical systems involve non-translational motion in open or closed trajectories. An important and frequently observed form of motion in systems of all dimensions, from a bound electron to a nucleus' atom to a planet orbiting its sun, could be approximated by radial motion. We shall devote a separate article to investigating the relativistic dynamics of radial motion. Here we confine ourselves to commenting on a common misconception in classical and modern physics, where it is the commonly accepted that radial motion with constant radial velocity differs from translational motion with constant linear velocity. While the latter is considered to be an inertial motion, the first is considered an accelerated motion. We claim that this distinction is fundamentally wrong and counterproductive. In fact, it is easy to see that the translational and radial systems of motion

are completely equivalent systems [185-186]. Because all the relationships between the various variables in one system are identical in their mathematical form to corresponding relationships between variables in the second system, the dynamics of the two system in time could be mapped one onto the other. Table 7 summarizes well know relationship between distance, linear velocity, acceleration, mass, force, work and kinetic energy, for translational motion, and the corresponding relationships between angular position, velocity, acceleration, inertia, torque, work and kinetic energy. The complete dynamical equivalence between the two types of motion is hard to miss. Thus to apply Information Relativity to radial motion, we can use the previous results derived for translational motion to write the equivalent results for radial motion, simply by replacing each translational variable by its corresponding radial variable.

**Table 7**
**Classical Translational and radial laws of motion**

| **Translational** | **Radial** |
|---|---|
| Position $x$ | Angular position $\theta$ |
| Velocity $v = \frac{dx}{dt}$ | Angular velocity $\omega = \frac{d\theta}{dt}$ |
| Acceleration $a = \frac{dv}{dt}$ | Angular acceleration $\alpha = \frac{d\omega}{dt}$ |
| Mass $m$ | Radial inertia $I$ |
| Newton's second law $F = ma$ | Newton's second law $\tau = I\,\alpha$ |
| Work $W = \int F dx$ | Work $W = \int \tau \; d\theta$ |
| Kinetic energy $E = \frac{1}{2} mv^2$ | Kinetic energy $E = \frac{1}{2} I\,\omega^2$ |

For the case of radial motion with constant radial velocity $w$, we can use the results in Table 1 inertial translational motion for to write the equivalent transformations relating physical measurements in one radial reference frame which rotates with respect to an observer's frame with radial velocity $w$. For example, the time duration transformation for constant radial motion could be written directly as:

$$\frac{\Delta t}{\Delta t'} = \frac{1}{1-\frac{\omega}{c}} = \frac{1}{1-\frac{v}{r\,c}} = \frac{1}{1-\frac{\beta}{r}} \tag{149}$$

And the length transformation becomes:

$$\frac{\Delta\theta}{\Delta\theta'} = \frac{1+\frac{\omega}{c}}{1-\frac{\omega}{c}} = \frac{1+\frac{\beta}{r}}{1-\frac{\beta}{r}} \tag{150}$$

The matter and dual wave energy densities could be also immediately written as:

$$\frac{e_k}{e_0} = \frac{1-\frac{\omega}{c}}{1+\frac{\omega}{c}} \left(\frac{\omega}{c}\right)^2 \tag{151}$$

And,

$$\frac{e_w}{e_0} = \frac{2\left(\frac{\omega}{c}\right)^3}{1+\frac{\omega}{c}} \tag{152}$$

For accelerated radial motion, in eq. 70 replacing the force $F$ by the angular torque $\tau$, the mass $m$ by the moment of inertia $I$ and the translational acceleration $a$ by the radial acceleration $\alpha$, gives:

$$\tau = \frac{1-2\frac{\omega}{c}-\left(\frac{\omega}{c}\right)^2}{\left(1+\frac{\omega}{c}\right)^2} \; I_0 \; \alpha \tag{153}$$

Other relationships could be derived using the same method.

**12. Summary and some concluding remarks**

The recent literature has witnessed many theories proposing a new physics. The main efforts were directed towards reconciliation between special relativity and quantum mechanics in what is broadly referred to as quantum field theory. This includes QED, QCD and the group of QG theories, which can be considered quantum field theories directed at a unification of gravity and quantum mechanics. More "extreme" theories abandoned both postulates of special relativity, included a preferred reference-frame, and allowed breaking of the time-translation invariance [187].

Information relativity theory constitutes a completely different approach to relativity by defining it epistemologically as a modulation in information about physical realities. Specifically, we extended classical physics to the realm of high velocities, simply by accounting for the time travel of information about a physical measurement, from the reference frame at which the measurement was taken, to an observer in another reference frame, which is in motion relative to the first frame. We demonstrated that this modification is capable of unifying the physics of moving bodies, regardless of their size and mass. The resulting model turns out to be in agreement with quantum mechanics predictions. However, it is advantageous in several important aspects including its axiom-free nature, universality, simplicity, continuity with classic physics, dependence only on observables, and explanatory power. Table 8 summarizes the main prediction presented in this article. The signs -, +, ?, and ?? in the table's cells, indicate no-prediction, successful prediction, disputed, and highly disputed predictions, respectively. Of particular significance are the solutions of the hydrogen atom problem and the mystery of the

double slit experiments, for which no satisfying explanations have been provided yet. No less important are the explanations proposed for the bewildering phenomena of dark matter and dark energy.

Generalization of the theory to include the gravitational force provided predictions and simple explanations for the strong force, quantum confinement, and quantum asymptotic freedom. Since the theory applies equally to the too-small and the too-big, we conjecture that similar forces and quantum processes may govern the interaction of black holes with matter gravitated by them.

**Table 8**
**Summary of main predictions**

| | **Experimental Result/ Observation** | **Special Relativity** | **General Relativity** | **Quantum theories** | **Information Relativity** | **Remarks** |
|---|---|---|---|---|---|---|
| | **1. Particle physics** | | | | | |
| 1 | Michelson-Morley "null" result | + | - | - | + | |
| 2 | Time dilation of decaying muons | + | - | - | + | |
| 3 | Radial and linear Sagnac effect | - | - | - | + | Contradicts Special Relativity |
| 4 | Higgs Boson mass | - | - | + | + | |
| | **2. Quantum mechanics** | | | | | |
| 5 | Matter-wave duality | - | - | + | + | Compatible with de Broglie-Bohm theory |
| 6 | Quantum phase transition | - | - | + | + | |
| | | | | + | + | |
| | Quantum criticality | - | - | + | + | At the Golden Ratio (Coldea, 2010) |
| 8 | Entanglement | - | - | + | + | Explained in physical terms |
| | | | | | | |
| 9 | Particle's diffraction in the double-slit experiment | - | - | + | + | Explained in physical terms |
| 10 | Hydrogen atom problem | - | - | ? | + | Quantization is concluded, not assumed |
| 11 | The strong force | - | - | + | + | Explained in physical terms see [10] |
| 12 | Quantum confinement | | | + | + | Explained in physical terms see [10] |
| 13 | Asymptotic freedom | | | + | + | Explained in physical terms, see [10] |
| | | | | | | |

| | **3. Cosmology** | | | | | |
|---|---|---|---|---|---|---|
| 14 | Dark matter | - | - | ? | + | Explained as cosmic quantum matter |
| | **Experimental Result/ Observation** | **Special Relativity** | **General Relativity** | **Quantum theories** | **Information Relativity** | **Remarks** |
| 15 | Dark energy | - | - | ?? | + | Explained as the energy of the matter's dual-wave at cosmic scales |
| 16 | GZK cutoff | - | - | - | + | Quantum criticality at cosmic scales |
| 17 | Predicting results Of ΛCDM cosmologies | - | ? | - | + | Explained as the amounts of cosmic dual-wave energy |
| 18 | Black hole radius | - | + | - | + | Without an interior singularity |
| 19 | Timeline of evolution of chemical elements | - | - | - | + | Not predicted by other theories |

We are fully aware of the fact that the proposed approach constitutes a huge paradigm shift in all physics. The difficulties in merging it with contemporary physics are enormous, and so are the social and psychological difficulties which would result from such merger. However, the fact that our theory is grounded only on physical facts with no theoretical axiom, coupled with its unquestionable successful in predicting and explaining a multitude of physical phenomena, should be enough to convince an unbiased reader, that it deserves a chance to be put for experimental testing. At present, the theoretical model of reality is fragmented, mathematically cumbersome, expressed in non-physical terms, full of inner contradictions, non-bridgeable with Newtonian physics, and incapable of answering fundamental questions like the nature of dark matter and dark energy. In contrast, we propose a unifying alternative which is coherent, non-axiomatic, simple and beautiful, consistent with Newton's physics, which provides plausible, and easy to test explanations of fundamental questions of physics. Unless directed by prejudice or conservatism, it is hard to understand why a true scientist will not want to consider the proposed theory.

**References**


[1] Einstein, A. On the electrodynamics of moving bodies (1905). In J. Stachel (Ed.), *The Collected Papers of Albert Einstein*, vol. 2 (pp 304–95), Princeton, NJ: Princeton University Press (1989).

[2] Amelino-Camelia, G. Testable scenario for relativity with minimum length. *Physics Letters* B 510, 255–263 (2001).

[3] Amelino-Camelia, G. Doubly-special relativity: first results and key open problems. *International Journal of Modern Physics* D 11 (10), 1643–1669 (2002).

[4] Amelino-Camelia, G. Doubly-special relativity: facts, myths and some key open issues.

S*ymmetry* 2, 230-271(2010).
[5] Albrecht, A., Magueijo, *J. Phys. Rev*. D 59, 043516 (1999).
[6] Barrow, J.D. *Phys. Rev*. D 59, 043515 (1999).
[7] Magueijo J. New varying speed of light theories. *Reports on Progress in Physics*, 66 (11), 2025 (2003).
[8] Magueijo, J. & Smolin, L. *Phys. Rev. Lett*. 88, 190403 (2002).
[9] Einstein, A. *Relativity: The general and special theory* (translated to English by Robert W. Lawson, University of Sheffield (1920).
[10] Suleiman, R. An epistemic relativizing of newton law of gravitation predicts the phenomenon of asymptotic freedom. Unpublished manuscript, 2016. https://www.researchgate.net/publication/301789366.
[11] Braxmaier, C., , H., Pradl, O., Mlynek, J., Peters, A., & Schiller, S. (2001) Tests of relativity using a cryogenic optical resonator. *Physical Review Letters*, 88 (1), 010401 [4 pages].
[12] Jacobson, T., Liberati, S., & Mattingly, D. Lorentz violation at high energy: concepts, phenomena and astrophysical constraints. *Annals of Physics*, 321, 150-196 (2006).
[13] Gambini, R., & Pullin, J. (1999) *Physical Review* D, 59, 124021. [4 pages]
[14] Colatto, L.P., Penna A.L.A, Santos, W.C. Charged tensor matter fields and Lorentz symmetry violation via spontaneous symmetry breaking. *The European Physical Journal* C, 36, 79–87 (2004).
[15] Abramowski A. (2011) Search for Lorentz Invariance breaking with a likelihood fit of the PKS 2155-304. Flare Data Taken on MJD 53944. *Astroparticle Physics*, 34, 738.
[16] Klapdor-kleingrothaus H V (2004) From nuclear physics to physics beyond the standard model: First evidence for Lepton number violation and the Majorana character of neutrinos. *Journal of Modern Physics* D, 13 (10, 2107-2126.
[17] Kostelecky V A, Russell N (2011). Data tables for Lorentz and CPT violation. *Review of Modern Physics*, 83, 11[arXiv:0801.0287].
[18] Devasiaa, S. (2010). Lorentz violation in high-energy ions. *The European Physical Journal* C, 69, 343–346.
[19] Cheng, H-C, Luty, M. A. Mukohyama, S., & Thaler, J. (2006). Spontaneous Lorentz breaking at high energies. *Journal of High Energy Physics*, 0605, 076.
[20] L. Hardy, *Phys. Rev. Lett***.** 68, 2981(1992).
[21] K. Berndl, D. Dürr, S. Goldstein and N. Zanghì, *Phys. Rev. A* 53, 2062 (1996).
[22] Bell, J. S. On the Einstein Podolsky Rosen paradox, *Physics*, 1 (3), 195 – 200 (1964).
[23] Bell, J.S. *Speakable and unspeakable in quantum mechanics*, 2nd Editionn. Cambridge University Press, Cambridge (2004).
[24] Norsen, T. Local Causality and Completeness: Bell vs. Jarrett. *Found Phys*., 39, 273-294 (2009).
[25] Aspect, A., Dalibard, J. & Roger, G. Experimental test of Bell's Inequalities using time-varying analyzers. *Phys. Rev. Lett*. 49, 1804-1807 (1982).
[26] Weihs, G., Jennewein, T., Simon, C., Weinfurter, H. & Zeilinger, A. Violation of Bell's Inequality under strict Einstein locality conditions. *Phys. Rev. Lett*. 81, 5039-5043 (1998).
[27] Matsukevich, D. N., Maunz, P., Moehring, D. L., Olmschenk, S. & Monroe, C. Bell inequality violation with two remote atomic qubits. *Phys. Rev. Lett*. 100, 150404 (2008).

[28] Horodecki, R. Horodecki, P. Horodecki, M., & Horodecki K. Quantum entanglement. *Rev. Mod. Phys*. 81, 865 (2009).
[29] Giustina, M. et al. Bell violation using entangled photons without the fair-sampling assumption. *Nature*, 497, 227-230 (2013).
[30] Hensen et al. Loophole-free Bell inequality violation using electron spins separated by 1.3 kilometers, *Nature*, 562, 682-686 526 (2015).
[31] O'Connor J. J., Roberston E. F. *Christian Andreas Doppler*. MacTutor History of Mathematics archive. University of St. Andrews (1998).
[32] Maulik D. Doppler Ultrasound in Obstetrics and Gynecology. Springer-Verlag (2005).
[33] Olsen S. *The Golden Section*. New York, Walker & Co. (2006).
[34] Livio M. *The Golden Ratio: The Story of Phi, the World's Most Astonishing Number*. New York, Broadway Books (2002).
[35] Coldea R., Tennant D. A., Wheeler E. M., Wawrzynska E., Prabhakaran D., Telling M., Habicht K., Smeibidl P., Kiefer K. Quantum criticality in an Ising chain: Experimental evidence for emergent E8 symmetry. *Science*, 327 (5962), 177–180 (2010).
[36] Hardy L. Nonlocality of a single photon revisited. *Phys. Rev. Lett*., 73, 2279–2283 (1994).
[37] de Broglie, L. Waves and quanta. *Nature*, 112, 540 (1923).
[38] de Broglie, L. The reinterpretation of wave mechanics, *Foundations of Physics*, 1, 5-15 (1970).
[39] Bohm, D. (1952a). A suggested interpretation of the quantum theory in terms of `hidden' variables, I. *Physical Review*, 85, 166-179.
[40] Bohm, D. (1952b). A suggested interpretation of the quantum theory in terms of `hidden' variables, II. *Physical Review*, 85, 180-193.
[41] Holland, P. R. *The quantum theory of motion: An account of the de Broglie-Bohm causal interpretation of quantum mechanics*. Cambridge University Press (1995).
[42] Douady, S., Couder, Y. Phyllotaxis as a physical self-otganizing growth process. *Physical Review Letters* 68 (13), 2098- 2101 (1992).
[43] Klar, A. J. S. Fibonacci's flowers. *Nature*, 417, 595 (2002).
[44] Zeng l., Wang G. Modeling golden section in plants. *Progress in Natural Science* 19, 255-260 (2009).
[45] Affleck, I. Golden ratio seen in a magnet. *Nature* 464 (18), 362-363 (2010).
[46] Stoudenmire E. M., Clarke D. J., Mong R. S., K., and Alicea, J. Assembling Fibonacci anyons from a Z3 parafermion lattice model. *Physical Review* B **91**, 235112 (2015).
[47] Lindner, J. F., Kohar, V. Kia, B., Hippke, M., Learned, J.G., and Ditto, W. L. Strange Nonchaotic Stars. *Phys. Rev. Lett.* 114, 054101 (2015).
[48] Kopell, N. J., and Whittington, M. A. Temporal interactions between cortical rhythms. *Frontiers in Neuroscience*, 2 (2), 145-154 (2008).
[49] Hammel, G. T., & Vaughan, K. C. *Math and Music: Harmonious Connections*. Dale Seymour Publications (1995).
[50] John F. Putz . The golden section and the piano sonatas of Mozart. *Mathematics Magazine* 68 (4), 275-282 (1995).
[51] Pittard, N., Ewing, M., & Jevons, C. Aesthetic theory and logo design: examining consumer response to proportion across cultures. *International Marketing Review*, 24(4), 457-473 (2007).

[52] van den Bos, K., Cropanzano, R. Kirk, J. Jasso, G., and Okimoto, T. G. Expanding the horizons of social justice research: Three essays on justice theory. *Soc. Just. Res*., 28, 229-246 (2015).
[53] Suleiman, R. Economic harmony: An epistemic theory of economic interactions. *Games*, 8(1), 2 (2017). doi:10.3390/g8010002.
[54] Dirac, P. The relationship between mathematics and physics. *Proceedings of the Royal Society* 59, 1038–39 (1939).
[55] Michelson, A.A., and Morley, E. On the relative motion of the Earth and the luminiferous ether. *American Journal of Science*, 34, 333-345 (1887).
[56] Suleiman, R. Information relativity theory and its application to time interval and length. Unpublished manuscript. http://vixra.org/pdf/1504.0154v3.pdf.
[57] Miller, D.C. (1925). Ether-drift experiments at mount Wilson. *Proceedings of the National Academy of Sciences* USA, 11(6), 306–314.
[58] Tomaschek, R. Über das verhalten des lichtes außerirdischer lichtquellen. *Annalen der Physik*, 378, 105–126 (1924).
[59] Illingworth, K. K. A repetition of the Michelson-Morley experiment using Kennedy's refinement. *Physical Review*, 30(5), 692-696 (1927).
[60] Piccard, A. & Stahel, E. L'expérience de Michelson, réalisée en ballonlibre. *Comptes Rendus*, 183(7), 420–421 (1926).
[61] Michelson, A. A., Pease, F. G. & Pearson, F. Results of repetition of the Michelson-Morley experiment. *Journal of the Optical Society of America*, 18(3), 181 (1929).
[62] Joos, G. Die Jenaer Wiederholung des Michelsonversuchs. *Annalen der Physik*, 399 (4), 385–407 (1930).
[63] Frisch, D., & Smith, J.H. Measurement of the Relativistic Time Dilation Using μ-Mesons. *American Journal of Physics*, 31, 342-355 (1963).
[64] Hall, R.E., Lind, D. A., and Ristinen, R. A. A simplified muon lifetime experiment for the instructional laboratory. *American Journal of Physics*, 38 (10), 1196-1200 (1970).
[65] Gaisser, T. K. *Cosmic rays and particle physics*, Cambridge University Press, Cambridge, (1990).
[66] Sagnac, M. G. C. *R. Acad. Sci*. 157, 708–710 (1913)
[67] Ashby, N. *Relativity in Rotating Frames,* Springer (2004).
[68] Post, E. J. *Rev. Modern Phys.* 39, 475–493 (1967).
[69] Anderson, R., Bilger, H. R., Stedman, G. E. "Sagnac" effect: A century of Earth rotated interferometers. *American Journal of Physics*, 62, 11, 975-985 (1994).
[70] Malykin, G. B. Earlier studies of the Sagnac effect. *Phys.-Usp*., 40 317 (1997).
[71] Ashby, N. Relativity and the Global Positioning System. *Physics Today*, 41-47 (2002).
[72] Chow, W.W. et al. The ring laser gyro. *Reviews of Modern Physics*, 57 (1), 61-104 (1985).
[73] Vali, V., & Shorthill, R. *Appl. Opt*. 16, 290 (1977).
[74] Leeb, W., Schiffner, G., & Scheiterer, E. *Appl. Opt*. 18, 1293 (1979).
[75] Lefevre, H. *The Fiber-Optic Gyroscope*. Artech House: Boston (1993).
[76] Burns, W. K. *Fiber Rotation Sensing,* Academic Press, Boston (1994).
[77] Malykin, G. B. The Sagnac effect: correct and incorrect explanations. *Phys.-Usp*., 43, 1229 (2000).
[78] Ashtekar, A., & Magnon, A. The Sagnac effect in general relativity. *J. Math. Phys*., 16,

341 (1975).
[79] Wang, R, Zheng, Y., Yao, A., & Langley, D. Modified Sagnac experiment for measuring travel-time difference between counter-propagating light beams in a uniformly moving fiber. *Physics Letters* A, 312 7–10 (2003).
[80] Wang, R., Zheng, Yi, & Yao, A. Generalized Sagnac effect. *Phys. Rev. Lett*., 93 (14), 143901 (3 pages) (2004).
[81] Adam T., et al. Measurement of the neutrino velocity with the OPERA detector in the CNGS beam (OPERA Collaboration). *Journal of High Energy Physics*, 10, 093 (2012).
[82] Adam, T., et al. Measurement of the neutrino velocity with the OPERA detector in the CNGS beam using the 2012 dedicated data. *Journal of High Energy Physics*, 1126-6708 (2013).
[83] Antonello, M., et al. Measurement of the neutrino velocity with the ICARUS detector at the CNGS beam. *Physics Letters* B, 713 (1), 17–22 (2012).
[84] Agafonova, N.Yu., et al. Measurement of the velocity of neutrinos from the CNGS beam with the Large Volume Detector. *Physical Review Letters*, 109, 070801 (2012).
[85] Alvarez Sanchez, P., et al. Measurement of CNGS muon neutrino speed with Borexino. *Physics Letters* B. 716, 401–405 (2012).
[86] Suleiman, R. A complete relativity theory predicts with precision the neutrino velocities reported by OPERA, MINOS, and ICARUS. *Progress in Physics*, 4, 53-56 (2013).
[87] Suleiman, R. A Relativistic Newtonian mechanics predicts with precision the results of recent neutrino-velocity experiments. *Journal of Advances in Physics*, 6 (1), 1032-1035 (2014).
[88] Suleiman, R. (2016). Spatial locality is the hidden variable in entanglement experiments, *Physics Essays*, 29, 503-505.
[89] Sachdev, S. *Quantum Phase Transitions*, 2nd Edition, Harvard University Press, Massachusetts (2007).
[90] Coleman, P., and Schofield, A. J. Quantum criticality. *Nature*, 433, 226-229 (2005).
[91] Einstein, A., Podolsky, B., & Rosen, N. Can quantum-mechanical description of physical reality be considered complete? *Physical Review*, 47, 777-780 (1935).
[92] Suleiman, R. If God plays dice, must we do the same? Quantum entanglement as a deterministic phenomenon. *SHS Web of Conferences*; Proceedings of ICNFP2015 (in press).
[93] P. Grangier, G. Roger, A. Aspect, *Europhys. Lett.* 1, 173 (1986).
[94] A. Zeilinger, G. Weihs, T. Jennewein, M. Aspelmeyer, *Nature* 433, 230 (2005).
[95] P. G. Merli, G. F. Missiroli, G. Pozzi, AJP 44, 306 (1976).
[96] A. Tonomura, J. Endo, T. Matsuda, T. Kawasaki, H. Ezawa, AJP 57, 117 (1989).
[97] J-Y Chesnel, A. Hajaji, R. O. Barrachina, F. Frémont, F. *Phys. Rev. Lett*. 98, 100403 (2007).
[98] A. Zeilinger, R. Gähler, C. G. Shull, W. Treimer, W. Mampe, *Rev. Mod. Phys*. 60, 1067 (1988).
[99] O. Carnal, J. Mlynek, *Phys. Rev. Lett*. 66, 2689 (1991).
[100] B. Zimmermann, D. Rolles, B. Langer, R. Hentges, M. Braune, S. Cvejanovic, OGeßner, F. Heiser, S. Korica, T. Lischke, A. Reinköster, J. Viefhaus, R. Dörner; V. McKoy, U. Becker, *Nature Phys*. 4 (8), 649-655 (2008).
[101] S. Eibenberger, S. Gerlich, M. Arndt, M. Mayor, J. Tüxen, *Phys. Chem. Chem. Phys*.

15, 14696-14700 (2013).
[102] R. Feynman, R. B. Leighton, M Sands. *The Feynman Lectures on Physics*, Vol. 3 (US: Addison-Wesley (1965).
[103] Suleiman, R. relativistic model of matter-wave duality explains the results of the double-slit experiment. Poster presented at the *5th International Conference on New Frontiers in Physics* ICNFP2016. Crete, 6-14 July 2016.
[104] S. Durr, T. Nonn, G. Rempe, *Nature* 395 (3), 33-37 (1998).
[105] Y. Aharonov, M. S. Zubairy, *Science* 307:875–879 (2005).
[106] R. Mir, J. S. Lundeen, M. W. Mitchell, A. M. Steinberg, J. L. Garretson, H. M. Wiseman, *NJP* 9, 287-287 (2007).
[107] S. Durr, T. Nonn, G. Rempe, *Nature* 395 (3), 33-37 (1998).
[108] V. Jacques, E. Wu, F. Grosshans, F. Treussart, P. Grangier, A. Aspect, J-F Roch, *Science* 315, 966-968 (2007).
[109] Mills, R. L. The hydrogen atom revisited. *International Journal of Hydrogen Energy*, 25 1171–1183 (2000).
[110] V.F. Weisskopf,. *Rev. Modern Phys*. **21,** 305, (1949).
[111] ] Mills, R. L. Maxwell's Equations and QED: Which Is Fact and Which Is Fiction? *Physics Essays* 19, 2, 225- 262 (2006).
[112] Dirac, P. The quantum theory of the electron. Proceedings of the Royal Society A, 117 (778): 610-624 (1928).
[113] Dirac, P. A theory of electrons and protons. Proceedings of the Royal Society A., 126 (801), 360 (1930).
[114] McGregor M.H. *The enigmatic electron*. Kluwer; Dordrecht (1992).
[115] Suleiman, R. The Dark Side Revealed: A Complete Relativity Theory Predicts the Content of the universe. *Progress in Physics*, 4, 34-40 (2013).
[116] Suleiman, R. A simple relativistic cosmology of the universe. Paper presented at the *International Conference on Relativistic Astrophysics: celebrating 100 years of Einstein's general relativity theory*, Lahore, Pakistan, Feb.10-14, 2015. http://vixra.org/pdf/1408.0002v5.pdf.
[117] Kazanas, D. *Astrophys. J*. 241, L59 (1980).
[118] Guth, A. H. *Phys. Rev*. D 23, 347 (1981).[51] Sato, K. *Phys. Lett*. B 99, 66 (1981).
[119] K. Greisen, *Phys. Rev. Lett*. 16, 748 (1966).
[120] G. T. Zatsepin and V. A. Kuz'min, *J. Exp. Theor. Phys. Lett*. 4, 78 (1966).
[121] Bergman, D.R., et al. Can experiments studying ultrahigh energy cosmic rays measure the evolution of the sources? astro-ph/,DanaInfo=arXiv.org+0603797v1 (2006).
[122] Thomson, G. The TA and TALE experiments. *Journal of Physics: Conference Series* 47, 248-254 (2006).
[123] Gilli, R., Cimatti, A., Daddi, E., et al. *ApJ*, 592, 721 (2003).
[124] Wittman, D. M., et al. Detection of weak gravitational lensing distortions of distant galaxies by cosmic dark matter at large scales. *Nature*, 405, 143-148 (2000).
[125] Samushia, L., & Ratra, B. Constraints on dark energy models from radial baryon acoustic scale measurements. *The Astrophysical Journal*, 701, 373–1380 (2009).
[126] Farooq, M. O. Observational constraints on dark energy cosmological model parameters. (Preprint) arXiv:1309.3710 (2013).

[127] Kunz, M, & Bassett, B. A. A tale of two distances. (Preprint) arXiv: astro-ph/0406013 (2004).
[128] Furlanetto, S. R. The global 21-centimeter background from high redshifts. *Mon. Not. R. Astron. Soc*. 371, 867–878 (2006).
[129] Oguri, M., et al. The Sloan digital sky survey quasar lines search. III Constrains on dark energy from the third data released quasar lens catalog. *The Astronomical Journal*, 135, 512–519 (2008).
[130] Viel, M, Haehnelt, M.G., & Springel, V. Inferring the dark matter power spectrum from the Lyman α forest in high-resolution QSO absorption spectra. *Mon. Not. R. Astron*. Soc. 354, 684 – 694 (2004).
[131] K. Schwarzschild. Über das Gravitationsfeld eines Massenpunktes nach der Einsteinschen Theorie, *Sitzungsberichte der Deutschen Akademie der Wissenschaften zu Berlin, Klasse fur Mathematik, Physik, und Technik,* 1916. pp 189.
[132] K. Schwarzschild, Über das Gravitationsfeld einer Kugel aus inkompressibler Flussigkeit nach der Einsteinschen Theorie, *Sitzungsberichte der Deutschen Akademie der Wissenschaften zu Berlin, Klasse fur Mathematik, Physik, und Technik*, 1916, pp 424.
[133] Hawking, S. W. Black Hole Explosions? *Nature*, 248: 30-31 (1974).
[134] Bekenstein, J. D. Black Holes and Entropy. *Physical Review D* 7: 2333-2346 (1973).
[135] Bowyer, S. et al. Cosmic X-ray Sources, *Science* 147 (3656): 394–398 (1965).
[136] Xiong, D. R., & Zhang, X. The connections between bulk Lorentz factor, black hole mass and accretion in Fermi FSRQs. *Astrophysics and Space Science* (2014).
[137] Ferrarese , L., & Ford, H. Supermassive black holes in galactic nuclei: Past, present and future research. *Space Science Reviews*, 116 (3-4): 523-624 (2005).
[138] John Kormendy, J., & Richstone, D. Inward bound – The search for supermassive black holes in galactic neuclei. *Annu. Rev. Astron. Astrophys*. 33:581-624 (1995).
[139] Doeleman, S., et al. Jet-launching structure resolved near the supermassive black Hole in M87. *Science*, 338: 355 – 358 (2012).
[140] Ferrarese, L., & Merritt, D. A fundamental relation between supermassive black holes and their host galaxies. *The Astrophysical Journal*, 539, L9–L12 (2000).
[141] Chokshi, A., & Turner, E. L. Remnants of the quasars. *Mon. Not. R. Astr. Soc*. 259: 421-424 (1992).
[142] Di Matteo, T., Springel, V., & Hernquist, L. Energy input from quasars regulates the growth and activity of black holes and their host galaxies. *Nature*, 433, 604-607 (2005).
[143] Bekenstein, J. D. Universal upper bound on the entropy-to-energy ratio for bounded systems. *Physical Review D* 23, 287-298 (1981).
[144] Bardeen, J. M., Carter, B., & Hawking, S. W. The four laws of black hole mechanics, *Communications in Mathematical Physics*, 31, 161-170 (1973).
[145] Bardeen, J., in *Proceedings of GR5*, Tiflis, U.S.S.R. (1968).
[146] Borde, A. *Phys. Rev*. D., 50, 3392 (1994).
[147] Borde, A., *Phys. Rev*., D55, 7615 (1997).
[148] Ay´on–Beato, E., *Asymptotic Behavior of Scalar Fields Coupled to Gravity,* Graduate Dissertation, Faculty of Physics, Havana Univ. (1993).
[149] Barrab`es, C., Frolov, V.P., *Phys. Rev*., D53, 3215 (1996).
[150] Mars, M., Mart´ın–Prats, M.M., Senovilla, J.M.M., *Class. Quant. Grav*., 13, L51 (1996).

[151] Cabo, A., Ay´on–Beato, E., *Int. J. Mod. Phys*., A14, 2013 (1999).
[152] Ayon-Beato, E., Garcia, A. Regular black hole in general relativity coupled to nonlinear electrodynamics. *Phys. Rev. Lett*., 80, 5056 (1998).
[153] Ashtekar, E., & Bojowald, M. Quantum geometry and the Schwarzschild singularity. *Class. Quantum Grav*. 23, 391 (2006).
[154] Ashtekar A., Pawlowski, T., & Singh, P. Quantum nature of the big bang: An analytical and numerical study. *Phys. Rev. Lett*., 96, 141301 (2006).
[155] Bojowald, M. Absence of singularity in loop quantum cosmology. *Phys. Rev. Lett.* 86, 5227 - 5230 (2001).
[156] Ashtekar A, Bojowald M and Lewandowski J. Mathematical structure of loop quantum cosmology. *Adv. Theor. Math. Phys*. 7, 233–268 (2003).
[157] Hawking, S. W. Particle creation by black holes", *Communications in Mathematical Physics*, 43, 199-220 (1975).
[158] Tseytlin, A.A., *Phys. Lett*., B363, 223 (1995).
[159] Callan, Jr. C. G., & Maldacena, J. M. D-Brane Approach to black hole quantum mechanics. *Nuclear Physics* B, 489, 65–94 (1997).
[160] Steinhardt, C. L., et al. SDSS 0956+5128: A broad-line quasar with extreme velocity offsets. *ApJ* 759 24 (2012).
[161] K. Hurley, K. et al. Interplanetary network localization of GRB 991208 and the discovery of its afterglow. *The Astrophysical Journal Letters*, 534 (2000).
[162] Calderone, G., Ghisellini, G., Colpi, M., and Dotti, M. B2 0954+25A: a typical Fermi blazar or a γ -ray loud Narrow Line Seyfert 1? *Mon. Not. R. Astron. Soc*. 424, 3081–3093 (2012).
[163] Xiong, D.R., & Zhang, X. The connections between bulk Lorentz factor, black hole mass and accretion in Fermi FSRQs. *Astrophysics and Space Science* (2014).
[164] Matsuoka, M. X-ray observations of high-z radio loud/quiet quasars. *A & Space Res*. 23, 1151- l 154 (1999).
[165] Elíasdóttir, Á., et al. Dust extinction in high-z galaxies with gamma-ray burst afterglow spectroscopy: the 2175 Å feature at z= 2.45. *The Astrophysical Journal*, 697:1725–1740 (2009)
[166] Hook, I. M. (Ed.), The science case for the European Extremely Large Telescope: The next step in mankind's quest for the Universe. *The Messenger*, 121, 2-10, (2005).
[167] ATLAS Collaboration. Combined search for the Standard Model Higgs boson using up to 4.9 fb−1 of pp collision data at $\sqrt{s}$ = 7 TeV with the ATLAS detector at the LHC. *Physics Letters B* 710, 49-66 (2012).
[168] CMS Collaboration. Observation of a new boson at a mass of 125 GeV with the CMS experiment at the LHC. *Physics Letters B* 716, 30–61 (2012).
[169] F. Englert, R. Brout, *Phys. Rev. Lett*. 13, 321 (1964).
[170] P.W. Higgs, *Phys. Lett*. 12, 132 (1964).
[171] G.S. Guralnik, C.R. Hagen, T.W.B. Kibble, *Phys. Rev. Lett*. 13, 585 (1964).
[172] P.W. Higgs, *Phys. Rev.* 145, 1156 ((1966).

[173] ATLAS Collaboration. Measurement of the parity violating asymmetry parameter $\alpha_b$ and the helicity amplitudes for the decay $\Lambda_b^0 \rightarrow J\psi\Lambda^0$ in the ATLAS experiment. ATLAS-CONF-2013-071, July 16 (2013).

[174] Malecki, P (on behalf of the ATLAS collaboration). Standard model and flavor physics measurements with the ATLAS detector. Cracow Epiphany Conference (2014).

[175] Weinberg, S. Cosmological Production of Baryons. *Phys. Rev. Lett*. 42, 850 (1979).

[176] Barvinsky, A. O., Kamenshchik, A. Yu., and Starobinsky, A. A. Inflation scenario via the Standard Model Higgs boson and LHC. *Journal of Cosmology and Astroparticle Physics*, 2008, (2008).

[177] Bezrukov, F., Shaposhnikov, M. The Standard Model Higgs boson as the inflation. *Physics Letters* B, 659, 3, 703–706 (2008).

[178] Moss, I. G. Higgs boson cosmology. *Contemporary Physics*, 56, 4, 468-476 (2005).

[179] Miralda-Escude, J., & Rees, M. J. High-redshift supernovae and the metal-poor halo stars: signatures of the first generation of galaxies. *The Astrophysical Journal Letters*, 478, 57–61 (1997).

[180] Bromm, V., & Loeb, A. The formation of the first low-mass stars from gas with low carbon and oxygen abundances. *Nature*, 425, 812-814 (2003).

[181] Wilczek, F.A. Asymptotic freedom: From paradox to paradigm. PNAS, 102 (24), 8403-8413 (2005).

[182] Jaffe, R., Wilczek, F. Quarks, diquarks and pentaquarks. Physics world, 17 (6), 25 -30 (2004).

[183] Aktas, A., et al. Evidence for a narrow anti-charmed baryon state. *Physics Letters* B, 588 (1–2), 17–28 (2004).

[184] Alt, C. et al. Evidence for an exotic S= -2, Q = -2 baryon resonance in proton-proton collision at the CERN SPS. *Physics Review Letters*, 92, 042003 (2004).

[185] Simon P´. L. *Differential Equations and Dynamical Systems*. Institute of Mathematics, Eötvös Loránd University (2012).

[186] Kalman, R. E. Mathematical description of linear dynamical systems. *J.S.I.A.M. Control* Ser. A, 1 (2), 152-192 (1963).

[187] Magueijo J. New varying speed of light theories. *Reports on Progress in Physics*, 66 (11), 2025 (2003).